NASA-CR-197000

THE OHIO STATE UNIVERSITY

Powder Agglomeration In a Microgravity Environment

James D. Cawley
Department of Materials Science and Engineering

(NASA-CR-197000) POWDER AGGLOMERATION IN A MICROGRAVITY ENVIRONMENT Final Report (Ohio State Univ.) 97 p

N95-14105

Unclas

G3/29 0028465

NASA Lewis Research Center
Cleveland, Ohio 44135

Grant No. NAG3-755
Final Report

October 1994

THE OHIO STATE UNIVERSITY

Powder Agglomeration In a Microgravity Environment

James D. Cawley
Department of Materials Science and Engineering

NASA Lewis Research Center
Cleveland, Ohio 44135

Grant No. NAG3-755
Final Report
RF Project No. 718986

October 1994

REPORT OF INVENTIONS AND SUBCONTRACTS

(Pursuant to "Patent Rights" Contract Clause) (See Instructions on Reverse Side.)

Form Approved
OMB No. 0704-0297
Expires Jun 30, 1992

Public reporting burden for this collection of information is estimated to average 5 minutes per response, including the time for reviewing instructions, searching existing data sources, gathering and maintaining the data needed, and completing and reviewing the collection of information. Send comments regarding this burden estimate or any other aspect of this collection of information, including suggestions for reducing this burden, to Washington Headquarters Services, Directorate for Information Operations and Reports, 1215 Jefferson Davis Highway, Suite 1204, Arlington, VA 22202-4302, and to the Office of Management and Budget, Paperwork Reduction Project (0704-0297), Washington, DC 20503.

1a. NAME OF CONTRACTOR / SUBCONTRACTOR	c. CONTRACT NUMBER	2a. NAME OF GOVERNMENT PRIME CONTRACTOR	c. CONTRACT NUMBER	3. TYPE OF REPORT (X one)
The Ohio State University Research Foundation	NAG3-755			a. INTERIM X b. FINAL
b. ADDRESS (Include ZIP Code) 1960 Kenny Road Columbus, OH 43210-1063	d. AWARD DATE (YYMMDD) 86/11/25	b. ADDRESS (Include ZIP Code)	d. AWARD DATE (YYMMDD)	4. REPORTING PERIOD (YYMMDD) a. FROM 86 11 25 b. TO 91 09 30

SECTION I – SUBJECT INVENTIONS

5. "SUBJECT INVENTIONS" REQUIRED TO BE REPORTED BY CONTRACTOR / SUBCONTRACTOR (If "None," so state) NONE

a. NAME(S) OF INVENTOR(S) (Last, First, MI)	b. TITLE OF INVENTION(S)	c. DISCLOSURE NO., PATENT APPLICATION SERIAL NO. OR PATENT NO.	d. ELECTION TO FILE PATENT APPLICATIONS				e. CONFIRMATORY INSTRUMENT OR ASSIGNMENT FORWARDED TO CONTRACTING OFFICER	
			(1) United States		(2) Foreign			
			(a) Yes	(b) No	(a) Yes	(b) No	(1) Yes	(2) No

f. EMPLOYER OF INVENTOR(S) NOT EMPLOYED BY CONTRACTOR / SUBCONTRACTOR		g. ELECTED FOREIGN COUNTRIES IN WHICH A PATENT APPLICATION WILL BE FILED	
(1) (a) Name of Inventor (Last, First, MI)	(2) (a) Name of Inventor (Last, First, MI)	(1) Title of Invention	(2) Foreign Countries of Patent Application
(b) Name of Employer	(b) Name of Employer		
(c) Address of Employer (Include ZIP Code)	(c) Address of Employer (Include ZIP Code)		

SECTION II – SUBCONTRACTS (Containing a "Patent Rights" clause)

6. SUBCONTRACTS AWARDED BY CONTRACTOR / SUBCONTRACTOR (If "None," so state) NONE

a. NAME OF SUBCONTRACTOR(S)	b. ADDRESS (Include ZIP Code)	c. SUBCONTRACT NO.(S)	d. DFAR "PATENT RIGHTS"		e. DESCRIPTION OF WORK TO BE PERFORMED UNDER SUBCONTRACT(S)	f. SUBCONTRACT DATES (YYMMDD)	
			(1) Clause Number	(2) Date (YYMM)		(1) Award	(2) Estimated Completion

SECTION III – CERTIFICATION

7. CERTIFICATION OF REPORT BY CONTRACTOR / SUBCONTRACTOR (Not required if [ ] Small Business or [X] Non-Profit organization.) (X appropriate box)

a. NAME OF AUTHORIZED CONTRACTOR / SUBCONTRACTOR OFFICIAL (Last, First, MI)	c. I certify that the reporting party has procedures for prompt identification and timely disclosure of "Subject Inventions," that such procedures have been followed and that all "Subject Inventions" have been reported.	
b. TITLE	d. SIGNATURE	e. DATE SIGNED

DD Form 882, OCT 90 Previous editions are obsolete. 971284

POWDER AGGLOMERATION IN A MICROGRAVITY ENVIRONMENT

Final Report for Grant NAG3-755

James D. Cawley
Ohio State University
Department of Materials Science and Engineering
2041 College Road
Columbus OH 43210-1178

ABSTRACT

This is the final report for NASA Grant NAG3-755 entitled "Powder Agglomeration in a Microgravity Environment." The research program included both two types of numerical models and two types of experiments. The numerical modeling included the use of Monte Carlo type simulations of agglomerate growth including hydrodynamic screening and molecular dynamics type simulations of the rearrangement of particles within an agglomerate under a gravitational field. Experiments included direct observation of the agglomeration of submicron alumina and indirect observation, using small angle light scattering, of the agglomeration of colloidal silica and aluminum monohydroxide. In the former class of experiments, the powders were constrained to move on a two-dimensional surface oriented to minimize the effect of gravity. In the latter, some experiments involved mixture of suspensions containing particles of opposite charge which resulted in agglomeration on a very short time scale relative to settling under gravity.

INTRODUCTION

The subject of the research program supported by this grant was powder agglomeration. The behavior of powder suspensions is one aspect of ceramic processing which is strongly influenced by gravity. In particular there is a strong coupling between agglomeration and settling under gravity. The extent of settling is determined by the competition between diffusion (Brownian motion) and convection due to gravity (Stoke's settling). The flux of particles towards, j (#/m^2-s) the bottom of the container may be written as

$$j = -D\,\partial c/\partial x + vc \qquad (1)$$

where D is the translational Brownian diffusion coefficient (m^2/s), c is the concentration of particles (#/m^3), x is position measured relative to the upper surface of the suspension (m), and v is the Stoke's settling velocity (m/s). At steady state the concentration of particles as a function of position for a suspension containing M particles per m^3 in a container of height h (m) is given by

$$c = B \exp(vx/D) \qquad (2)$$

where B is a constant which depends on the experimental conditions and may be written

$$B = vM/[DA(\exp(vh/D)-1)] \qquad (3).$$

It is readily seen by inspection that the degree of segregation of particles is determined by the ratio of v/D. For very small values of v/D, Eqn. 3 yields B=M/A and Eqn. 2 yields c=B. Therefore the value of c becomes independent of position and equal to the original concentration, i.e. no segregation occurs. On the contrary, as the ratio v/D becomes increasingly larger more of the particles tend to collect near the bottom of the container.

Since Stoke's velocity can be written

$$v = B' r^2 \qquad (4)$$

where r is the hydrodynamic radius of the particle and B' is a constant given by

$$B' = (\rho_s-\rho_l)g/(18\pi\eta) \qquad (5)$$

where ρ_s and ρ_l are the densities of the solid and liquid respectively (kg/m^3), g is the gravitational constant (9.8 m/s^2) and η is the viscosity of the liquid (). The Brownian motion diffusion coefficient can be written

$$D = B''/r \qquad (6)$$

where B", another constant is given by

$$B'' = kT/(8\pi\eta) \qquad (7)$$

where kT is the product of Boltzmann's constant () and absolute temperature (K). It is evident for the the ratio of Eqn. 4 to 5

$$v/D = (B'/B'')\, r \qquad (8)$$

that the tendency for particle segregation decreases with decreasing particle size. A suspension consisting of dispersed and very finely divided particles will tend to be very homogeneous and only weakly affected by gravity. A system undergoing agglomeration, however, loses this stability.

The process of agglomeration is the accretion of particles into increasingly larger flow units. As long as the applied shear field field is kept low, these behave as

"particles" with an effective density which is intermediate between that of the fluid an the solid and a large hydrodynamic radius. The former tends to decrease the magnitude of B", but the effect is slight and the ratio v/D tends to increase in a nearly linear fashion as r increases. The consequence is that inducing agglomeration results in very rapid settling. This generally regarded as a technical problem in the processing of ceramics. Indeed it also hampers the scientific investigation of an agglomeration process(es).

Recently there has been revived interest in understanding the processes which are important in the aggregation of colloids. This is driven by a combination of scientific and technical achievements. Firstly, the production of colloidal ceramic powders has been greatly developed. Very fine powders are now routinely produced using such methods as precipitation, aerosol decomposition, sol-gel, and flame spraying. Controlling the colloidal stability of these powders requires an increased understanding of the important forces on the particles. Secondly, the technical tools which are currently available (small angle light scattering, small angle x-ray scattering, and advanced electron microscopy) provide information about the structure of aggregates which was previously very difficult to obtain. This, coupled with the now popular fractal description of irregular structures, has allow a more rigorous comparison between model and experiment. Lastly, the widespread availability of powerful computational facilities has allowed numerical models to be developed which are much more sophisticated.

The research program funded under NASA grant NAG3-755 addressed involved the development of both numerical models and two qualitatively different experimental approaches. Research personnel fully or partially supported were: J. D. Cawley, P.I.; J. F. Dirkse; J. L. LaRosa, K. Langguth, J. Marra and Y. H. Rim. Both K. Langguth and J. Marra left the University after a relatively short time; neither received a degree. Both J. F. Dirkse and J. L. LaRosa successfully completed M.S. degree programs.Copies of their respective theses have been supplied to the grant monitor, Dennis Fox (NASA Lewis). Dr. Y. H. Rim was a post-doctoral researcher who was partially supported by this grant during his 1 1/4 year stay at Ohio State University.

J. L. LaRosa's research program focussed on the development of a method for directly observing the agglomeration of 0.4 μm aluminum oxide particles using optical microscopy. Two important aspects of this work were that this experiment allowed a critical test of the assumptions employed in subsequent, as well as prior, numerical models and it also provided an excellent set of data to test the appropriateness of using fractal geometry to describe the aggregate of commercial ceramic powders. The experiments of both Langguth and Marra contributed to the development of the experimental procedure employed by LaRosa.

J. F. Dirske's thesis research focussed on the development of numerical models for simulating the aggregation process. Two standard approaches were pursued; the Monte Carlo method and "Molecular" Dynamics. In the latter method particles, rather than molecules were the basic flow units, however it would be inappropriate to refer to our approach as Brownian Dynamics since we modeled the case in which convection (due to, for example, gravity) dominates the process. Two different processes were investigated in detail. These were agglomeration during settling and rearrangement of particles in contact with a container wall and under a strong gravitational field.

The research of Y. H. Rim was a collaborative program, carried out with R. Ansari and W. V. Meyer of NASA Lewis, and directed at the use of light scattering to measure the characteristics of very finely divided colloidal suspensions during the agglomeration process. In the experiments, agglomeration was induced by one of two methods. In one set of experiments the pH of the suspension was adjusted such that the particles were uncharged and agglomeration results from short range van der Waals forces. In the other type of experiment two suspensions were mixed; one containing positively charged particles and the other containing negatively charged particles. Since the suspensions were maintained at low ionic strength, agglomeration resulted from long range electrostatic forces. Thus, these experiments correspond to physical realizations of the two limiting cases of computer models; purely diffusive and purely convective.

The seven reprints of research fully or partially supported under this grant are presented in chronological order:

J. D. Cawley, "Two Dimensional Agglomeration of Al2O3," pp. 52-54 in Materials Research Society EA-13, Fractal Aspects of Materials: Disordered Systems, Edited by A. J. Hurd, D. A. Weitz, and B. B. Mandelbrot, 1987.

J. D. Cawley, "Two Dimensional Agglomeration of Ceramic Powders," pp. 155-157 in Materials Research Society EA-17, Fractal Aspects of Materials: Disordered Systems, Edited by D. A. Weitz, L. M. Sander, and B. B. Mandelbrot, 1988.

J. D. Cawley, J. LaRosa, and J. F. Dirkse, "Agglomeration of Ceramic Powders,"pp. 185-197 in LLS/ATD 1988 Workshop Proceedings, Edited by W. V Meyer, NASA Conference Publication 10033, 1989,.

Y. H. Rim, J. D. Cawley, W. V. Meyer, and R. Ansari, "In-Situ Light Scattering Study of Agglomeration," pp. 54-65 in Ceramic Transactions vol. 26: Forming Science and Technology, Edited by M. Cima, American Ceramic Society, Columbus OH (1992)

J. L. LaRosa and J. D. Cawley, "Fractal Dimension of Alumina Aggregates Grown in Two Dimensions," Journal of the American Ceramic Society, 75 [7] 1-6 (1992).

J. F. Dirkse and J. D. Cawley, "A Modified Ballistic Aggregation Process," submitted to the Journal of Colloid and Interface Science.

J. F. Dirkse and J. D. Cawley, "Numerical Simulation of Particle Rearrangement Within an Agglomerate During Settling Under Gravity," submitted to the Journal of the American Ceramic Society.

Reprints

TWO DIMENSIONAL AGGLOMERATION OF Al_2O_3

J. D. CAWLEY
Department of Ceramic Engineering, Ohio State University, 2041 College Road, Columbus OH, 43210

INTRODUCTION

In many situations particle agglomeration takes place within environments that experience substantial convection, e.g. thermophoretic deposition, stirred colloidal suspensions, and smoke formation. It is therefore of interest to understand the role of convection in determining the collision probability between particles and clusters of particles. The examination of real time video taped movies of the agglomeration of Al_2O_3 particles constrained to two dimensions suggests that the situation is more complicated than a simple random rain model.

The video tapes also provide information on rearrangement processes during agglomerate growth.

EXPERIMENTAL PROCEDURE

Low volume fraction, between 0.01 and 0.03%, suspensions of either 0.4 or 4.0 μm Al_2O_3 particles were prepared. Drops of these suspensions were placed in a hole on an aluminum microscope slide and observed using a inverted optical microscope focused on the lower side of the droplet. Due to the low volume fraction, the particles had a very low collision probability in the bulk and settled to the surface almost entirely as singlets. In several experiments the air striking the fluid surface produced a particle drift and allowed the effect of convection on the agglomeration process to be observed.

RESULTS

The agglomerates observed for 0.4 μm Al_2O_3 at a pH~8 (the pzc for Al_2O_3) bear a strong resemblance to computer generated agglomerates using the cluster-cluster aggregation model, as is apparent is this image digitized from a video tape.

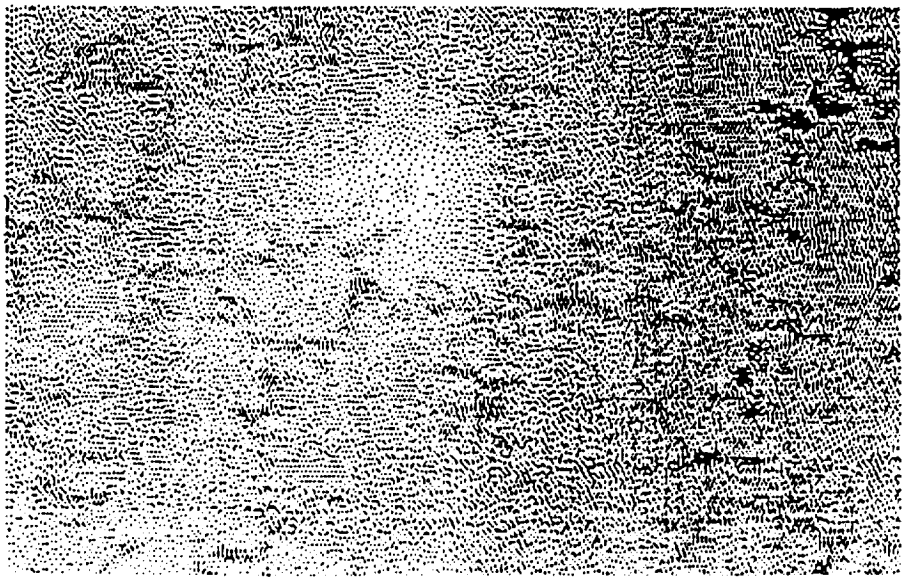

The effect of convection is seen in the deposition of small agglomerates, 10 - 25 particles, onto a large immobile agglomerate of several thousand particles. The sketchs below are tracings of digitized images from a video tape where the microscope was focused on the tip of a dendrite extending nearly to the center of the drop. The arrows indicate the direction of particle drift in the free stream to the left of the observed area. The time interval between images 1-3 is roughly 12 seconds, and between images 3-6 is 20 seconds.

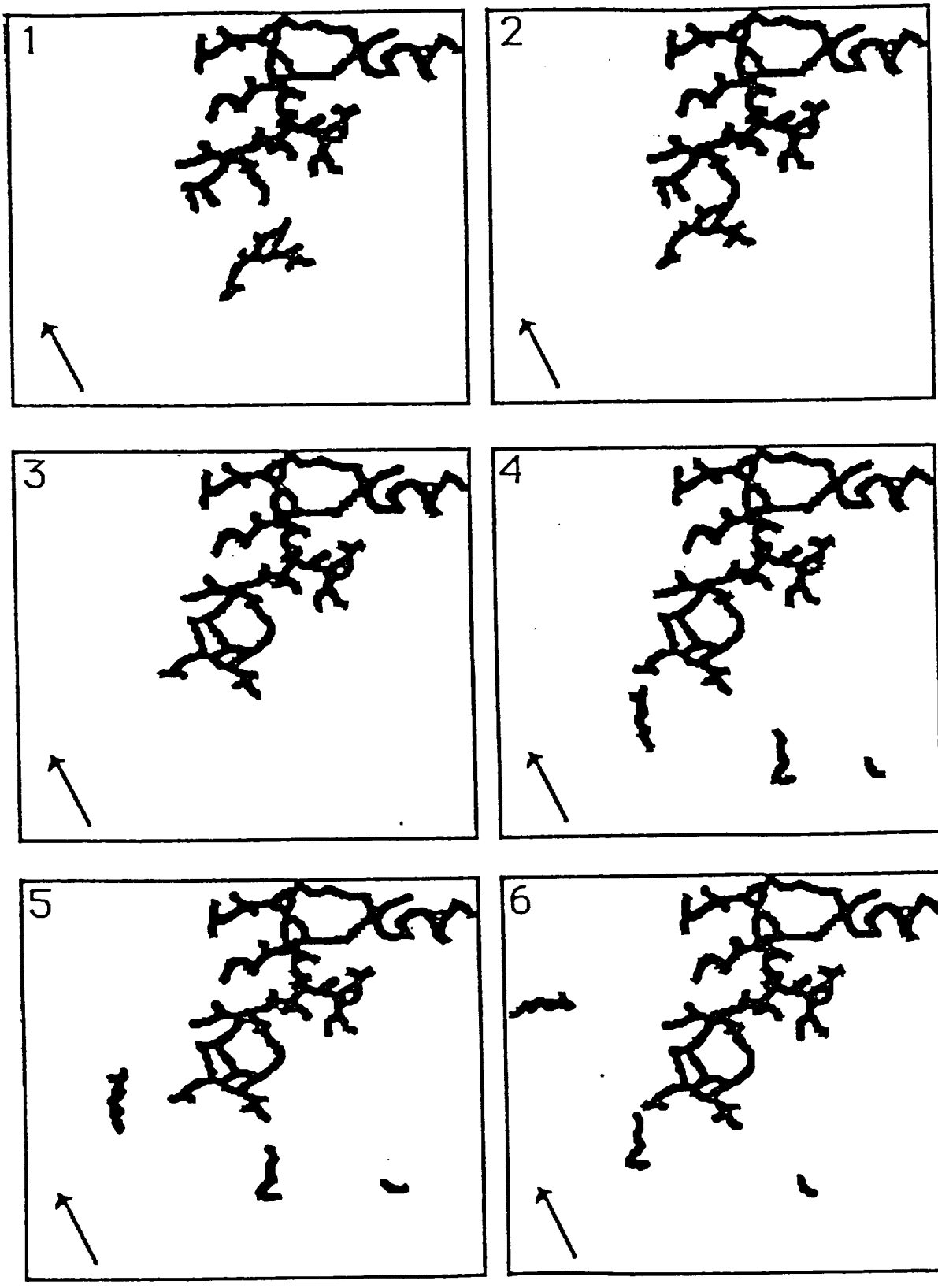

The area on the right in the images is a 'bay' along the edge of the large immobile agglomerate. The fluid flow in this region is impeded by the dendrite arm along the top of the images which acts as a 'reef'. The sequence 1-3 shows the motion of an agglomerate of roughly 25 particles. The agglomerate attempts to follow motion of the fluid around the tip of the dendrite. However it is sufficiently massive that it strikes the dendrite near the tip and becomes attached. Note that it continues to move via rotation until it becomes attached it two locations. The sequence 4-6 shows that less massive agglomerates, less than 10 particles, are able to follow the fluid around the tip. These sequences suggest that:

a) the magnitude of convection is dependent on the local geometry (single particles deep within the bay display only Brownian motion while those near the surface show significant drift);

b) the role of convective transport varies for different sized agglomerates and is probably more important for cluster-cluster aggregation;

c) it appears that convection can lead to preferential growth near the tips of dendrites, thus convectively driven agglomeration may give rise to mass fractals.

Observations on restructuring indicate that:

a) restructuring occurs through deformation of dendrite arms rather than single particle dettachment and re-attachment;

b) restructuring is more prevalent with 4.0 μm particles than with 0.4 μm particles, it appears that the van der Waals attraction between adjacent dendrites of 4.0 μm particles can induce collapse;

c) preliminary results suggest that restructuring may be sensitive to pH.

The use of Brownian dynamics calculations to model a mixed convection/diffusion system is being investigated.

Two Dimensional Agglomeration of Ceramic Powders

J. D. Cawley, Department of Ceramic Engineering, 2041 College Road, Columbus OH 43210

INTRODUCTION: DLA simulations have been used to study the competitive growth of clusters on a two dimensional surface. A region of a square lattice is defined (typically a square or circle region) and a given number of the sites are populated and considered fixed. A single mobile particle is allowed to randomly occupy any unoccupied site. This particle is allowed to execute an off lattice random walk until its center is within a lattice site adjacent to an occupied site. At this point it is fixed and a further mobile particle is introduced. This model contains many of the essential attributes of the agglomeration of particles in a two dimensional experiment in which particles settle to, and are mobile on, the lower surface of a dilute suspension [1]. It may also represent the growth of thin film on the surface of a substrate by condensation from a vapor.

EXPERIMENTS: Three types of simulations were performed. In the first a 200x200 square lattice was initially populated with 10 fixed particles. The top and bottom of the square were subjected to periodic boundary conditions, while the left and right were treated as impermeable surfaces, but did not trap random walkers. Random walkers were randomly added and clusters were allowed to grow until a left to right percolation path was created. The results of this experiment is shown in figure 1. In the initial phase of the experiment lacy clusters (that have a visual appearance consistent with fractals) form and grow such that they tend to fill the tessellation. As they approach one another they tend to densify rather that link together. This is a direct consequence of the fact that the random walker has a higher probability of entering the system in between adjacent dendrite arms on a single cluster than in the small area left between neighboring clusters. When percolation does occur the filled fraction of the lattice is ϕ_c=18,344/40,000 = 0.4586 in striking agreement with the value of 0.45 for percolation in 2-D by random population of sites[2].

The second experiment was designed to test whether the clusters which grow in this competitive situation are indeed fractal. This experiment involved seeding the center of a circular region in a square lattice with a single particle and introducing random walkers at random within the circle. To make the circular region equivalent to the cell surrounding each agglomerate in the first experiment the boundary was treated as impermeable. Four stages of growth are illustrated in figure 2, along with a standard log-log plot of number versus radius of the sampling interval. The cluster is clearly not fractal. The amount of mass near the periphery is substantially in excess of the expectation for a fractal. This is manifest as a bump in the log-log plot between values of 4 and 4.5 on the horizontal axis. It is interesting to note that clusters occurring when sputter depositing films of Nd_3Ge onto a quartz substrate show precisely the same deviation from fractal behavior[3]. This results from the geometric situation that the most probable location for the random walker to be introduced (or the most area available for a sputtered atom to be adsorbed) is the large openings between the dendrite tips. The magnitude of the discrepancy decreases as the cell fills, finally converging to a straight line with a slope of 2 upon complete filling.

The third experiment was a simple simulation on a 200x200 square lattice identical to the first except one edge was completely seeded and a single seed placed in the center with respect to the horizontal axis and 50 lattices away from the seeded edge. The left and right boundaries are periodic and the bottom is impermeable. The result, illustrated in figure 3, presents another manifestation of the consequence of competitive growth. The isolated cluster grow away from the seeded edge and its presence inhibits effectively screens the center of the seeded edge. The result of this is that the growth from the wall begins to surround the isolated cluster and a clearly defined region devoid of particles prevents them from linking together. This is commonly observed in the formation of frost (condensed from the air) on a window pane (a substrate) as illustrated in figure 3 b.

CONCLUSIONS: Competitive growth of DLA clusters give rise to nonfractal structures and can explain the development of some patterns in the formation of thin films on substrates.

REFERENCES

1. J. D. Cawley, "Two Dimensional Agglomeration of Alumina," MRS Extended Abstracts, Fractal Aspects of Materials: Disordered Systems, A. J. Hurd, D. A. Weitz, B. B. Mandelbrot, Eds., 1987.
2. R. Zallen, The Physics of Amorphous Solids, (John Wiley and Sons, 1983) p. 191.
3. S. A. Wolf, W. T. Elam, J. Sprauge, D. U. Gubster, D. van Vechten, and P. Meakin, "Sputter Deposited Fractal Aggregates," MRS Extended Abstracts, Fractal Aspects of Materials: Metal and Catalyst Surfaces, Powders and Aggregates, B. B. Mandelbrot and D. E. Passoja, Eds. 1984.
4. W. A. Bentley and W. J. Humphreys, Snow Crystals, (Dover Publications, Inc, 1962), p.218.

PRECEDING PAGE BLANK NOT FILMED

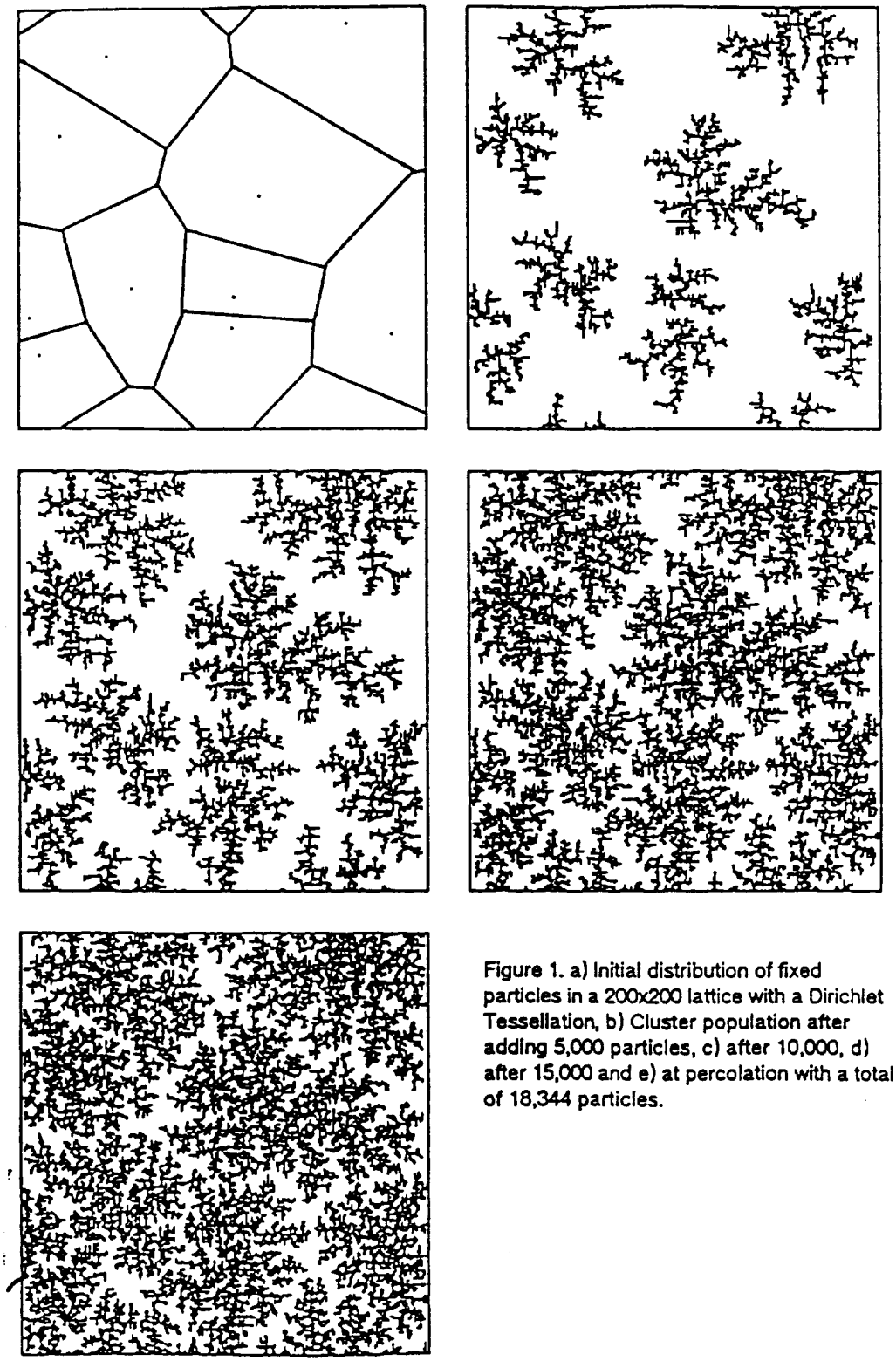

Figure 1. a) Initial distribution of fixed particles in a 200x200 lattice with a Dirichlet Tessellation, b) Cluster population after adding 5,000 particles, c) after 10,000, d) after 15,000 and e) at percolation with a total of 18,344 particles.

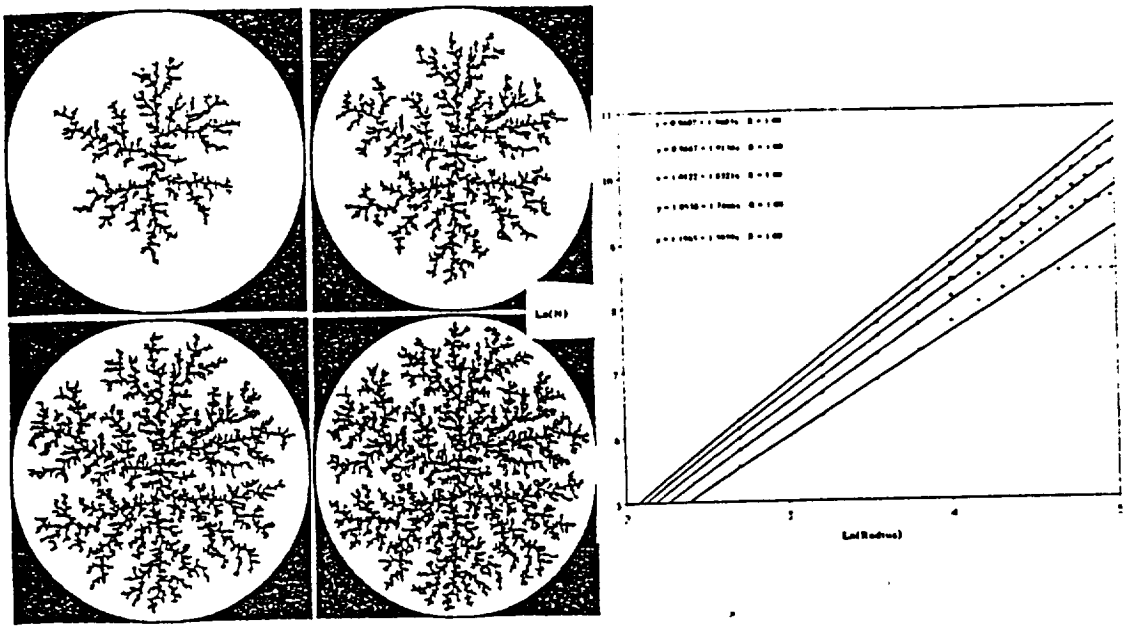

Figure 2. DLA agglomerates grown in a circular region bounded by an impermeable surface. The four illustrations represent clusters of: 5,000; 10,000; 15,000; and 20,000, respectively. The curves represent data taken on agglomerates of: 5,000; 15,000; 25,000; 35,000; 45,000 particles. Best fits to the first four data points on each data set produced the straight lines on the figures and apparent fractal dimensions appear as the coefficients on x in the upper left hand corner.

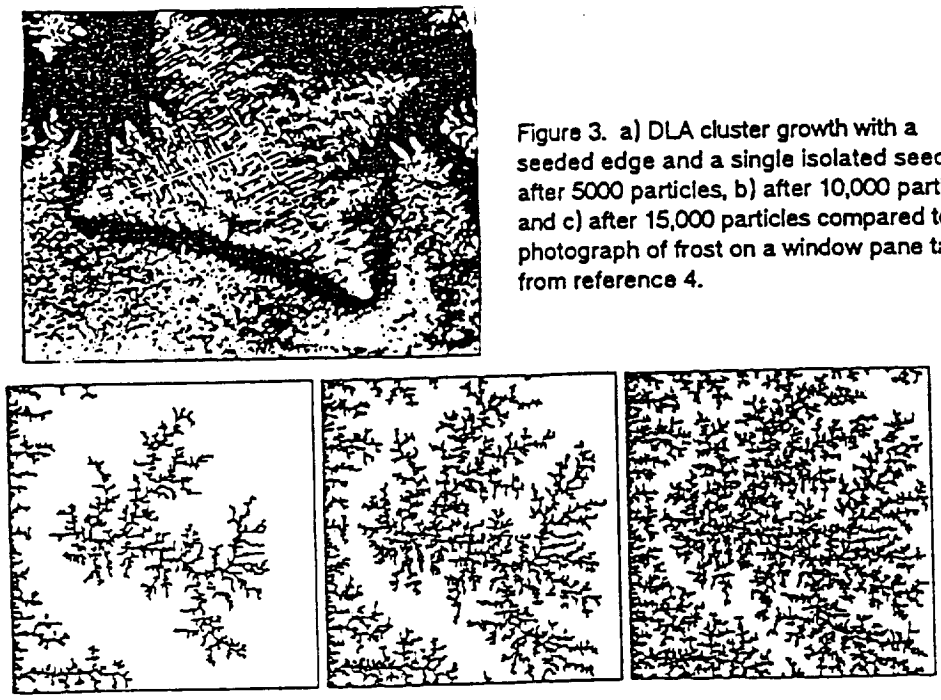

Figure 3. a) DLA cluster growth with a seeded edge and a single isolated seed after 5000 particles, b) after 10,000 particles and c) after 15,000 particles compared to a photograph of frost on a window pane taken from reference 4.

AGGLOMERATION OF CERAMIC POWDERS

James D. Cawley, Judith LaRosa, and Fredrick Dirkse
Department of Ceramic Engineering
The Ohio State University
Columbus, Ohio

A research program directed at a critical comparison of numerical models for powder agglomeration with experimental observations is currently underway. Central to this program is the quantitative characterization of the distribution of mass within an agglomerate as a function of time. Current experiments are designed to restrict agglomeration to a surface, which is oriented perpendicular to the force of gravity. These experiments are discussed with reference to: their significance to ceramic processing; artifacts which may be avoided in microgravity experiments; and the comparison of information available in real space (from optical microscopy) to that in reciprocal space (from light scattering). The principal machine requirement appears to be a need to obtain information at small scattering angles.

Introduction

In general, ceramic processing is a powder technology in which powders are manufactured, formed into a compact, and consolidated through heat treatment. Although the final piece may have the same chemical composition as the starting powders, it is often the case that a mechanical mixture of different powders is used which undergo a desired chemical reaction during the heat treatment.

Control of the state of agglomeration is important for technological reasons[1]. Agglomerates are necessary for many conventional forming operations such as dry pressing, slip casting, and plastic forming. However, the residual porosity in a fired ceramic, which can strongly affect the optical, thermal, and mechanical properties of the material, is an artifact of the porosity in the green body. This is intimately related to the packing of the primary particles within the agglomerate and the packing of the agglomerates to form the compact. Frequently, it is desired to crush agglomerates in the latter stages of powder compaction in order to achieve high packing densities. Clearly, the control of the agglomerate population is an important process control variable, and successful control implies the ability to quantify agglomerate characteristics in a meaningful way.

PRECEDING PAGE BLANK NOT FILMED

It has long been realized that a quantitative characterization of the agglomerate geometry is important to a complete understanding of colloidal suspensions. For example, Michaels and Bolger[2] quantitatively characterize agglomerate structure through a term C_{ap} which is the reciprocal of the solids packing density within the agglomerate. Firth[3] and Firth and Hunter[4] have shown C_{ap} to be an important parameter in describing the rheology of agglomerated colloidal suspensions.

Beginning with the seminal work of Forrest and Witten[5] on the structure of agglomerates of metallic smoke particles, it has been realized that many agglomerates are fractals. In a fractal agglomerate, the average packing density of the agglomerate decreases as it grows, so that within an agglomerate, the density is a maximum at the center of the agglomerate and drops off as a power law when increasingly larger volumes are considered, i.e. for a three dimensional system,

$$\rho = \beta \cdot r^{(D-3)} \qquad \text{Eqn-1}$$

where ρ is the density of solids within a sphere of radius r around the agglomerate's center of mass, β is a geometrical constant, and D is defined as the fractal dimension. A significant feature of fractal growth is that both β and D are constants which do not depend on variables such as time available for agglomeration.

The objective of the research currently underway is to examine the effects of process variables on the structure of agglomerates. The approach is to follow the evolution of the agglomerate on the scale of the individual particles. The process variables are viewed in terms of the forces resolved on the particles. For example: alterations in the electrolyte chemistry change the magnitude (and sometimes the sign) of interparticle forces; mixing introduces shear forces; the presence of a suspension medium gives rise to both Brownian motion, or stochastic force, as well as hydrodynamic forces; and the presence of gravity adds a systematic force. The influence of these process variables is being studied principally through the effect each has on the geometry of resultant agglomerates. This is quantified following a fractal approach. Numerical simulations, both Monte Carlo and Molecular Dynamics, are being investigated in addition to experimentation. The results of the simulations will not be discussed here except for their role in guiding experimentation.

Monte Carlo simulations have shown that (in the absence of rearrangement within the agglomerate) interparticle forces do not have a significant effect on the distribution of mass within the agglomerate. As a result, experiments are currently being restricted to agglomeration at the zero point of charge, i.e. when the only significant contribution to the interparticle force is van der Waals attraction. The importance of Brownian motion, or random walk particle trajectories, has been clearly established by the numerical simulation of Witten and Sander[6] and the large body of work which has followed, notably that of Meakin[7]. The current research focus is the role of hydrodynamic forces, principally how collision probabilities depend on fluid flow around and through existing agglomerates. The effect of gravity is being examined to determine how it complicates experimentation.

The most obvious complication introduced by the existence of gravity is that particles initially suspended in a liquid medium will settle to the bottom of the container. Further, larger agglomerates settle more rapidly. Although the density of fractal agglomerates decreases with increasing size, the settling rate increases since it also depends on size to the second power. Thus, experiments in three dimensions are subject to agglomerate collisions due to relative velocities between agglomerates (that are not typically included in numerical models). The typical densities associated with ceramics, 3.0 - 4.0 g/cm^3, make it impractical to restrict experimentation to particles sufficiently small to avoid settling. For this reason, ground based experimentation is currently being restricted to two dimensions.

Experimentation

The experimental arrangement is very straightforward and is based on the work of Onoda[8]. A small hole is drilled through an aluminum slide, and a drop of a very dilute ceramic powder suspension is placed in this hole and is supported by surface tension. The powder particles settle under the influence of gravity to the lower surface. Since the particle concentration in the volume in low, virtually all of the particles settle to the lower interface without experiencing a collision. Once settled, the particles are constrained to move on a surface and agglomeration occurs. A schematic of the experiment in shown in figure 1. The upper portion of the figure illustrates the physical arrangement, and the lower portion shows the distribution of particles within the drop once agglomeration has started. Typical conditions are the following: 0.4 μm Al_2O_3 powder (3.96 g/cm^3) at 0.001 volume percent; pH = 8.2; 4 mm hole in a 2 mm thickness. The agglomeration process has been observed in real time using optical microscopy (focussed on the lower surface of the drop) and is currently being approached using static light scattering.

It is useful to analyze how this experimental arrangement is similar to and differs from the situation being modeled in either Diffusion Limited Aggregation[6] or Cluster Cluster Aggregation[9,10]. The standard DLA algorithm is executed within a lattice (typically a square lattice) which is seeded at the center. Subsequent particles are added randomly along an approximate circle which is far away from the growing agglomerate. The only path by which a particle may be incorporated into the agglomerate is by a random walk from the region outside the agglomerate. In the case of CCA, the lattice is initially populated with a given number of particles which are then allowed to undergo simultaneous random walks. The number of particles in the system is not a function of time. Neither situation completely describes the experiments.

In the initial stage of the experiment, the number of particles per unit area is low, and the growth of agglomerates appears to take place independently, resulting in structures reminiscent of DLA. At later stages these agglomerates collide and link to form large structures like those predicted by CCA (however agglomerates appear to collide as a result of drift rather than Brownian motion). The early stage in not truly DLA for two reasons: one is that neighboring agglomerates compete for particle additions; the other is because there exists a finite probability that particles can settle to the

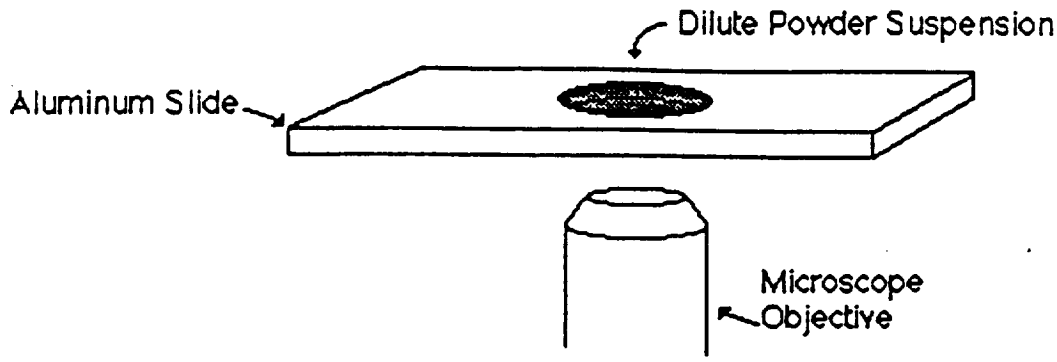

Figure 1a. Schematic illustration of the experimental arrangement for observing agglomeration on the lower surface of a drop.

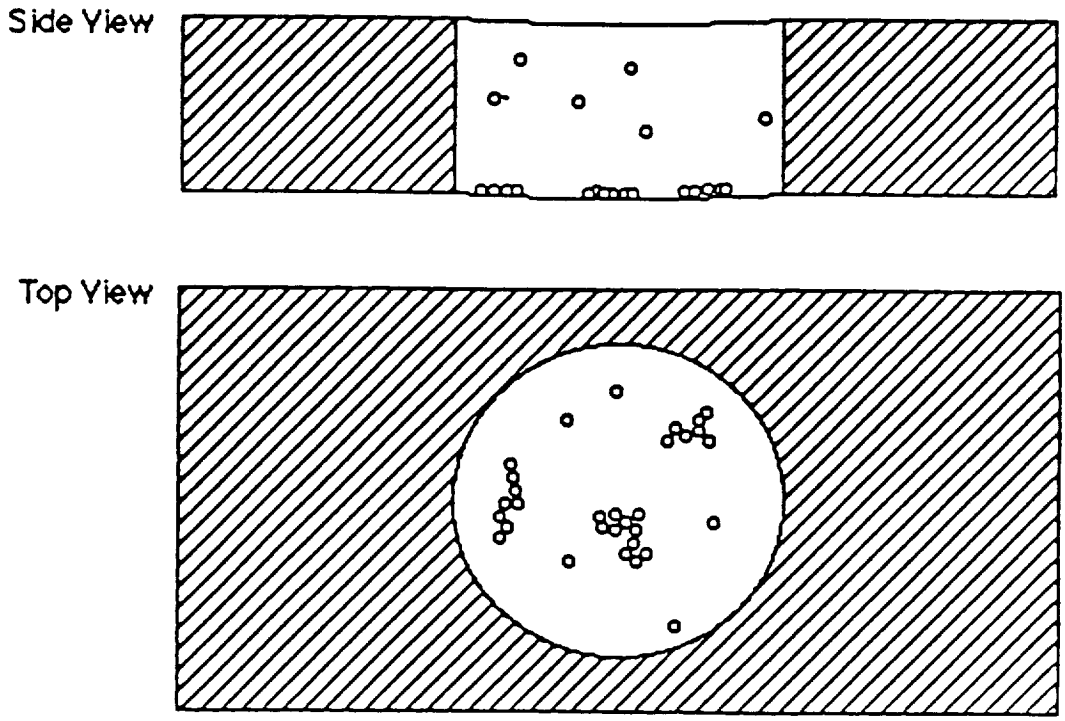

Figure 1b. Schematic illustration of the distribution of particles within the drop. Particles within the volume of the drop rarely collide and agglomeration is restricted to the lower surface of the drop.

interface such that they arrive in the plane within the interior of the agglomerate. The first effect biases the growth of agglomerates away from neighboring agglomerates. The second gives rise to agglomerates which have densities greater than what is predicted by DLA. This second effect also allows the interior of rings (commonly occurring in CCA) to be filled. The end result of these experiments is typically a plane filling structure, i.e. D = 2. Thus, in these experiments a fractal dimension (if at all appropriate) is not truly a constant since it appears to be time dependent. A time sequence of agglomerates* of 0.4μm Al_2O_3 at a pH of 8.2 which illustrates the time dependence of the particle number density is shown in figure 2.

These effects can be seen in two Monte Carlo simulations which are distinguished from simple DLA because particle additions are allowed to occur within any unoccupied lattice site to simulate particles settling from above. In the first simulation, a 200x200 square lattice was initially populated with 10 fixed particles. The rationale for using a set of fixed nucleation sites is that in the experiments, several clusters will simultaneously form on the lower surface of the drop. After some time, these will become sufficiently large to be regarded as immobile relative to the singlets. The cluster population which grows from the fixed nucleation sites will mimic this set. The top and bottom of the square were subjected to periodic boundary conditions while the left and right were treated as impermeable surfaces that did not trap random walkers. Random walkers were randomly added, and clusters were allowed to grow until a left to right percolation path was created. The results of this experiment are shown in figure 3. In the initial phase of the experiment, ramified clusters (that have a visual appearance consistent with fractals) grew with a tendency to fill the tessellation. As they approached one another they tended to densify rather than link together. This is a direct consequence of the fact that the random walker has a higher probability of entering the system in between adjacent dendrite arms on a single cluster than in the small area left between neighboring clusters. When percolation does occur, the filled fraction of the lattice is ϕ_c=18,344/40,000 = 0.4586 in striking agreement with the value of 0.45 for percolation in two dimensions by random population of sites[11].

The second simulation was designed to test whether the clusters which grow in this competitive situation are indeed fractal. In order to maximize statistics, the growth of a single agglomerate in a single "cell" was monitored. This experiment involved seeding the center of a circular region in a square lattice with a single particle and introducing random walkers at random within the circle. To make the circular region equivalent to the cell surrounding each agglomerate in the first experiment, the boundary was treated as impermeable. Four stages of growth are illustrated in figure 4 along with a standard log-log plot of number versus radius of the sampling interval. Although a typical ramified cluster was formed, it is clearly not fractal. The amount of mass near the periphery is substantially in excess of the expectation for a fractal as evidenced by the bump in the log-log plot between values of 4 and 4.5 on the horizontal axis. Again this is a purely geometrical result. The most probable location for the random walker to be introduced is the large openings between the dendrite tips. This is equivalent to particles having a higher probability of settling to the surface in regions which are

*Photo sequence taken by K. Langguth while a graduate student at OSU.

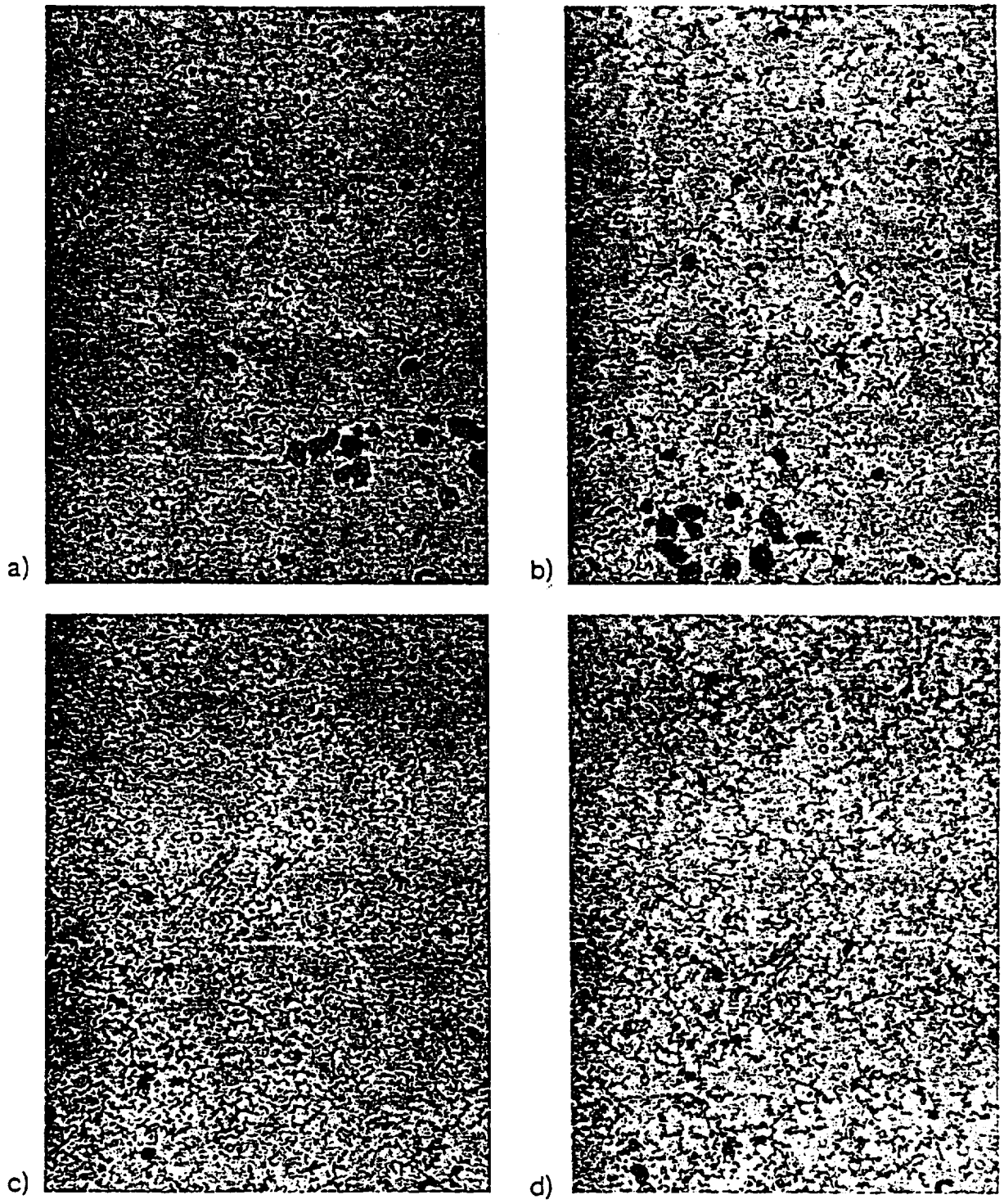

Figure 2. Optical photomicrographs of the lower surface of a 0.003 % suspension of Al_2O_3 after a) 7.5 min., b) 11 min., c) 15.5 min., d) 20 min. Both the increase in the number density of particles as a function of time and the two dimensional character of the agglomerates are clearly evident. The small particles in the image are nominally 0.4 μm and the large are 4.0 μm.

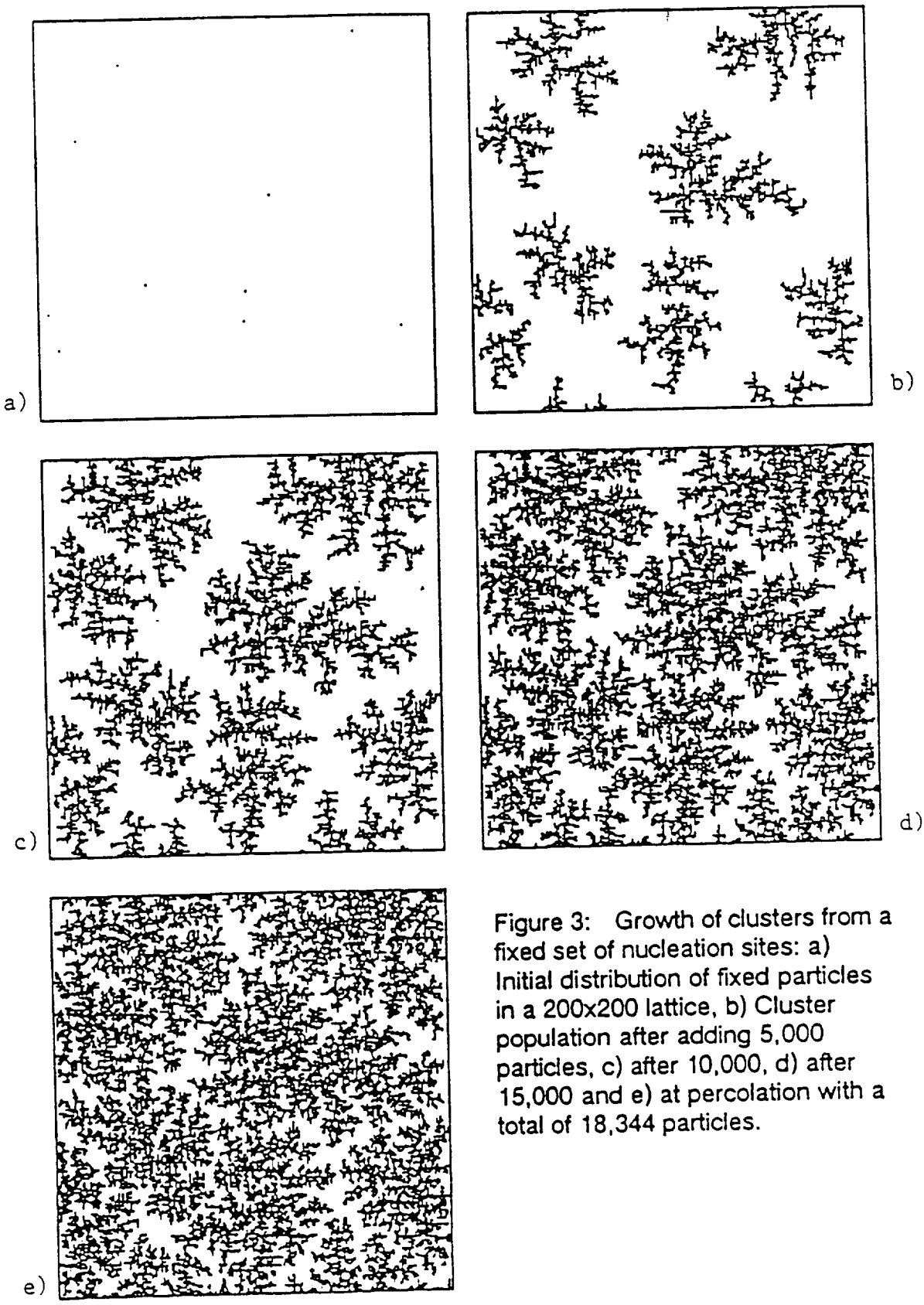

Figure 3: Growth of clusters from a fixed set of nucleation sites: a) Initial distribution of fixed particles in a 200x200 lattice, b) Cluster population after adding 5,000 particles, c) after 10,000, d) after 15,000 and e) at percolation with a total of 18,344 particles.

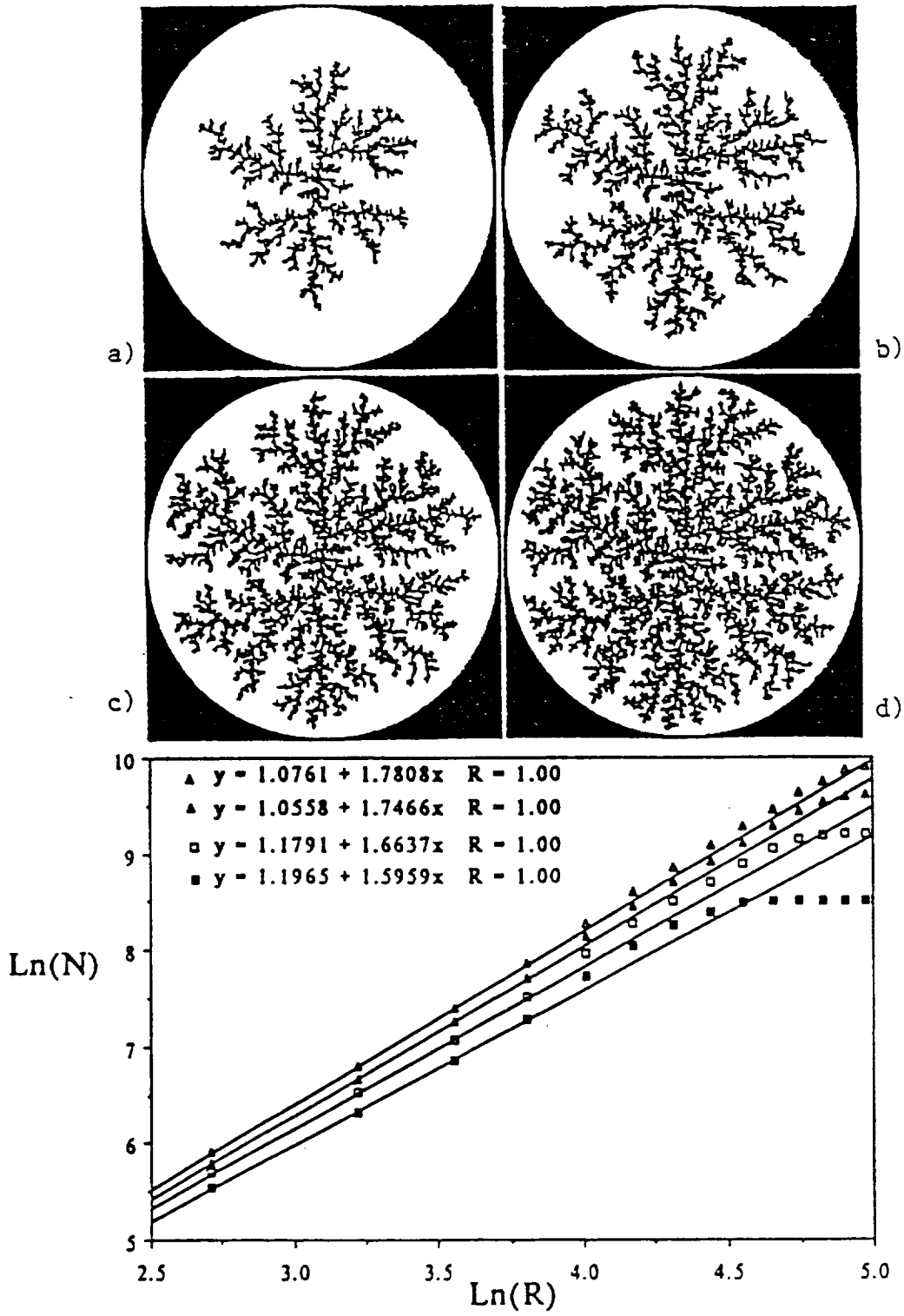

Figure 4: Modified DLA simulation in which particles are added at random to any unoccupied site. The upper portion of the figure shows the evolution of the agglomerate after: a) 5,000; b) 10,000; c) 15,000; and d) 20,000 particle additions. The lower portion of the figure is log-log plots which clearly indicate that the resultant structures are not fractal.

sparsely populated. The magnitude of the discrepancy decreases as the cell fills, finally converging to a straight line with a slope of 2 upon complete filling.

Experimental confirmation of this result is necessary. In the simulation, particles are not allowed to settle to already filled sites. This is equivalent to assuming that particles which settle onto the top of a second particle stick to the top and therefore never arrive in the plane of observation. In real systems, however, particles which settle on top of another may rotate into the plane. This would increase the rate of filling near the center of the agglomerate and might compensate for the mass accumulation near the tips and restore the agglomerate to fractal status.

The only experimental results which have been quantified resulted from agglomeration of 0.4 μm Al_2O_3 in a mildly convective environment (Peclet number on the order of 10). In this situation, small agglomerates are driven together by convection in the liquid and lead to structures reminiscent of CCA agglomerates. A tracing of a large agglomerate, which formed 22.5 minutes into the experiment, is shown in figure 5 along with its log-log plot of number of particles within circles of systematically varied radii. It can be seen that apart from a transient near the agglomerate center, it is well described by a fractal dimension of 1.54 which is in good agreement with CCA simulation. Further quantification is underway to determine precisely the degree to which the agglomerates resulting from this geometrical set-up are fractal, and in particular, the role of convection is being examined.

Application of Light Scattering and Optical Fourier Transforms

Our experiments will be restricted to the use of static light scattering. The analysis of total intensity versus scattering angle has been used in the determination of fractal dimensions of agglomerates imbedded in both two dimensional [12] and three dimensional space [13]. Earth based experimentation will initially be restricted to the analysis of two dimensional agglomerates using the experimental set-up pictured in figure 6. This represents a sample cell which has been designed to fit into the NASA Lewis Laser Light Scattering Facility. Two principal features of this design should be noted: first, the path of the laser beam is modified by the presence of the prism such that it will probe the sample perpendicular to the plane on which agglomeration takes place; secondly, a charge coupled device video camera will be used as a two dimensional array detector allowing the simultaneous collection of data over a range of scattering vectors.

The signal that results from the ground based experiments is expected to be an Optical Fourier Transform of the two dimesional agglomerates which form on the lower surface of the cuvette combined with a background signal resulting from the population of singlets which remain suspended in the fluid above. Characterization of the background may be approached using a horizontal laser beam which does not sample the agglomerates. Interpretation of the signal will follow the analysis of Allain and Cloitre[12].

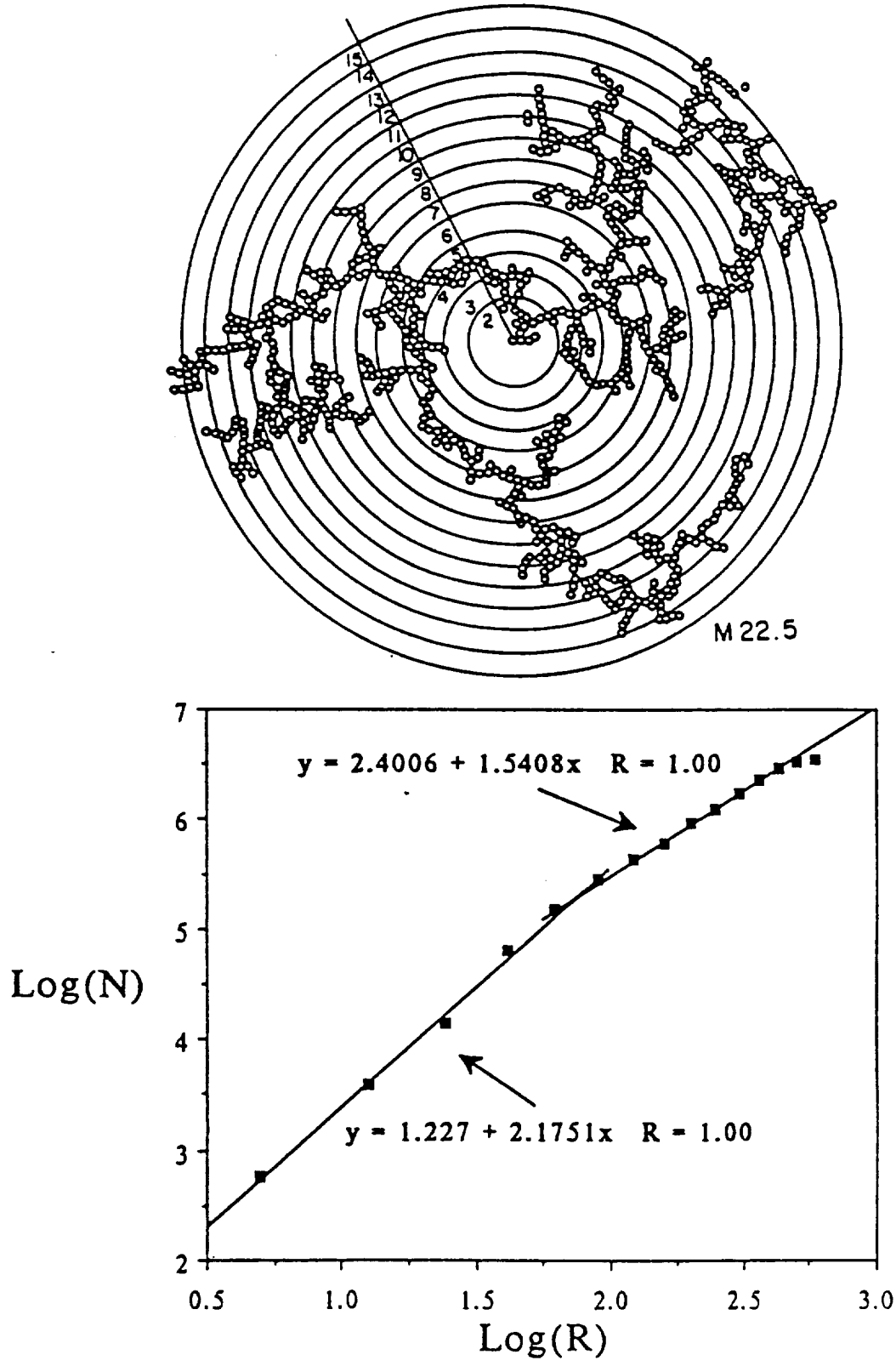

Figure 5: Tracing of an agglomerate of 0.4 μm Al_2O_3 formed on the lower surface of a drop along with a log-log plot which suggests it is fractal and has a dimension of 1.54.

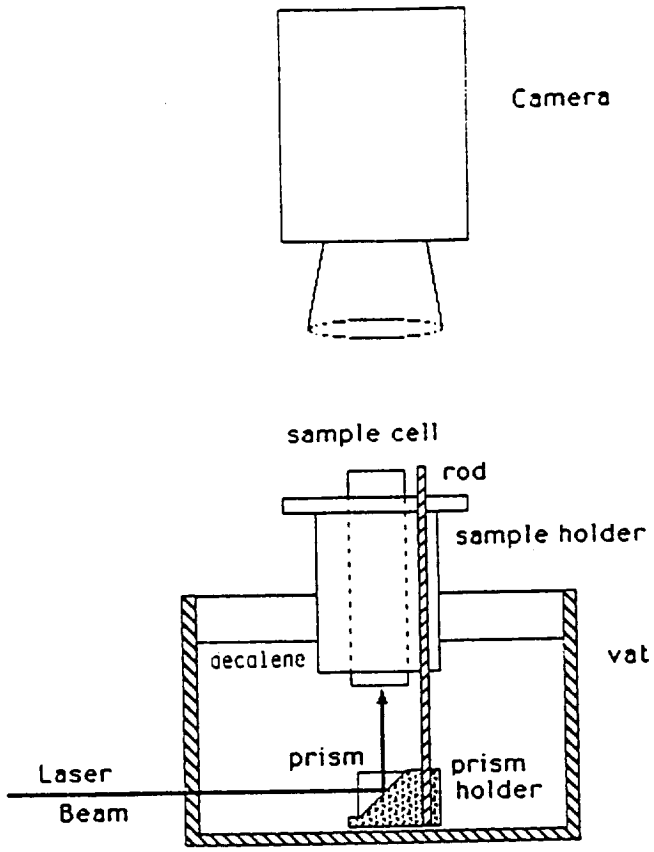

Figure 6: Schematic of the sample cell to be used in conjunction with the NASA Laser Light Scattering Facility.

The distribution of particles in the agglomerate is probed only with scattering vectors, k, which satisfy the inequalities

$$1/R_g \leq k \leq 1/a \qquad \text{Eqn-2}$$

where R_g is the radius of gyration, and a is the particle size[12]. The scattering vector is defined as

$$k = 4 \pi n \lambda^{-1} \sin(\theta/2) \qquad \text{Eqn-3.}$$

This equation may be used to define the parameters for a particular experiment. For instance, it is useful to calculate the scattering angle, θ, which satisfies the right hand inequality of Eqn-2 since only scattering from angles below this value will contain information about the agglomerate. Its value depends on the wavelength of the illuminating radiation, λ, the index of refraction of the suspension medium, n, and the particle size. The results of calculations for this upper scattering angle are presented in Table 1. These results emphasize the importance of small angle measurements. Many powders of interest in ceramic processing are on the order of 0.5 microns. Even with illumination with red light, 680 nm, the information is compressed below 17°. For

Table 1. Upper Scattering Angles Calculated for a Range of Particle Sizes Using Two Wavelengths of Radiation

Particle Size	Upper Scattering Angle λ = 680nm, n = 1.3	Upper Scattering Angle λ = 514nm, n = 1.3
0.1	50°	36°
0.2	42°	18°
0.3	28°	12°
0.4	21°	9°
0.5	17°	7°
0.6	14°	6°
0.7	12°	5°
0.8	10°	4°
0.9	9°	4°
1.0	5°	4°

the purposes of analyzing agglomerates of these relatively large particles, the maximum wavelength is preferred. Clearly, the most sensitive variable is the actual particle size, and in experiments using Fe_2O_3, this can be controlled during powder synthesis[14].

The prospect of obtaining information in both real space (using mass distribution obtained by optical microscopy) and reciprocal space (using light scattering) will provide the opportunity to make critical evaluations of the respective techniques. Such information will greatly increase the reliability of information gathered from three dimensional agglomeration experiments since obtaining real space information with the necessary spatial resolution is very difficult. For example, the consequences of polydispersity can be directly tested.

Summary

Agglomeration experiments are underway which are restricted to two dimensions in order to eliminate artifacts due to settling under the influence of gravity. Simulations of this experiment suggest that in a purely diffusive environment, this experimental set up will likely produce agglomerates which are not fractal due to competition between growing neighbors. However, the experimental data which have been collected on agglomerates grown under mild convection is consistent with interpretation as a fractal and has a dimensionality consistent with CCA. A significant advantage to the two dimensional experiments is the ability to collect information in both reciprocal space and real space.

Three dimensional agglomeration experiments are more relevant to the issues associated with ceramic processing. These experiments will require a microgravity environment to avoid both settling under gravity and thermal convection currents in the fluid. These structures will be most easily probed in reciprocal space, and information gathered from the two dimensional experiments will be of direct use in subsequent interpretation.

References

1. J. W. Halloran, "Role of Powder Agglomerates in Ceramic Processing," in Adv. in Ceramics Vol. 9, Forming of Ceramics, (American Ceramic Society, 1984)

2. A. S. Michaels and J. C. Bolger, "Sediment Height and Sedimentation Rate of Kaolinite Suspensions," Ind. Eng. Chem. Fund., 1, 153 (1962).

3. B. A. Firth, "Flow Properties of Coagulated Colloidal Suspensions, II. Experimental Properties of the Flow Curve Parameters," J. Colloid Interface Sci., 57, 257 (1976).

4. B. A. Firth and R. J. Hunter, "Flow Properties of Coagulated Colloidal Suspensions, I. Energy Dissipation in the Flow Units," J. Colloid Interface Sci., 57, 248 (1976) and "Flow Properties of Coagulated Colloidal Suspensions, III. The Elastic Floc Model," J. Colloid Interface Sci., 57, 266 (1976).

5. S. R. Forrest and T. A. Witten, "Long Range Correlations in Smoke-Particle Aggregates," J. Phys. A12, 1109 (1979).

6. T. A. Witten and L. M. Sander, "Diffusion Limited Aggregation, A Critical Phenomena," Phys. Rev. Lett. 47, 1400 (1981).

7. P. Meakin, "Diffusion-Controlled Cluster Formation in 2-6 Dimensional Space," Phys. Rev. A27, 1495 (1983).

8. G. Y. Onoda, personal communication.

9. P. Meakin, "Formation of Fractal Clusters and Networks by Irreversible Diffusion Limited Aggregation," Phys. Rev. Lett., 51, 1119 (1983).

10. M. Kolb, R. Botet, and R. Julien, "Scaling of Kinetically Growing Clusters," ibid 51, 1123 (1983).

11. Zallen, The Physics of Amorphous Solids (Wiley-Interscience1983).

12. C. Allain and M. Cloitre, "Optical Fourier Transforms of Fractals," in Fractals in Physics, L. Pietronero and E. Tosatti, Eds. (Elsevier Science Publishers 1986).

13. D. W. Schaefer, J. E. Martin. P. Wiltzius, and D. S. Cannell, "Fractal Geometry of Colloidal Aggregates," Phys. Rev. Lett. 52, 2371 (1981).

14. S. Hamada and E. Matijevic,"Ferric Hydrous Oxide Sols: IV. Preparation of Cubic Hematite Particles by Hydrolysis of Ferric Chloride in Alcohol-Water Solutions," J. Col. Inter. Sci., 84, 274 (1981).

IN-SITU LIGHT SCATTERING STUDY OF AGGREGATION

Young Hoon Rim and James D. Cawley
Department of Materials Science and Engineering, The Ohio State University, 2041 College Rd., Columbus, OH 43210-1178

Rafat R. Ansari and William V. Meyer
NASA Lewis Research Center, 21000 Brookpark Rd., Cleveland, OH 44135

ABSTRACT

The results of both static and dynamic light scattering experiments on the aggregation of colloidal particles is reported. Commercial sols of silica and aluminum monohydroxide were employed. Aggregation was induced either by increasing salt concentration of a sol or mixing sols with oppositely charged particles, i.e. mutual flocculation or heterocoagulation. The agglomeration process was characterized by determination of the mean hydrodynamic radius and fractal dimension. The results of experiments on salt induced agglomeration of silica were consistent with prior studies. Mutual flocculation results yield a fractal dimension close to that predicted from the ballistic cluster cluster aggregation model.

INTRODUCTION

The process of aggregation or the flocculation of small particles to form larger clusters and the structures that result are important technologically and scientifically. A complete characterization of aggregation involves describing the kinetics of the process as well as the geometrical distribution of particles within individual aggregates. Dynamic, or quasielastic, light scattering (DLS) and static light scattering (SLS) provide complementary information towards this goal. DLS, which measures the time dependence of intensity fluctuations in the scattered light, has proven quite useful in study of the kinetics of aggregation and in the determination of particle size distributions.[1,2] Static light scattering, in which the angular dependence of time averaged intensity is measured, provides information on the internal structure of the aggregates. Both types of scattering experiments may be performed on the same sample and in-situ during aggregation.

Recently, the aggregation of colloidal gold and silica has been extensively studied

PRECEDING PAGE BLANK NOT FILMED

and analyzed in the framework of fractal geometry.[3-12] In the context of colloidal aggregates, fractal geometry may be summarized with the following relations involving the fractal dimension, D:[13,14]

$$R_g \propto M^{1/D} \tag{1}$$

$$g(r) \propto \frac{1}{r^{(d-D)}} \qquad a << r << R_g \tag{2}$$

where R_g and M are the radius of gyration and mass of the aggregate respectively, $g(r)$ is the pair correlation function, a is the radius of the primary particles, and d is the spatial dimension (d=3 for all experiments discussed in this paper). The fractal approach to the description of aggregate structure has been recently fully discussed in the context of sol-gel processing of ceramics.[15]

The structures of experimental aggregates may be compared to those predicted from numerical models in order to infer the mechanism(s) of growth. The numerical models may be broken down into two principal classes: particle-cluster or cluster-cluster.[16,17] In the former, aggregate growth is considered to result only from the addition of singlets to an existing cluster, or aggregate, while the latter allows collisions between growing aggregates. Each of these broad classes may be further refined to account for Brownian motion (diffusion limited models), convection (ballistic models) or the presence of a significant barrier to aggregation (reaction limited models). Typically, the experimental fractal dimension is compared to the values from various numerical simulations and when a match is found it is inferred that the mechanism included in the model dominated under the given experimental conditions.

The kinetics of aggregation can be analyzed by following either the time dependence of R_g, i.e. the upper limit of Eqn-2, using SLS or through a determination of the hydrodynamic radius using DLS.

In DLS the initial decay rate of the fluctuations in the scattered light intensity may be determined from a cumulant analysis of the measured autocorrelation function. The ratio of this decay rate to the square of the wave vector may be used to obtain a measure of the translational diffusion coefficient which in turn may be analyzed using the Stoke's Einstein equation to yield a hydrodynamic radius, R_h. The wave vector, q, is defined by

$$q = (4\pi n/\lambda_0) \sin(\theta/2) \tag{3}$$

where n is the index of refraction, λ_0 is the wavelength of the light, and θ is the

laboratory scattering angle. DLS studies have indicated that R_h follows an exponential time dependence under reaction limited conditions (slow aggregation)[9] and a power law under diffusion limited conditions (fast aggregation).[11]

Static light scattering may be analyzed to yield R_g by analyzing the transition between the power law regime and the Guinier regime. The scattered light intensity, $I(q)$, is directly proportional to the static scattering factor $S(q)$,[13,18] i.e.

$$\frac{I(q)}{I_0} = M^2 S(q) \tag{4}$$

Given an appropriate expression for $S(q)$, it is possible to analyze the measured intensity as a function of q, or equivalently θ, to determine R_g and D. One such expression which has been used in the analysis of colloidal silica aggregates[7,12] is

$$S(q) \propto \left[1 + \frac{2(qR_g)^2}{3D}\right]^{-(D/2)} \tag{5}$$

The function was selected based on its simplicity and the fact that it shows the correct limiting cases, which are:

$$I(q) \propto q^{-D} \qquad qR_g >> 1 \tag{6}$$

and

$$I(q) \propto \left[1 - \frac{(qR_g)^2}{3} \cdots\right] \qquad qR_g << 1 \tag{7}$$

Since the R_h and R_g can be independently determined it is possible to evaluate the relationship between the two. Both experiments and simulations[12] suggest that the two are related by a simple proportionality and that the proportionality constant is near unity (although it has been pointed out that this analysis neglects the effect of polydispersity).

We used a slightly different approach. It is possible to relate $S(q)$ to a volume integral involving $g(r)$[13,14] and therefore an assumed form for $g(r)$ can be used to obtain the expression for $S(q)$. Since the integration volume is large compared to the size of the cluster it is necessary to multiply Eqn-2 by a cutoff function, $f(r)$, to account for finite size of the cluster. The form of this cutoff function must be such that $f(r) = 1$ for $r << R_g$ and $f(r) \rightarrow 0$ for $r >> R_g$. Several functions have been investigated[12,13] including a step function, a Gaussian decay, $f(r) = \exp(-(r/R_g)^2)$, and an exponential, $f(r) = \exp(-r/R_g)$. We have employed the latter. Assuming $g(r) = \exp(-r/R_g)/r^{(d-D)}$

and performing the appropriate integration, with the assistance of an appropriate handbook,[20] yields

$$S(q) \propto \sin[(D-1)\tan^{-1}(qR_g)]\left[\frac{R_g^{(D-1)}}{q(1+(qR_g)^2)^{(D-1)/2}}\right] \quad (8)$$

Although this expression has a more complicated form than Eqn-5 substitution of the appropriate series obtains the same limiting forms.

The results of the SLS and DLS may be compared in two ways. Firstly, a relationship can be assumed between R_h and R_g may be assumed (e.g. $R_h = R_g$). This allows the data from DLS to be used to define R_g leaving only a single fitting parameter, D, for the SLS data. Alternatively, the data from DLS and SLS may be independently analyzed and the values of R_g and R_h compared.

EXPERIMENTS

Light scattering experiments were carried out on specimens in which aggregation was induced by one of two qualitatively different mechanisms: i) electrostatically stabilized single phase (silica) sols were rendered unstable through the addition of salt leading to aggregation as a consequence of van der Waals attraction or ii) two sols containing particles of opposite charge (negative silica and positive aluminum monohydroxide) were mixed leading to mutual flocculation, i.e. aggregation as a result of electrostatic attraction.

Materials

Scattering samples were made through dilution of commercial sols of either colloidal SiO_2 (Ludox-AM, DuPont Co., Wilmington DE) or AlO(OH) (Nyacol AL-20, Nyacol Products Inc., Ashland MA) using doubly distilled and deionized water (resistivity of ≈2.3 MΩ-cm). Ludox-AM is supplied as a sol of 30 wt.% (15.7 vol.%) silica. The particles are nearly spherical and closely sized. The surface of these particles have been modified by substitution of aluminum into the tetrahedral sites normally occupied by silicon. This produces a negative charge which is insensitive to pH. The suspension is supplied at a pH of 8.8, but was adjusted to 4 after dilution using nitric acid. Most experiments on salt induced aggregation were conducted at 0.5 wt.% which corresponds to a particle number density of 2.34×10^{15} cm^{-3}. The sol was diluted to 1.0% and an equal volume of a 2M NaCl solution was added yielding sample which was 0.5% SiO_2 and 1M NaCl. In some experiments the sample was agitated after the addition of the NaCl while in others extreme care was taken not to vibrate or shake the sample.

The Nyacol-AL20 is supplied as an electrostatically stabilized suspension (iep≈8 and as-supplied pH ≈4) with 27.6 wt.% (11.2 vol.%) AlO(O)OH). In contrast to the

Ludox, AlO(OH) particles are high aspect ratio plates (≈5 nm x ≈50 nm x ≈50 nm) and have a wider size distribution. For the mutual flocculation experiments, this suspension was diluted using a pH=4 nitric acid solution, and vigorously mixed with an equal volume of equally diluted Ludox.

To remove dust, sols were multiply filtered using either a LID/X filter syringe with a 0.2 μm membrane or a 0.2 μm Miller-FGS filter unit. The characterization of stable dilute sols included the determination of particle size distribution using DLS and confirmed using transmission electron microscopy.

All light scattering experiments were carried out using a commercial LLS system (Brookhaven Instrument Corporation) at the Laser Light Scattering Laboratory of the NASA Lewis Research Center. Our experiments employed a range of scattering angles from 20° to 150° for the SLS experiments. Most DLS data was collected at 90°. A vertically polarized 10 mW Ar laser (λ_0 = 5145Å) was used as the incident light source. In some experiments the incident beam intensity was reduced using neutral density filters. The scattered light was detected using a photomultiplier mounted on a precision goniometer. The reported SLS data represents the average of five 5-second runs at each scattering angle. The time necessary to complete an angular scan (≈15 min) was short compared to the aggregation rate observed in the salt induced experiments and long relative to that observed in the mutual flocculation experiments (i.e. the aggregate structure is not expected to change on the time scale of the scan in either case).

In the DLS experiments a second cumulant analysis was used to determine the mean aggregate size as a function of time. The reported hydrodynamic radius must be regarded as an *apparent* hydrodynamic radius since the measurements were taken at 90° and therefore did not satisfy the criterion that $qR << 1$. It is known that failure to account for the q-dependence of the apparent value of R_h will result in an underestimate for a polydisperse system.[11,19]

RESULTS AND DISCUSSION

Salt Induced Aggregation of Ludox

Two types of experiments were performed. Our initial experiments were designed to grow large aggregates in order to minimize finite size effects. In these experiments, samples were prepared by allowing an agitated mixture of the diluted Ludox-AM and NaCl solution to rest undisturbed for a period on the order of a month. In all cases sedimentation was observed. The samples were resuspended using an ultrasonic probe and a specimen was extracted for SLS measurements. Power law behavior is observed over the entire range of scattering vectors and D was determined to be 2.21. This relatively high value for D is consistent with similar experiments on Ludox.[8,11]

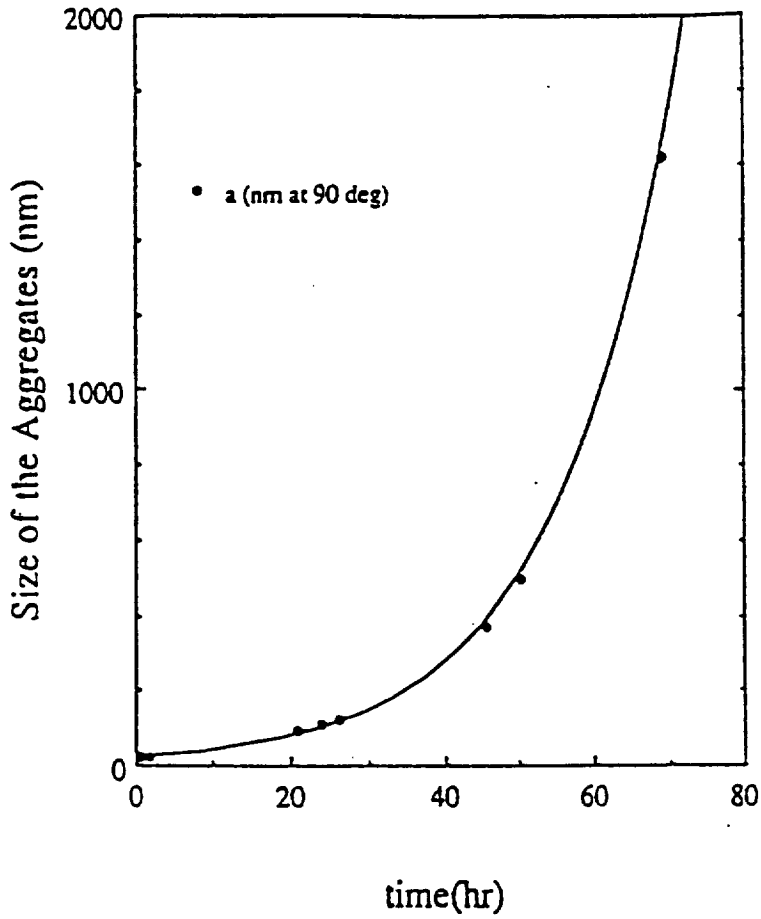

Figure 1 The value of the apparent hydrodynamic diameter determined from DLS on a salt induced aggregated silica 0.5 wt. % sol as a function of time. Zero time is defined by the addition of a salt solution to produce 1 M NaCl. The kinetics are best described by an exponential growth law.

The second set of experiments involved quiescent samples. In these experiments the 2 M NaCl solution was slowly poured into a cuvette containing the diluted Ludox. The cuvette was then placed directly into the light scattering sample holder and both SLS and DLS measurements were performed.

The kinetics of aggregation were found to follow an exponential growth law which is characteristic of reaction limited cluster aggregation.[11] The results from DLS experiments on a 0.5 Wt.% Ludox-AM sols with 1M NaCl is shown in Fig. 1. The apparent hydrodynamic diameters, a, presented in this figure were derived from a second cumulant analysis. The solid line represents a best fit to the displayed data which may be written as

$$a = 23.1 \exp(0.062 \cdot t) \tag{9}$$

where t is time expressed in hours and a is expressed in nm. The value of the constant in the argument of the exponent was not analyzed, but it is related to the concentration of particles and the magnitude of the residual repulsive interparticle forces.

It is surprising that exponential kinetics are observed since the experimental conditions (i.e. 1 M NaCl) were expected to yield fast diffusion limited aggregation and power law kinetics. This is particularly puzzling since the results of the SLS experiments indicate that the system was indeed undergoing diffusion limited aggregation.

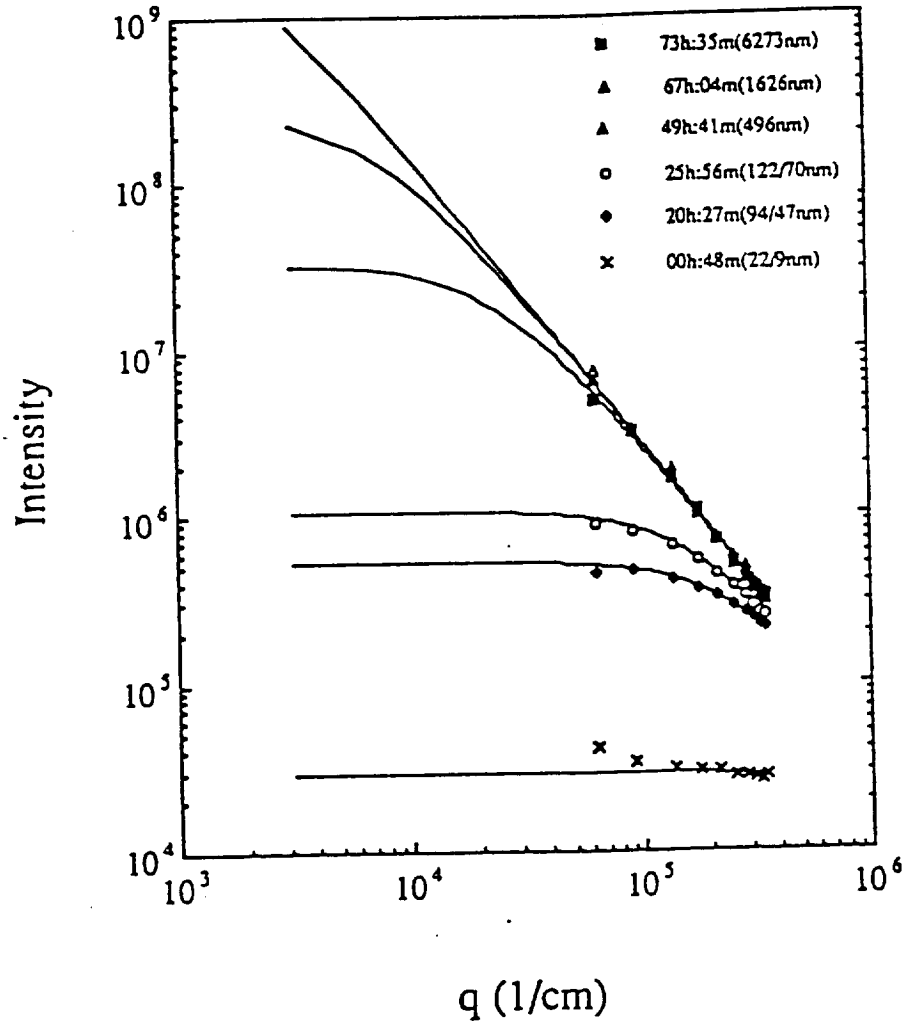

Figure 2 SLS profiles on the same sample as Fig. 1 as a function of time. The solid lines represent fits using Eqn-8 in the text for the static scattering factor, $S(q)$, with $D = 1.75$ and R_g assumed to be equal to one half of the hydrodynamic diameter determined for DLS. The hydrodynamic diameter for each fit is shown in the legend.

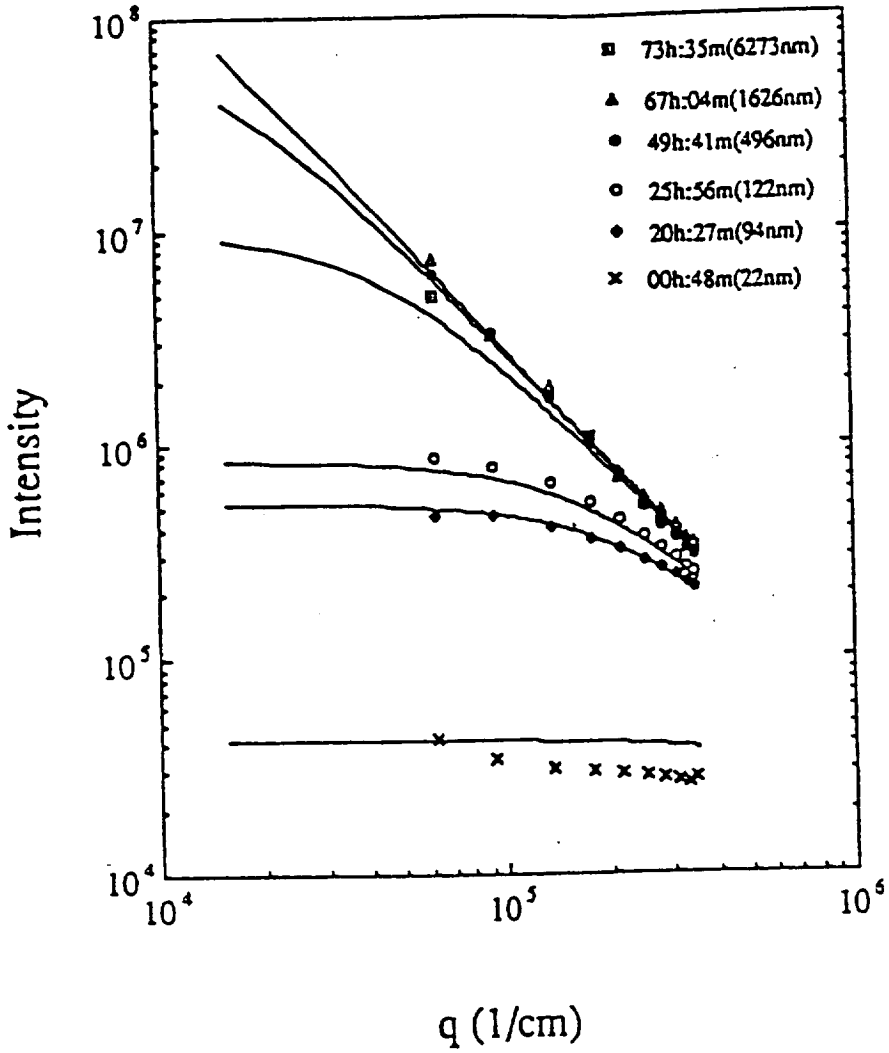

Figure 3 The same data as Fig. 2, but the solid lines are calculated using R_g as a fitting parameter in Eqn-8 (D still assumed to be 1.75). Significantly better fits are obtained particularly for times less than 49 hrs. R_g was assumed to be equal to the hydrodynamic diameter for the three uppermost curves and equal to the number to the right of the slash in the legend for the three lower curves.

The SLS results on the same sample are presented in Figs. 2 and 3. The same data points are plotted in each figure and the solid curves were all calculated using $S(q)$ as defined in Eqn-8 assuming d=1.75 which is very close to the value of 1.74 previously determined for fast diffusion limited aggregation of colloidal silica.[11] The difference between the two figures was the procedure used in evaluating R_g.

The curve in Fig. 2 were calculated assuming R_g was equal to the apparent R_h determined from DLS (one half of the hydrodynamic diameter given in parentheses in the legend). In order to calculate intensity it is necessary to determine the

Table 1 R_h and R_g Determined from SLS and DLS, Respectively.[a]

Time (hrs.)	R_h (nm)	R_g (nm)	qR_g	R_h/R_g
0.80	11	9	0.2	1.2
20.45	47	47	1.1	1.0
25.93	61	70	1.6	0.9
49.68	248	496	11.5	0.5
67.07	813	1626	37.8	0.5
73.58	3137	6273	145.9	0.5

[a]Values determined on a 0.5 wt. % sol of Ludox-AM in a 1 M NaCl solution as a function of time. The value of R_g was determined by fitting the data in Fig. 3 using Eqn-8. The value of R_h was determined from DLS at 90° using an Ar Laser yielding $q = 1/43$ (nm^{-1}).

magnitude of the proportionality constant in Eqn-8. This was empirically done for one set of data and the same value was used for all subsequent calculations. The calculated curves are in good, though not perfect, agreement with the experimental data both in terms of the systematic increase in intensity and the shift of break in slope to lower values of q. This indicates that the assumption of a simple proportionality between the characteristic aggregate sizes measured in DLS and SLS is a good approximation.

Somewhat better fits to the SLS data can be obtained if the value of R_g is used as a free fitting parameter. This was done in generating the solid curves presented in Fig. 3. A summary of the values of R_g determined from SLS and R_h determined from DLS as a function of the dimensionless parameter qR_g presented in Table 1 shows that when qR_g is on the order of 1 or smaller the ratio R_h/R_g is nearly unity and that when $qR_g >> 1$ this ratio is =0.5 (it should be noted that the fit to the SLS becomes insensitive to R_g as aggregation proceeds and therefore small differences from 0.5 cannot be resolved). These results are consistent with the fact that the effective diffusion coefficient observed in DLS increases as qR_g exceeds 1 as a result of the increasing importance of rotational diffusion.[18,19] The magnitude of the effect, i.e. a factor of 2, is in very good agreement with the predictions that have been made for diffusion limited aggregation over the range of qR_g used in our DLS experiments.[18,19]

Mutual Flocculation of Ludox-Nyacol Mixtures

Mutual flocculation was observed to be very rapid. Even at particle concentrations of 0.1 wt. % the process was complete before the sample could be inserted into the light scattering system (1-2 min.). As a result of the rapid growth of large aggregates power law behavior was observed throughout the entire range of q investigated.

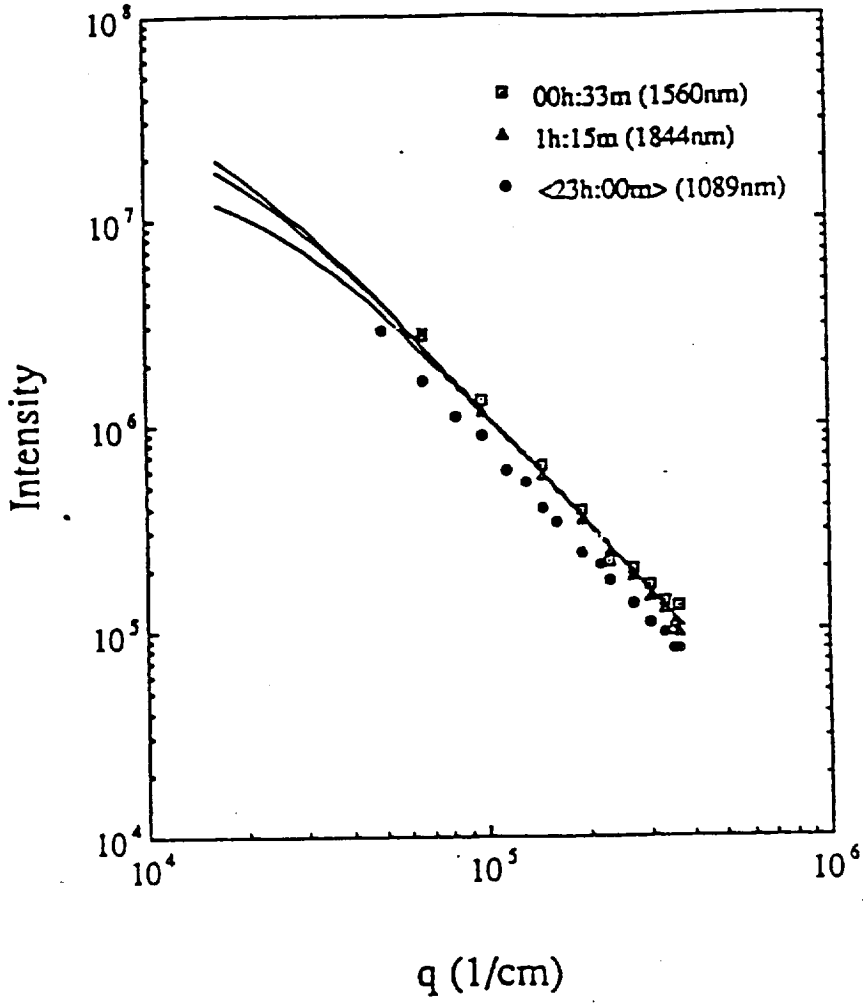

Figure 4 SLS profiles determined from a mixture of Ludox and Nyacol sols of 0.1 wt. % as a function of time. R_h values determined from DLS are given in the legend. Power law behavior is observed and the intensity decreases as a function of time which is attributed to large aggregates settling out of the path of the primary beam.

The results of a typical experiment using 0.1 wt. % suspensions are shown in Fig. 4. The best fits using Eqn-8 and the $2R_h$ from DLS yield $D = 1.84$ which is significantly higher than that observed for the salt induced silica aggregates. The value of D observed for mutual flocculation of 0.5 wt. % suspensions was significantly higher, ≈2.03. The only change in the SLS with time was a slow uniform decrease in the intensity of the signal, ≈40% after 23 hrs. DLS indicates that the aggregate size first increases and then decreases. Both of these observations are consistent with settling under gravity. The net effect being the reduction of the number of scattering centers in the path of the beam as the larger clusters settle down.

The high fractal dimensions observed in the mutual flocculation experiments may be qualitatively rationalized in terms of electrostatic interactions. The fact that the aggregation kinetics are very rapid indicates that the electrostatic interaction is relatively long range. Thus it is expected that particle motion will not be dominated by Brownian motion, rather particles of opposite charge will tend to follow ballistic trajectories towards each other. Such a process is consistent with a higher fractal dimension.[16,17] In addition, it is plausible (though unproven) that electrostatic interaction between neighboring branches within an aggregate will increase as the aggregate grows and lead to restructuring. This would also be expected to drive D to higher values.

CONCLUSIONS

1) The assumption of an exponential cutoff on $g(r)$ yields a form of $S(q)$ which is consistent with the SLS results on both salt induced single phase aggregates and aggregates produced by mutual flocculation.

2) Silica aggregates grown in a 1 M NaCl solution yield $D = 1.75$. Aggregates allowed to settle and then resuspended exhibit $D = 2.21$. Both observations are consistent with prior work. The scaling relationship between R_g (determined by SLS) and R_h (determined from DLS) is also consistent with prior calculations and experiments.

3) Mixtures of silica and aluminum monohydroxide aggregate very rapidly and exhibit higher fractal dimensions suggesting ballistic aggregation and possibly restructuring.

ACKNOWLEDGMENTS

RA and WVM would like to acknowledge support from the NASA microgravity Science Application Division, Code SN, of NASA. YHR and JDC would like to acknowledge support through NASA grant #NAG3-755 and a seed grant from the Ohio State University Center for Materials Research.

REFERENCES

1. B. J. Berne and R. Pecora, Dynamic Light Scattering, Wiley, New York, 1976.
2. B. E. Dahneke, Measurement of Suspended Particles by Quasi-Elastic light Scattering, Wiley, New York, 1983, Ch.1.
3. D. A. Weitz and M. Oliveria, "Fractal Structures Formed by Kinetic Aggregation of Aqueous Gold Colloids", Phys. Rev. Lett. 52, [16] 1433-36 (1984).
4. D. A. Weitz, J. S. Huang, M. Y. Lin, and J. Sung, "Limits of Fractal Dimension for Irreversible Kinetic Aggregation of Gold Colloids," Phys. Rev. Lett, 54, [13] 1416-19 (1985).
5. D. W. Schaefer, J. E. Martin, P. Wiltzius, and D. S. Cannell, "Fractal Geometry of

Colloidal Aggregates", Phys. Rev. Lett. 52, [26] 2371-74 (1984).
6. D.W. Shaefer and K. Keefer, "Fractal Aspects of Ceramic Synthesis," p. 277-88 in Better Ceramics through Chemistry II, Edited by C.J. Brinker, D.E. Clark, and D.R. Ulrich, Mat. Res. Soc. Symp. Proc. 73 (1986).
7. D. S. Cannell and C. Aubert, "Aggregation of Colloidal Silica," p. 187-197 in On Growth and Form: Fractal and Non-Fractal Patterns in Physics, Edited by H. Eugene Stanley and N. Ostrowsky, Martinus Nijhoff Publishers, Boston MA, 1986.
8. C. Aubert and D. S. Cannell, "Restructuring of Colloidal Silica Aggregates," Phys. Rev. Lett. 56, [7] 738-41 (1986).
9. J. E. Martin, "Slow Aggregation of Colloidal Silica," Phys. Rev. A 36, [7] 3415-26 (1987).
10. H. M. Lindsay, M. Y. Lin, D. A. Weitz, P. Sheng, Z. Chen, R. Klein, and P. Meakin, "Properties of Fractal Colloid Aggregates," Faraday Discuss. Chem. Soc. 83, 153-65 (1987).
11. J. E. Martin, J. P. Wilcoxon, D. Schaefer, and J. Odinek, "Fast Aggregation of Colloidal Silica," Phys. Rev. A 41, [8] 4379-91 (1990).
12. P. Wiltzius, "Hydrodynamic Behavior of Fractal Aggregates," Phys. Rev. Lett. 58, [7] 710-15 (1987). Z. Y. Chen, P. Meakin, J. M. Deutch, "Comment on 'Hydrodynamic Behavior of Fractal Aggregates'," Phys. Rev. Lett. 59, [18] 2121 (1987). P. N. Pusey, J. G. Rarity, R. Klein, and D. A. Weitz "Comment on 'Hydrodynamic Behavior of Fractal Aggregates'," Phys. Rev. Lett. 59, [18] 2122 (1987). P. Wiltzius and W. van Saarloos, Reply, Phys. Rev. Lett. 59, [18] 2123 (1987).
13. J. E. Martin, "Static and Dynamic Scattering From Fractals," Phys. Rev. A 31 [2] 1180-82 (1985).
14. J. E. Martin and A. J. Hurd, "Scattering From Fractals," J. Appl. Cryst. 10 61-78 (1987).
15. C. J. Brinker and G. W. Scherer, Sol-Gel Science: The Physics and Chemistry of Sol-Gel Processing, Academic Press, San Diego, CA, 1990.
16. P. Meakin, "Models for Colloidal Aggregation," Ann. Rev. Phys. Chem. 39, 237-67 (1988).
17. R. Jullien and R. Botet, Aggregation and Fractal Aggregates, World Scientific, Singapore, 1987, p. 64, p.77.
18. D. A. Weitz and M. Y. Lin, "Laser Light Scattering as a Probe of Fractal Aggregates," p. 173-184 in NASA Laser Light Scattering Advanced Technology Workshop-1988, NASA CP 10033, Edited by W.V. Meyer.
19. H. M. Lindsay, R. Klein, D. A. Weitz, M. Y. Lin, and P. Meakin, "Effect of Rotational Diffusion on Quasielastic Light Scattering From Fractal Colloids," Phys. Rev. A 38 [5] 2614-26 (1988).
20. I. S. Gradshteyn and I. M. Ryzhik, Table of Integrals, Series, and Products, Academic Press, New York, 1980, p. 490.

Journal of the American Ceramic Society

J. Am. Ceram. Soc., 75 [7] 1981–84 (1992)

Fractal Dimension of Alumina Aggregates Grown in Two Dimensions

Judith L. LaRosa*,* and James D. Cawley*,†

Department of Materials Science and Engineering, The Ohio State University, Columbus, Ohio 43210

The concepts of fractal geometry are applied to the analysis of 0.4-μm alumina constrained to agglomerate in two dimensions. Particles were trapped at the bottom surface of a drop of a dilute suspension, and the agglomeration process was directly observed, using an inverted optical microscope. Photographs were digitized and analyzed, using three distinct approaches. The results indicate that the agglomerates are fractal, having a dimension of approximately 1.5, which agrees well with the predictions of the diffusion-limited cluster–cluster aggregation model. [Key words: alumina, aggregates, fractals, geometry, suspension.]

I. Introduction

Control over the extent of agglomeration is fundamental to powder processing of ceramics. Quantitative measures of the state of agglomeration, such as average size and reciprocal packing efficiency,[1] are therefore of value. Recently, the fractal dimension[1] has proven useful in quantifying the geometry of colloidal aggregates of both metallic and oxide particles[2–16] as well as structures observed in sol–gel processing of ceramics.[17] In particular, the fractal dimension provides a quantitative measure which allows comparison of experimental observations to computer-generated structures.[18]

This study focused on agglomeration of submicrometer commercial alumina (Sumitomo AKP30) constrained to a surface, i.e., two dimensions using the technique of Onoda.[19] In the experiments, gravity acted perpendicular to the surface and, therefore, played no role in the agglomeration process. This allowed the results to be compared to diffusion-limited aggregation computer models. Real-time qualitative observations of the agglomeration process confirmed the models' applicability. In addition, analyzing digitized photographs of the agglomerates revealed that the structures were indeed fractal, having a fractal dimension of about 1.5.

II. Background

Fractal geometry can be used to describe a wide range of physical phenomena.[20,21] A fractal agglomerate occupies simultaneously a Euclidian dimension d and a fractal dimension D. For an arbitrarily large agglomerate, the maximum possible D equals d, and when considering completely connected agglomerates, the lower limit of D is one. In general, a lower fractal dimension indicates a more tenuous structure, while a higher fractal dimension means that the structure is more space-filling.

The fractal dimension is determined from several relationships which are unique to fractal geometry.[2,16,18,20,21] One of these relationships incorporates the density correlation function $C(r)$:

$$\langle C(r)\rangle \propto r^{-\alpha} \tag{1}$$

$$C(r) = (1/N)\sum_i \rho(r_i)\,\rho(r_i + r) \tag{2}$$

where N is the number of particles or occupied sites in the agglomerate, i is the observation point or occupied site, $\rho(r_i)$ is the density at the observation point = 1, and $\rho(r_i + r)$ is the density of occupied sites located a distance r from the observation point and

$$-\alpha = D_\alpha - d \tag{3}$$

where D_α is the fractal dimension, and d is the Euclidian dimension in which the agglomerate is grown.

The $-\alpha$ indicates that density decreases at larger distances. $C(r)$ in Eq. (2) represents the probability of finding a particle or occupied site at a distance r from another particle or occupied site. This probability, in turn, is proportional to the density of the agglomerate at a distance r from a particle. Experimentally, $C(r)$ is found by calculating the density at a distance r from a chosen occupied site or observation point. For monosized particles, number density can replace the mass density. In two dimensions, the number density at r equals the number of particles N divided by the area of a ring containing the N particles. For an inner ring radius of r and an outer radius of $(r + \Delta r)$ where Δr is small, $\langle C(r)\rangle$ is approximated by

$$\langle C(r)\rangle \approx \langle N(r)\rangle/2\pi r\Delta r \tag{4}$$

In Eq. (1), $\langle C(r)\rangle = (1/N_T)\Sigma_i C_i(r)$ where $C_i(r)$ is measured at a distance r from a single point i in the agglomerate. The distance r is constant over all i, and N_T is the total number of i points sampled from the agglomerate. A graph of ln $\langle C(r)\rangle$ vs ln (r) yields a slope equal to $-\alpha$ from which D_α is calculated.

Fractal dimension can also be obtained from the equation

$$\langle M(r)\rangle \propto r^{D_\beta} \tag{5}$$

M is the mass enclosed by some distance r (Eq. (5) may be obtained from an integration of Eq. (4)). For example, M may be the mass contained in a circle of radius r. Then $\langle M(r)\rangle$ is the mass averaged over the total number of i point origins for each r. D_β equals the fractal dimension. If each particle has the same mass, M may be replaced by the number of particles N contained in a sphere of radius r:

$$\langle N(r)\rangle \propto r^{D_\beta} \tag{6}$$

As a result, the graph of ln $\langle N\rangle$ vs ln (r) has a slope equal to D_β.

A third measure of fractal dimension is yielded by the relationship between the radius of gyration R_g of an agglomerate and its total mass M:

$$\langle R_g(M)\rangle \propto M^{(1/D_\gamma)} \tag{7}$$

where

$$R_g = \sqrt{\textstyle\sum_i m_i r_i^2/M}$$

and m_i is the mass of particle i at r_i from the origin, and D_γ is the fractal dimension.

But for monosized particles, $M = mN_T$, where m is the mass of particle, and N_t is the total number of particles in

D. R. Clarke—contributing editor

Manuscript No. 196259. Received November 5, 1991; approved March 18, 1992.

Supported by NASA under Grant No. NAG3–755 and an IBM Faculty Development grant.

*Member, American Ceramic Society.

*Currently at Materials Research Laboratory, Pennsylvania State University, University Park, PA 16802.

†Currently at Department of Materials Science and Engineering, Case Western University, Cleveland, OH 44106.

PRECEDING PAGE BLANK NOT FILMED

the agglomerate:

$$\langle R_g(N) \rangle \propto N_T^{(1/D_\gamma)} \tag{8}$$

where

$$R_g = \sqrt{\left(\sum_i r_i^2 / N_T\right)}$$

Therefore, the slope of ln $\langle R_g \rangle$ vs ln (N_T) is the multiplicative inverse of D_γ. In principle, both R_g and N_T are measured from one agglomerate during the course of its growth, although in practice,[15] R_g and N_T from each of several agglomerates may be used, assuming that the agglomerates grew under the same conditions.

Averaged values are used in Eqs. (1) and (4)–(8), because experimental agglomerates are not deterministic. A deterministic fractal has exactly the same structure over all length scales. Since this does not hold exactly for real agglomerates, the relationships described above are true only in a statistical sense.

One experimental test for the appropriateness of the fractal approach is whether $D_\alpha = D_\beta = D_\gamma$.

Although complex computer simulations have been developed to include structural arrangements and reversible agglomeration,[16,18] the simpler models provide clear insight into agglomeration growth in two, three, and more dimensions. One of the most influential of these has been the diffusion-limited aggregation (DLA) model. In this model, the first particle is released at a randomly chosen position some distance away from a fixed seed particle. It diffuses through space following a random-walk course which simulates Brownian motion. If it comes in contact with the seed, it sticks. Additional particles are released one at a time and stick to the agglomerate upon contact. One variation of DLA is diffusion-limited cluster aggregation (DLCA). Unlike DLA, in which single particles are continuously added to the agglomerate upon particle-to-cluster collisions, the DLCA starts with a fixed number of initially dispersed particles which simultaneously undergo random walks. The ensuing collisions involve particle clusters of all sizes. When the Euclidian dimension is two, DLA produces an agglomerate with a fractal dimension of 1.71, while DLCA yields 1.45.

III. Experimental Procedure

Suspensions of 0.001 vol% alumina were prepared by adding 0.4-μm-diameter α-Al_2O_3 to a buffer solution of HCl and tris(hydroxymethyl)aminomethane. The buffer had an ionic strength of 0.2M, and it provided a stable pH near the point of zero charge for alumina measured to be ≈8.2. This ensured that agglomeration would result upon collision of two particles. In order to observe the agglomeration process, a drop of the suspension was placed over a 4-mm hole in a 2-mm-thick aluminum slide. The particles settled under the influence of gravity to the lower surface, where they were observed through an inverted optical microscope. The particle number density in the drop was low, making particle–particle collisions in the bulk rare, and virtually all of the particles which were observed settled as singlets. Therefore the entire agglomeration process took place on the two-dimensional lower surface of the drop.

Videotaping and conventional metallographic photographs were taken as a function of time. The photographs were digitized, using a high-resolution video camera and a frame grabber board mounted in a personal computer. Fractal dimensions for individual agglomerates were calculated from Eqs. (1) and (6), using the X–Y coordinates of the particles. In addition, pictures of computer-simulated agglomerates from other investigators[18] were digitized in order to check the reliability of the data processing methods.

Fig. 1. Photomicrograph taken of the bottom surface of a drop of a 0.001 vol% suspension of 0.4-μm alumina (Sumitomo, AKP30) after 22 min. Agglomerates of a wide variety of sizes are present, ranging from several to several hundred particles. Out-of-focus singlet particles which are in the process of settling to the lower interface are also apparent.

IV. Results and Discussion

Real-time observation of the aggregation process indicated that the overwhelming majority of particles settle to the interface as singlets. Vigorous Brownian motion within the plane of the interface was observed. This caused particles to collide and agglomerate. At first, collisions were between either two particles or a singlet and a small cluster of particles. These types of collisions occurred throughout the experiment, since single particles were constantly settling to the interface. However, as time elapsed, cluster–cluster collisions dominated the aggregation process. One assumption frequently made in the fractal analysis of aggregate growth is that agglomeration is irreversible. No bond breaking was expected, or observed, in these experiments. It is also generally assumed that no rearrangement takes place. This was also generally consistent with experimental observation. However, multiple bonds were occasionally formed between clusters as part of one would stick to the other, rotate slightly, and attach in one or two other places.

The observed resistance to rearrangement is believed to result from the fact that the primary particles in the aggregate are not true spheres but somewhat irregular. This leads to local minimums in the interparticle energy as a function of rotation.

The larger agglomerates contained 30 to 100 particles. Figure 1 is a photograph of an interface taken 22 min after a drop was placed in the slide. Visual inspection of this micrograph reveals a strong qualitative similarity to the results of computer simulations using DLCA.[16,18]

The results obtained from digitized images of some computer-simulated agglomerates (the algorithms used to simulate these agglomerates are not relevant to the experiments discussed here) are shown in Table I. Good agreement was

Table I. Fractal Dimensions of Digitized Two-Dimensional Computer-Simulated Agglomerates (from Ref. 18)

	Expected[18]	D_α	D_β
Diffusion-limited particle–cluster	1.71	1.71	1.67
Ballistic cluster–cluster	1.55	1.63	1.53
Reaction-limited cluster–cluster	1.61	1.59	1.56

Table II. Fractal Dimensions of Alumina Agglomerates

Agglomerate	D_α $\Delta r = 0.4\ \mu m$	D_α $\Delta r = 0.8\ \mu m$	D_β
	Photograph A: t = 22 min, pH 8.5		
1	1.46	1.47	1.45 ± 0.06
2	1.54	1.55	1.41 ± 0.10
3	1.55	1.45	1.40 ± 0.07
4	1.41	1.31	1.45 ± 0.04
5	1.38	1.29	1.36 ± 0.07
6	1.44	1.31	1.48 ± 0.05
7	1.56	1.54	1.51 ± 0.05
8	1.57	1.55	1.52 ± 0.06
9	1.51	1.50	1.59 ± 0.07
10	1.51	1.37	1.41 ± 0.05
11	1.63	1.58	1.62 ± 0.03
12	1.55	1.44	1.45 ± 0.04
13	1.30	1.22	1.35 ± 0.06
14	1.61	1.56	1.52 ± 0.05
15	1.61	1.51	1.55 ± 0.07
16			1.41 ± 0.03
17			1.60 ± 0.06
18			1.41 ± 0.06
	Photograph B: t = 25 min, pH 8.5		
1	1.69	1.64	
2	1.68	1.62	
3	1.56	1.48	
4			1.55 ± 0.07
5			1.64 ± 0.03
	Photograph C: t = 40 min, pH 8.6		
1			1.47 ± 0.05
2			1.48 ± 0.04
	Photograph D: t = 20 min, pH 7.9		
1			1.35 ± 0.04
2			1.42 ± 0.05
3			1.39 ± 0.04
4			1.44 ± 0.04
	Photograph E: t = 30 min, pH 7.9		
1			1.45 ± 0.05
2			1.42 ± 0.05
Avg:	1.53	1.47	1.47 ± 0.03
SD:	0.10	0.12	0.08
Range:	1.30–1.69	1.22–1.64	1.35–1.64

found between the results obtained using the computer programs and the prior published values. Additional checks on the programs including analyzing sections of the a circle (one-quarter and one-half circles) which yielded D_β of 1.0 and the determination of the pair correlation function for an fcc lattice with the program used to calculate D_α.

Table II lists the fractal dimensions obtained for the alumina agglomerates. Time elapsed, t, and pH are also given for each of the photographs. In calculating $C(r)$, values of Δr were used corresponding to the particle diameter and twice the diameter. The average values of D_α are 1.53 and 1.47 for $\Delta r = 0.4$ and 0.8 μm, respectively. Confidence intervals of 95% are indicated for values of D_β, for which the average is 1.47. Typical plots used to determine D_α and D_β from a typical digitized agglomerate are shown in Figs. 2 and 3, respectively. Attempts were also made to determine D_γ from a plot of ln (R_g) vs ln (total number of points); however, the results were inconclusive. It was observed that the values obtained were strongly dependent on the number of data points used, which implies that the total number of agglomerates analyzed is too small to yield a well-determined value for D_γ.

These results of D_α and D_β are in agreement with the expected value of 1.45 based on DLCA computer simulations,[18] indicating that the experiment is a physical realization of this model. These values are also significantly higher than the ≈1.2 observed by Hurd and Schaefer[15] for two-dimensional aggregation of silica spheres. In their experiments, however, a strong interparticle electrostatic interaction (which was not

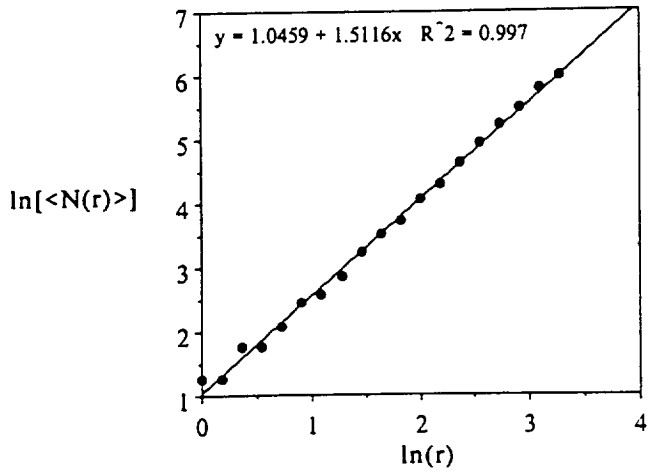

Fig. 2. A plot of the natural logarithm of the average number of particles within a sampling interval as a function of the natural logarithm of the size of the sampling interval. The straight line represents the best fit using Eq. (6), and the slope is equal to the fractal dimension.

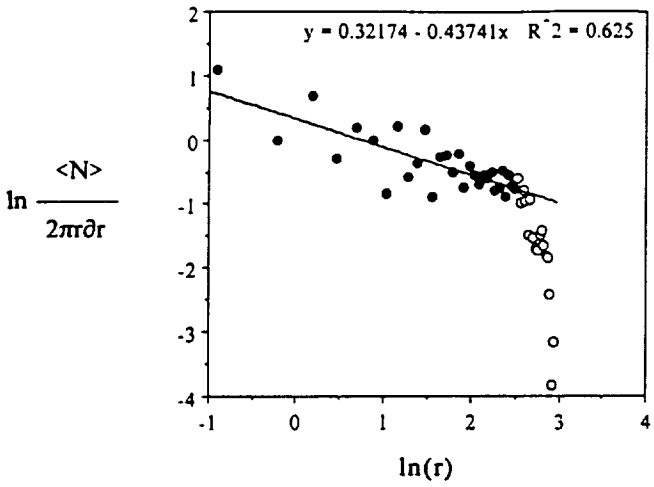

Fig. 3. A plot of the pair correlation function for the same agglomerate as Fig. 2. The straight line represents the best fit using Eq. (1) up to a cutoff radius. The solid squares represent the points used in the fitting procedure.

present in our experiments) was believed to be responsible for the lower observed dimension.

V. Conclusion

The random and disorderly agglomerates grown in these experiments can be meaningfully described in terms of a fractal dimension of ≈1.5. This value is close to the value expected from the diffusion-limited cluster–cluster aggregation model.

References

[1]J. W. Halloran, "Role of Powder Agglomerates in Ceramic Processing"; pp. 67–75 in Advances in Ceramics, Vol. 9, *Forming of Ceramics*. American Ceramic Society, Columbus, OH, 1986.

[2]S. R. Forrest and T. A. Witten, Jr., "Long-Range Correlations in Smoke-Particle Aggregates," *J. Phys. A*, **12** [5] L109–L117 (1979).

[3]D. A. Weitz and M. Oliveria, "Fractal Structures Formed by Kinetic Aggregation of Aqueous Gold Colloids," *Phys. Rev. Lett.*, **52** [16] 1433–36 (1984).

[4]D. A. Weitz, J. S. Huang, M. Y. Lin, and J. Sung, "Limits of Fractal Dimension for Irreversible Kinetic Aggregation of Gold Colloids," *Phys. Rev. Lett.*, **54** [13] 1416–19 (1985).

[5]D. W. Schaefer, J. E. Martin, P. Wiltzius, and D. S. Cannell, "Fractal Geometry of Colloidal Aggregates," *Phys. Rev. Lett.*, **52** [26] 2371–74 (1984).

[6]D. W. Shaefer and K. Keefer, "Fractal Aspects of Ceramic Synthesis"; pp. 277–88 in *Better Ceramics through Chemistry II*. Edited by C. J. Brinker, D. E. Clark, and D. R. Ulrich. Materials Research Society, Pittsburgh, PA, 1986.

[7]D. S. Cannell and C. Aubert, "Aggregation of Colloidal Silica"; pp. 187–97 in *On Growth and Form: Fractal and Non-Fractal Patterns in Physics*. Edited by H. E. Stanley and N. Ostrowsky. Martinus Nijhoff Publishers, Boston, MA, 1986.

[8]C. Aubert and D. S. Cannell, "Restructuring of Colloidal Silica Aggregates," *Phys. Rev. Lett.*, **56** [7] 738–41 (1986).

[9]J. E. Martin, "Slow Aggregation of Colloidal Silica," *Phys. Rev. A*, **36** [7] 3415–26 (1987).

[10]H. M. Lindsay, M. Y. Lin, D. A. Weitz, P. Sheng, Z. Chen, R. Klein, and P. Meakin, "Properties of Fractal Colloid Aggregates," *Faraday Discuss. Chem. Soc.*, **83**, 153–65 (1987).

[11]J. E. Martin, J. P. Wilcoxon, D. Schaefer, and J. Odinek, "Fast Aggregation of Colloidal Silica," *Phys. Rev. A*, **41** [8] 4379–91 (1990).

[12]P. Wiltzius, "Hydrodynamic Behavior of Fractal Aggregates," *Phys. Rev. Lett.*, **58** [7] 710–15 (1987); (b) Z. Y. Chen, P. Meakin, and J. M. Deutch, "Comment on 'Hydrodynamic Behavior of Fractal Aggregates'," *Phys. Rev. Lett.*, **59** [18] 2121 (1987); (c) P. N. Pusey, J. G. Rarity, R. Klein, and D. A. Weitz, "Comment on 'Hydrodynamic Behavior of Fractal Aggregates'" *Phys. Rev. Lett.*, **59** [18] 2122 (1987); (d) P. Wiltzius and W. van Saarloos, Reply, *Phys. Rev. Lett.*, **59** [18] 2123 (1987).

[13]J. E. Martin, "Static and Dynamic Scattering from Fractals," *Phys. Rev. A*, **31** [2] 1180–82 (1985).

[14]J. E. Martin and A. J. Hurd, "Scattering From Fractals," *J. Appl. Crystallogr.*, **20**, 61–78 (1987).

[15]A. J. Hurd and D. W. Schaefer, "Diffusion-Limited Aggregation in Two Dimensions," *Phys. Rev. Lett.*, **54** [10] 1043–46 (1985).

[16]R. Jullien and R. Botet, *Aggregation and Fractal Aggregates*. World Scientific, Singapore, Republic of Singapore, 1987.

[17]C. J. Brinker and G. W. Scherer, *Sol–Gel Science: The Physics and Chemistry of Sol–Gel Processing*. Academic Press, San Diego, CA, 1990.

[18]P. Meakin, "Models for Colloidal Aggregation," *Ann. Rev. Phys. Chem.*, **39**, 237–67 (1988).

[19]G. Y. Onoda, "Direct Observation of Two-Dimensional, Dynamical Clustering and Ordering with Colloids," *Phys. Rev. Lett.*, **55** [2] 226–29 (1985).

[20]B. B. Mandelbrot, *The Fractal Geometry of Nature*. W. H. Freeman, New York, 1984.

[21]L. M. Sander, "Fractal Growth," *Sci. Am.*, **256**, 94–100 (1987). □

A Modified Ballistic Aggregation Model

J. F. Dirkse* and J. D. Cawley**
Department of Materials Science and Engineering
Ohio State University

Abstract

The standard ballistic aggregation model assumes that the particles which are added to a growing agglomerate follow straight line trajectories. The finite viscosity of real fluids, however, bias the flow of liquid around rather than through the agglomerate. The result of this is that particles, which follow sreamlines in the fluid, will tend to be deposited near the periphery of the growing agglomerate. A modification is made to the ballistic aggregation model in order to account for this effect and the geometry of the resultant structures is characterized. The simulation results suggest that even under conditions where convection dominates particle motion, branched open structures are likely to be formed.

This work was supported by the National Areonautics and Space Administration under grant NAG3-755.

* currently with Tresp Associates, Energy Associates Group, Oakland, CA.
** currently with Case Western Reserve University, Dept. of Materials Science, Cleveland, OH.

1. Introduction

Agglomerates are generally formed as a result of collisions between primary particles, and small clusters of particles, in a suspension. The size, shape, and internal pore distributions of agglomerates are dependent on how the agglomerate was assembled and the response of the bonded particles to external forces. Computer simulation has proven a powerful method for improving our understanding of the mechanisms involved in agglomeration.

Several types of numerical models are available to study colloidal aggregation. Particle or aggregate transport in these models can be tailored to include either ballistic, diffusive, or mixed components of motion. The mode of transport is distinguished by the particle or aggregate trajectory: ballistic motion follows a curvilinear path, and diffusive motion imitates a random walk. Probability models, such as diffusion-limited aggregation or ballistic growth, and molecular models, such as Brownian dynamics, are commonly used to simulate colloidal aggregation[1-10].

Fig. 1 schematically illustrates the ballistic growth and diffusion-limited aggregation models (DLA and BA, respectively). Typical 2-dimensional aggregates grown from these models are shown in Fig. 2. The typically open nature of a DLA agglomerate is in sharp contrast to the compact nature of the BA agglomerate.

In Table 1 the fractal dimensions of the aggregation models discussed thus far are tabulated from a review by Meakin[7]. Results are included for both particle-cluster and cluster-cluster models. In the former, agglomerates are generated by successive additions of single particles to a growing agglomerate whereas the latter begins with a fixed number of isolated particles and allows growth through the motion of both single particles and clusters. One difference between particle-cluster and cluster-cluster aggregation is that with cluster-cluster aggregation the fractal dimension is relatively insensitive to the type of transport.

2. Motivation for the present work

The relationship between the mechanism of particle addition to a growing agglomerate and geometrical aspects of resultant structure was investigated. The interest in examining colloidal aggregation, from the perspective of convective dominated transport, stems from direct observation of alumina aggregation at an air-water interface[11]. In these experiments, low volume fraction, 0.01%, suspensions of 0.4 μm alumina (Sumitomo AKP-30) were prepared. Drops of these suspensions were placed in a hole in an aluminum microscope slide and observed using an inverted optical microscope focussed on the lower surface of the droplet. Due to the low volume fraction of solids, the particles had a very low collision probability in the bulk and were observed to settle to the lower surface almost entirely as singlets. Therefore it was possible to directly observe the entire agglomeration process. In several experiments, drafts in the room air produced significant convection. (It was possible to carry out experiments in which the role of convection could be neglected[12], but these are not discussed in this paper). A diagram made by superimposing a series of images collected using a video camera is shown in Fig. 3. The large unshaded figure represents a portion of a large agglomerate which was fixed to aluminum slide and was therefore immobile. The observed direction of drift is indicated by the arrow.

The positions of two smaller agglomerates are shown as a function of time; one of which (shaded black) was shielded from the convective flow due to its location in a "bay" and was observed to move only by Brownian motion while the other (shaded gray) displayed movement which was dominated by convection. As noted on the figure, the elapsed time is nearly equal between the first and last image for each. It is evident that the net displacement due to drift is much larger than that due to diffusion. In addition, it appears from these, and other, results that the probability of attachment in the presence of a fluid with a finite viscosity will be highly dependent on the degree of convection and the local geometry. The regions which extend into the fluid effectively screen the regions of the agglomerates associated with bays suggesting that under conditions of that convective transport, similar to the diffusive or Brownian case, preferential tip growth is to be expected.

This analogy leads to the idea that the resultant structures may be fractals, since one of the characteristics of "fractal growth" by Brownian motion is the high growth probability for dendrite tips relative to interior of agglomerate. Several authors have investigated the region of a growing aggregate which is available for new growth,

termed an active zone[13], in order to examine the screening behavior of fractal structures, i.e. the shielding the interior from diffusive growth[13-19].

In this work, the standard ballistic growth model was modified to include the contribution of hydrodynamic screening by the agglomerate. The approach was to assume that convective flow was approximated by fluid flow around a circular geometry imposed on a growing aggregate as an approximation to hydrodynamic screening where interior fluid flow in porous materials is inhibited. Growth of the aggregate was restricted to single particle additions which followed the streamlines around the circular geometry. This type of fluid flow leads to preferential tip growth by excluding growth within a circle with a radius related to the radius of gyration of the aggregate. The simulations are restricted to 2-dimensional particle-cluster models since this class of models is most sensitive to the effects of particle transport. The influence of different relationships between the radius of gyration and the hydrodynamic radius was examined by characterizing structures produced using computer simulations.

Analyzing aggregate geometry is usually a difficult task since they are generally highly irregular structures. The outputs of the numerical model developed in this work were characterized using four quantitative measures: i) average coordination number of the particles making up the agglomerate; ii) the fractal dimension determined from the scaling of the radius of gyration during growth, the distribution of mass within the agglomerate, and the pair correlation function; iii) measurement local density fluctuations within the agglomerate; and iv) a characterization of the active zone of the growing agglomerate.

The average coordination number is a measure of connectivity (for a completed connected structure the minimum value is two and for a two-dimensional structure of equal sized particles the maximum is six). The coordination number was calculated by determining the number of particles with center-center distances below a certain distance, 1.1 or 2.0, and averaging the result. The number of nearest neighbors is determined using the 1.1 cutoff while the total number of first, second and third nearest neighbors was determined using 2.0.

The fractal dimension[20] has become a standard measure for agglomerates. It can be determined from a number of different scaling relations, in this work the following set were used:

$$R_g \alpha M_t^{1/D} \quad (1)$$

$$M(r) \alpha r^D \quad (2)$$

$$\langle c(r) \rangle \alpha r^{d-D} \quad (3)$$

where R_g is the radius of gyration, M_t is the mass of the agglomerate at time t, M(r) is the mass contained in a circle of radius r centered on the center of mass of the agglomerate, $\langle c(r) \rangle$ is the density correlation function, r is the distance between two points within the agglomerate, and D is the fractal dimension[11,21].

Local density was measured by randomly choosing 100 points located $\leq R_g$ and determining the density of particles within both 4 and 10 diameters from this point. These values were then normalized using the overall density for the particular agglomerate (10,000 divided by $2\pi R_{max}^2$) .

4. Numerical Model Development

Colloidal particles dispersed in an aqueous suspension encounter one another through the influence of several forces; external fields such as gravity, convection, or applied voltages, interparticle forces including Van der Waals and electrostatic, hydrodynamic interaction, and Brownian forces. These forces are not explicitly evaluated in the model. In the experiment, gravity simply serves to populate the plane of interest. Particles are kept at the near the point of zero charge so that the only operative interparticle force is Van der Waals which is only considered to result in irreversible bonding when particles come into contact. The only external field is a convection flow which is considered to overwhelm any contribution from Brownian motion.

The issue of hydrodynamic screening in the presence of mild convection was addressed by approximating the flow field around the agglomerate by that around an infinitely long cylinder having the same hydrodynamic radius. The axis of the cylinder is perpendicular to the plane of aggregate growth and passes through the center of mass of the aggregate which defines the origin of the coordinate system. An aggregate is depicted in Fig. 4 along with the flow field of the cylinder including several streamlines of constant potential. The stream function Ψ describing the streamlines of fluid flow around a cylinder geometry are calculated by the potential flow equation

$$\Psi = V [y - yR_h^2/(x^2+y^2)] \quad (4)$$

where V is the undisturbed fluid velocity at a distance $x^2+y^2 >> R_h^2$ such that V=-

$\partial\Psi/\partial y=V_x$ and $V_y=\partial\Psi/\partial x=0$ with R_h equal to the cylinder radius[22]. Eqn. 4 assumes laminar (low Reynolds number) and irrotational flow of an ideal fluid (i.e. constant density and zero viscosity)[23]. The resultant description of the pressure at the upstream half of the cylinder (i.e. the side from which particles arrive) is close to what is found experimentally[24].

Fluid flow around an aggregate is incorporated into the ballistic growth model by treating growth particles as point masses and confining their trajectories to streamlines. Eqn. 4 when rewritten as a cubic in y can be solved exactly[25]; however, a linear iteration solution for nonlinear equations[26] was used to approximate the streamline of constant potential. The three pieces of information needed for this method are the random initial coordinates of the incoming particle, the undisturbed fluid velocity, and the hydrodynamic radius. The particle is moved downstream in increments of 0.01 μm. Each new position is found by iterating the until the stream function is within a tolerance of ±1% of $\Psi(x_o,y_o)$. The routine continues until contact with the aggregate. A particle is considered to be in contact with the aggregate when the center-center separation distance is within ±1% of the particle diameter. A particle is discarded if it travels past the aggregate. Several procedures were used to increase the computational efficiency[27].

The undisturbed fluid velocity in the stream function is determined from an approximate settling velocity of the aggregate in water using Stokes law. This velocity is recalculated after each particle addition by setting the radius equal to the hydrodynamic radius of the agglomerate. The values used to calculate the velocity in the growth simulations are for alumina in room temperature water: $\Delta\rho=3x10^3$ kg/m^3, g=9.8 m/s^2, and $\eta=10^{-3}$ kg/m·s.

One of the principal objectives of this study was to investigate the influence of form for the relation between R_g and the hydrodynamic radius, R_h, on the structure of the aggregate. R_h can be defined from the abbreviated Einstein-Stokes relation of the translational diffusion coefficient D_t by

$$D_t = (kT)/(6\pi\eta R_h) \qquad 5)$$

where kT is the thermal energy[28]. A colloidal aggregate consisting of a porous network of primary particles has a hydrodynamic radius dependent on the connectivity and distribution of these particles. The greater value of R_h; the greater the screening of the

interior.

It has been shown from theory and experimental observation that the hydrodynamic radius may be related to the radius of gyration[28-31] by

$$R_h = \beta \cdot R_g \qquad 6)$$

where ß is defined as the hydrodynamic ratio. Several different relationships have been used to approximate ß[29-32]. Three cases will be considered here: ß is a constant; Kirkwood-Riseman theory applies; or the Porous-Sphere model applies.

The Kirkwood-Riseman approximation takes into account the hydrodynamic interaction of flexible macromolecules in solution[33] and can be used to define ß[19,34]. Analysis of spherically symmetric fractals indicates that the hydrodynamic radius and radius of gyration are proportional to size of the structure and the fractal dimension[28,35]. ß is then independent of agglomerate size, but is sensitive to fractal dimension following

$$(R_h/R_g)^2 = [2(2+D)(D-1)^2]/[D^3] \qquad 7)$$

in three dimensions[28]. Using the fractal dimension of 2.10 from the silica aggregate experiment the hydrodynamic ratio has a value on the order of 1.04.

The porous sphere model[35] uses the Navier-Stokes equation to describe fluid flow around a stationary structure. With this approximation ß is a function of both fractal dimension and the size of the structure according to

$$R_h/R_g = [(D+2)/D]^{1/2} [1-\kappa^{-1/2}\tanh(\kappa^{1/2})] [1+3/2(\kappa-\kappa^{-3/2}\tanh(\kappa^{1/2}))] \qquad 8)$$

where κ is given by $N^{(D-1)/D}$. The expression leads to a weaker decreasing dependence on the fractal dimension than in the Kirkwood-Riseman approximation. Using a value of $\kappa \approx 100$, appropriate for Wiltzius' experiments[35], and D=2.10, ß = 1.24.

Most of the simulations run in these experiments were carried out assuming ß was a constant. The range of different values used for ß sample the range reported from theory and experiment. It is difficult to apply the Kirkwood-Riseman model in the form developed here since it requires a-priori knowledge of the fractal dimension which is not available in our simulations. Some simulations were carried out using an approximation to the porous sphere model. When data points calculated using Eqn. 8 are plotted as a function of N-particles with an arbitrary fractal dimension near 2.0, the behavior is roughly logarithmic in that there is a rapid increase in ß followed by asymptotic behavior. Therefore an approximation, i.e.

$$\beta = 0.3\text{Log}(N) \qquad 9)$$

was used as an approximation. The constant, 0.3, was chosen to so that the hydrodynamic ratio approaches 1.2 when N=10,000. A comparison of the predictions of Eqn. 8 to that of Eqn. 9 for two typical values of D is shown in Fig. 5.

The model only allows particle attachment over the range of radial distances greater than R_h and less than or equal to R_{max}; R_{max} is defined as the maximum radial distance of a particle in the agglomerate from the center of mass. The growth probability distribution in this zone, where growth is allowed, is also expected to be strongly influenced by the choice of ß. For an N-particle aggregate the interval R_{max}-R_h will depend on the spatial distribution of particles.

The numerical procedure starts with a seed of two particles in contact oriented randomly with their combined center of mass at the coordinate origin. The undisturbed fluid velocity is directed in the positive x direction and has an initial value of 5.44×10^{-7} m/s times ß. The initial range of velocities is therefore $2.82\text{-}7.84 \times 10^{-7}$ m/s. Each incoming particle is introduced upstream along a line segment parallel to the y-axis which intersects the x-axis x_{min}-3r; x_{min} is most negative x-coordinate of a particle in the agglomerate and r is the particle radius, 0.5 μm. The y coordinate of the incoming particle is randomly chosen between y_{min} and y_{max} which are the minimum and maximum y-coordinates of particles in the agglomerate. A streamline of constant potential is determined from the particle's initial coordinates, the undisturbed fluid velocity, and the hydrodynamic ratio. The incoming particle is constrained to follow this streamline until contact, and then a new center of mass, radius of gyration, and fluid velocity are calculated. The center of mass is shifted to the origin, and the aggregate is randomly rotated about this point to maintain uniform growth from any direction. The aggregate does not rotate during particle transport.

Fig. 4 depicts aggregation scheme and shows several streamlines superimposed over an aggregate of 500 particles. The stream function at the random release site is equal to 6.31×10^{-9} m^2/s. In this illustration the hydrodynamic ratio is unity and particles can not penetrate the region bounded by the circle.

Typical simulations consisted of 10,000 particles. The radius of gyration was calculated and stored after each particle addition. The coordinates of all particles and the order in which they were added were also recorded.

5. Modeling Results

Typical structures generated from these simulations are shown in Figs. 6-9. These structures were grown with hydrodynamic ratios of 0.72, 0.85, 1.0, and 1.2, respectively. The circles superimposed on the 10,000 particle aggregates are the final hydrodynamic radii. A total of 5 structures were grown for each of the values of ß with the exception of ß=1.2 for which only 3 structures were grown. As is discussed in section 6, ß=1.2 represents a marginally stable case for agglomeration.

By comparing the structures, it is evident that the degree of ramification was dependent on ß. Increasing the hydrodynamic radius lead to more open structures with distinct large scale branching. The size of the aggregates was interpreted using the radius of gyration and also the maximum radius from the center of mass of a particle in an aggregate. In Fig. 10 is a plot of the mean final radial dimensions with respect to the hydrodynamic radius. These results indicate that increasing R_h leads to larger structures and thus more open since the total number of particles is constant. Between ß=0.72 and 1.0 the effect is nearly linear but deviates from linearity at ß=1.2. The average radius of gyration of these structures was about 60-65% of the average maximum radius.

The average number density was examined to quantify the degree of aggregate ramification. The mean number density was evaluated at 100 randomly chosen points within the radius of gyration for sampling areas 4 and 10 μm in radius. The results indicate that, as evident in Figs. 6-9, the short range number density is inversely proportional to the final value of R_{max}. In addition, the standard deviation associated with the sampling is directly proportional to the value of ß also consistent with the visual appearance of the agglomerates.

The average particle coordination was examined to determine the local connectivity with nearest neighbors. The average number of nearest neighbors is shown in Table 2. There is almost no effect of ß on the local connectivity (the single outlier is at ß=1.2, which is nearly unstable). The coding of the run numbers in corresponds to the initial seed for the random number generator and the value of the hydrodynamic ratio.

Also included for comparison is an effective average coordination number for particles within two diameters of each other. These results indicate that the structures are not densely packed (which would yield CN=18), but it also indicates that they are far from 1-dimensional strings (which would yield CN=4).

The fractal dimension gives an indication of the overall mass distribution of particles within an aggregate. The fractal dimension for each structure was determined by averaging the fractal dimension calculated from three methods: the dependence of the radius of gyration on agglomerate size (evaluated every one hundredth particle addition); the scaling of mass from the center of mass; and the scaling behavior of the pair correlation function. Typical plots of these three methods are shown in Fig. 11 and correspond to the structures shown in Fig. 6 (ß=0.72). The overall average fractal dimension was calculated for 5 aggregates for each value of ß=0.72-1.0 and over 3 aggregates with ß=1.2 then averaged. The length scale over which self-similarity holds was chosen from a visual inspection of the log-log plots to determine the appropriate range for fitting the slope with a linear least squares fit. The fractal dimensions from the correlation function and the point counting method were calculated from length scales covering approximately 6-42% (Ln(r)=-12 to -10) of the maximum radius of the structures. The fractal dimension from the radius of gyration was calculated by excluding the initial growth of 700 particles (Ln(r)=-11 to approximately -9.65). In all cases this interval tested for scaling was several decades in ln(N). When calculating a fractal dimension it was found that the value would fluctuate depending on the choice of length scale, but the fluctuations were very small ±0.05 over the range included in the calculation. The data points used in the calculations are indicated in bold on the figures.

The results of the simulations are tabulated in Table 3, and indicate that ß had almost no effect on the value of the fractal dimension; in all cases the average was ≥1.90. This value is similar to, though slightly less than, the values reported for similar sized simulations using the simple ballistic aggregation model[36]. The average fractal dimension, <D>, was significantly lower, <D>=1.81, in the case of size dependent ß, i.e. the approximation to the porous sphere model. A typical structure resulting from these simulations is shown in Fig. 12 and Table 4 gives the results from 5 simulations.

The fractal dimensions of the aggregate surfaces were calculated using the Plischke and Racz definition of the active zone[13]. The average deposition distance <r> from the center of mass of the growing aggregate was calculated for each one hundredth particle addition. The fractal dimension was then calculated from slope of the log-log plot of N versus <r>. The average surface fractal dimension ($<D_s>$=1.97) was similar to, though slightly greater than, the overall average fractal dimension, and

was also insensitive to the size of the hydrodynamic radius.

Figs. 13 and 14 show the location of the last 2000 particles added to the surfaces of the agglomerates grown with ß=0.72 and ß=1.2. These figures give an indication of the structure of the active zone. The two circles superimposed on these figures represent the location of the hydrodynamic radius at N=8,000 particles and N=10,000 particles, respectively.

The growth probability was examined for two structures ß=0.72 and 1.0 (runs 11 and 13). This probability was measured by releasing probe particles along the y-axis at specified points and determining the point of contact on the aggregate from the center of mass. After contact the particles were discarded and the aggregate was randomly rotated about its center of mass. The points from which the particles were released were: -1.5 μm from the aggregate surface, and y=0.0 to 0.8 by 0.1 increments of the maximum radius. For each of these sites (9 total) 5,000 particles were released, and they were constrained to follow streamlines of constant potential as during growth.

These results are shown in Fig. 15 for ß=0.72 and 1.0 respectively. Distance is normalized by the maximum radial distance from the center of mass of a particle in the respective aggregate. With increasing release height the particles are more likely to strike the aggregate at further radial distances from the center of mass. The mean contact distance for each release height is also given in these figures.

6. Discussion

Modifying the ballistic growth model to include hydrodynamic screening lead to preferential tip growth, which is clearly illustrated in Figs. 13 and 14. When the hydrodynamic radius is much smaller than the maximum radial dimension of the aggregate, the structures are circularly symmetric and relatively compact; nearly indistinguishable from structures grown using the simple ballistic model. Fewer growth sites are available as the hydrodynamic radius approaches the maximum radial dimension of the aggregate. The only branches which will continue to grow will be the ones that offer a substantial number of contact sites beyond the hydrodynamic radius. The active zone in this instance is distinguished by spiked tips touching the hydrodynamic radius. This is the principal difference between structures grown with differing values of ß. The quantitative measures: density (within R_h); aggregate fractal dimension; surface fractal dimension and average particle coordination number (both within 1.1 and 2.0 diameters) are very similar in all cases. The increased standard deviation in the mean local number density with increasing hydrodynamic screening is

a direct reflection of the larger blocks of open space encountered as ß is increased.

One result of these experiments was to define a maximum value for ß at which agglomerate growth is possible. It was found that growing aggregates with ß=1.2 was dependent on the choice of the random number seed. In some instances, relatively few particles were outside of the hydrodynamic radius. These simulations could not maintain continued growth unless extensive computer time was allowed. In the case of ß=1.4, the maximum radius of a particle in the aggregates from the center of mass eventually equaled the hydrodynamic radius and growth was effectively stopped after a short time.

The preferential tip growth observed in these simulations is qualitatively consistent with that observed experimental in two dimensional colloidal aggregation and in DLA simulations. However, the spatial distribution is not equivalent. The higher fractal dimensionality indicates that the density ($\rho \propto r^{D-d}$) of the aggregates in these simulations is less sensitive to agglomerate size. The observed fractal dimensions of these structures are nearly equivalent to those observed using the simple ballistic growth which suggests that $D \rightarrow d$ as $N \rightarrow \infty$.

The fractal dimension was significantly reduced when the hydrodynamic radius was dependent on the aggregate size. This type of simulation produced structures with fractal dimensions about 6% greater than in colloidal aggregation or DLA growth. The precise nature of the scaling function between R_h and N is therefore an area worthy of further investigation.

The expression used to relate ß to size was an approximation to the porous sphere model. The function used, $R_h/R_g = 0.3\text{Log}(N)$, closely followed the behavior of a 10,000 particle structure with D=1.5 although the resulting fractal dimension was <D>=1.81. This lower fractal dimension, when compared to the other simulations, can be explained in terms of the growth conditions as related to the radius of gyration. Initially, the hydrodynamic radius is extremely small and a proportionately smaller region of the interior is screened. As the agglomerate grows the hydrodynamic radius rapidly increases and the amount of screening is increased causing the density to drop as the size increases.

The modified ballistic simulations may provide information on the crossover regime between DLA and ballistic growth, particularly when the drift component is dominant but not strong enough to impose straight line trajectories into the interior of

the aggregate.

REFERENCES

[1]M. P. Allen and D. J. Tildesley, Computer Simulation of Liquids, Oxford Science Publications, Oxford, 1987.

[2]M. J. Vold, "Computer Simulation of Floc Formation in a Colloidal Suspension," J. Coll. Sci., **18** 684-95 (1963).

[3]D. N. Sutherland, "Comments on Vold's Simulation of Floc Formation," J. Coll. Inter. Sci., **22** 300-02 (1966).

[4]P. Meakin, "Models for Colloidal Aggregation," Ann. Rev. Phys. Chem., **39** 237-67 (1988).

[5]D. N. Sutherland, "A Theoretical Model of Floc Structure," J. Coll. Inter. Sci., **25** 373-80 (1967).

[6]D. N. Sutherland, "Chain Formation of Fine Particle Aggregates," Nature, **226** 1241-2 (1970).

[7]D. N. Sutherland and I. Goodarz-Nia, "Floc Simulation: The Effect of Collision Sequence," Chem. Eng. Sci., **26** 2071-85 (1971).

[8]T. A. Witten and L. M. Sander, "Diffusion-Limited Aggregation, A Critical Phenomenon," Phys. Rev. Lett., **47** [19] 1400-03 (1981).

[9]P. Meakin, "Formation of Fractal Clusters and Networks by Irreversible Diffusion-Limited Aggregation," Phys. Rev. Lett., **51** [13] 1119-22 (1983).

[10]M. Kolb, R. Botet, and R. Jullien, "Scaling of Kinetically Growing Clusters," Phys. Rev. Lett., **51** [13] 1123-26 (1983).

[11]J. D. Cawley, "Two Dimensional Agglomeration of Al_2O_3," p. 162-4 in EA-13: Fractal Aspects of Materials: Disordered Systems, A. J. Hurd, D. A. Weitz, and B. B. Mandelbrot, Materials Research Society, Pittsburgh, 1987.

[12]J. L. LaRosa and J. D. Cawley, "Fractal Dimension ofAlumina Aggregates Grown in Two Dimensions," J. Am. Ceram. Soc., **75** [7] 1981-4 (1992).

[13]M. Plischke and Z. Racz, "Active Zone of Growing Clusters: Diffusion-Limited Aggregation and the Eden Model," Phys. Rev. Lett., **53** [5] 415-18 (1984).

[14]P. Meakin and T. A. Witten, "Growing Interface in Diffusion-Limited Aggregation," Phys. Rev. A, **28** [5] 2985- (1983).

[15]P. Meakin, "Structure of the Active Zone in Diffusion-Limited Aggregation, Cluster-Cluster Aggregation, and the Screened Growth Model," Phys. Rev. A, 32 [1] 453-9 (1985).

[16]M. Matsushita, Y, Hayakawa, S. Sato, and K. Honda, "Scaling Properties for the Unscreened Surfaces of Fractal Patterns," Phys. Rev. Lett., **59** [1] 86-89 (1987).

[17]A. Coniglio and H. E. Stanley, "Screening of Deeply Invaginated Clusters and the Critical Behavior of the Random Superconducting Network," Phys. Rev. Lett., **52** [13] 1068-71 (1983).

[18]P. Meakin, H. E. Stanley, A. Coniglio, and T.A. Witten, "Surfaces, Interfaces, and Screening of Fractal Structures," Phys. Rev. A, **32** [4] 2364 (1985).

[19]P. Meakin, H. E. Stanley, A. Coniglio, and T.A. Witten, "Scaling Properties for the

Surfaces of Fractal and Nonfractal Objects: An Infinite Hierarchy of Critical Exponents," Phys. Rev. A, **3 4** [4] 3325-40 (1986).
[20]B. Mandlebrot, The Fractal Geometry of Nature, W. H. Freeman and Co., N.Y., 1983.
[21]J. E. Martin and A. J. Hurd, "Scattering from Fractals," J. Appl. Crystallogr., **20**, 61-78 (1987).
[22]K. Brenkert, Jr., Elementary Theoretical Fluid Mechanics: p301, John Wiley and Sons, Inc., New York, 1960.
[23]*ibid.*, pp. 89 and 300.
[24]K. Brenkert, Jr., Elementary Theoretical Fluid Mechanics: p307, John Wiley and Sons, Inc., New York, 1960.
[25]P. L. Alger, Mathematics for Science and Emgineering: p101, McGraw-Hill Book Co., New york, 1957.
[26]C. F. Gerald and P. O. Wheatley, Applied Numerical Analysis: p21, 3rd Ed., Addison-Wesley Publishing Co., Reading MA., 1984.
[27]J. Fredrick Dirkse, Numerical Simulation of Colloidal Aggregation, M. S. Thesis, Ohio State University, 1990.
[28]Z. Chen, P. Meakin, and J. M. Deutch, "Comment on 'Hydrodynamic Behavior of Fractal Aggregates'," Phys. Rev. Lett., **5 9** [18] 2121 (1987).
[29]P. N. Pusey, J. G. Rarity, R. Klein, and D. A. Weitz, "Comment on 'Hydrodynamic Behavior of Fractal Aggregates'," Phys. Rev. Lett., **5 9** [18] 2122 (1987).
[30]W. Hess, H. L. Frisch, and R. Klein, "On the Hydrodynamic Behavior of Colloidal Aggregates," Z. Phys. B, **64** 65-67 (1986).
[31]P. Wiltzius, "Hydrodynamic Behavior of Fractal Aggregates," Phys. Rev. Lett., **5 8** [7] 710-12 (1987).
[32]P. Meakin, Z. Y. Chen, and J. M. Deutch, "The Translational Frictional Coefficient and Time Dependent Cluster Size Distribution of Three Dimensional Cluster-Cluster Aggregation," Phys. Rev. Lett., **8 2** [8] 3786-89 (1985).
[33]J. G. Kirkwood and J. Riseman,"The Intrinsic Viscosities and Diffusion Constants of Flexible Macromolecules," J. Chem. Phys., **16** [6] 565-73 (1948).
[34]P. Meakin and R. Jullien, "Restructuring Effects in the Rain Model for Random Deposition," J. Physique, **48** 1651-62 (1987).
[35]W. Van Saarloos, "On the Hydrodynamic Radius of Fractal Aggregates," Physica, **1 47A** 280-96 (1987).
[36]P. Meakin, "Accretion Processes with Linear Particle Trajectories," J. Colloid Interface Sci., **105** [1] 240-46 (1985).

Figure Captions

1. Schematic illustration of diffusion limited aggregation (DLA) and ballistic aggregation (BA). In both models a succession of single particles is added to a growing agglomerate (which is an accurate model for very dilute suspensions). The difference between the models is the nature of the trajectory which the particle follows; a straight line for BA and a random walk for DLA. Although the DLA schematic illustrates a lattice based random walk, off-lattice random walks may also be used.

2. Typical results of the DLA and BA models (from ref. 4). The DLA clusters are characteristically open and branched whereas the BA clusters are compact and circularly symmetric.

3. Tracing of images obtained using an optical microscope to observe agglomeration of alumina particles on the lower surface of a drop of a dilute alumina suspension. The large unshaded figure represents a large immobile agglomerate. The direction of a weak convection current is indicated by the arrow. Small agglomerates located with in 'bays,' such as that shaded black, were observed to exhibit only Brownian Motion, whereas those outside the large agglomerate exhibited motion dominated by convection.

4. Schematic snapshot during numerical modeling which illustrates the procedure utilized in the modified ballistic aggregation process. R_h is calculated for the agglomerate using Eqn. 6 with either an assumed value for ß or one calculated with Eqn. 9. R_h for this particular simulation is given by the circle about the agglomerate center of mass. Particles are released at a random location along a line segment up stream from the agglomerate. Particles follow streamlines, calculated using Eqn. 4, until contact with the agglomerate. Any particles which pass the agglomerate are discarded.

5. Plot of the hydrodynamic ratio, either R_h/R_g or ß, as a function of the number of particles in the agglomerate. The open symbols represent data calculated using Eqn. 8 using two different values for the fractal dimension and the crosses that calculated using Eqn. 9.

6. Typical agglomerate calculated using the modified ballistic aggregation model and ß=0.72.

7. Typical agglomerate calculated using the modified ballistic aggregation model and ß=0.85.

8. Typical agglomerate calculated using the modified ballistic aggregation model and ß=1.00.

9. Typical agglomerate calculated using the modified ballistic aggregation model and

ß=1.20.

10. Plot of the maximum radius (distance between the center of mass and the most remote particle) and the radius of gyration for agglomerates of 10,000 particles as a function of hydrodynamic ratio.

11. Typical result used in determining the fractal dimension of a particular agglomerate grown using the modified ballistic aggregation process with ß=0.72: a) the density-density correlation function; b) the number of particles within distance r of the agglomerate center of mass; and c) the radius of gyration as a function of the number of particles in the agglomerate (evaluated for during growth). In all cases the line represents the best fit to the data points indicated by the bold symbols.

12. Typical agglomerate grown using the Eqn. 9 to calculate ß. Note the striking resemblance to the DLA agglomerate in Fig. 2.

13. Illustration of the location 2000 particles added to the agglomerate grown with ß=0.72.

13. Illustration of the location 2000 particles added to the agglomerate grown with ß=1.00.

14. Growth probability as a function of radial distance for agglomerates grown with ß=0.72 and ß=1.20. The growth probability was determined by allowing 5,000 trial particles released randomly along a line segment upstream to strike the agglomerate and averaging the results. No growth was allowed during these trials and the agglomerate was randomly rotated between each trial.

TABLE 1: Fractal Dimensions from Diffusion-Limited Aggregation and Ballistic Growth from Meakin[4] (* off-lattice, † lattice)

Space Dimension	Particle-Cluster	Cluster-Cluster
	Diffusion-Limited Aggregation	
2	1.71*	1.45*
3	2.50*	1.80*
	Ballistic Growth	
2	2.0*†	1.55*
3	3.0*†	1.95*

TABLE 2: Average Coordination Numbers for Singlet Aggregation

	RUN	$CN_{1.1}$	CN/CN_{max}	$CN_{2.0}$	CN/CN_{max}
ß=0.72	11	2.15	0.36	6.00	0.33
	21	2.15	0.36	5.96	0.33
	31	2.15	0.36	5.93	0.33
	41	2.15	0.36	5.96	0.33
	51	2.14	0.36	5.94	0.33
ß=0.85	12	2.18	0.36	6.09	0.34
	22	2.15	0.36	5.96	0.33
	32	2.16	0.36	6.03	0.34
	42	2.16	0.36	6.01	0.33
	52	2.15	0.36	6.00	0.33
ß=1.0	13	2.29	0.38	6.47	0.36
	23	2.16	0.36	6.00	0.33
	33	2.15	0.36	6.07	0.34
	43	2.16	0.36	6.13	0.34
	53	2.16	0.36	6.07	0.34
ß=1.2	14	2.88	0.48	8.48	0.47
	24	2.17	0.36	6.27	0.35
	54	2.17	0.36	6.21	0.35
average	ß=0.72	2.15	0.36	5.96	0.33
	ß=0.85	2.16	0.36	6.02	0.33
	ß=1.0	2.18	0.36	6.15	0.34
	ß=1.2	2.40	0.40	6.99	0.39

TABLE 3: Fractal Dimensions for Singlet Aggregation

	RUN	$D_{C(r)}$	$D_{N(r)}$	$D_{Rg(N)}$	row average	R_g (μm)
ß=0.72	11	1.87	1.89	1.94	1.90	64.1
	&	1.92	1.89	1.96	1.93	63.3
	31	1.90	1.91	1.93	1.91	64.7
	41	1.91	1.89	1.97	1.92	63.4
	51	1.94	1.91	1.94	1.93	63.8
ß=0.85	12	1.88	1.92	1.90	1.90	64.7
	22	1.93	1.90	1.96	1.93	65.1
	32	-	1.92	2.02	1.97	65.9
	42	1.99	1.92	1.98	1.96	66.7
	52	1.91	1.86	1.96	1.91	67.3
ß=1.0	13	2.00	1.86	2.00	1.95	68.3
	23	1.94	1.92	1.91	1.92	71.2
	33	1.93	1.89	1.97	1.93	72.9
	43	1.96	1.89	1.99	1.95	64.8
	53	1.84	1.88	1.87	1.87	71.2
ß=1.2	14	–	1.95	1.99	1.97	81.3
	24	1.86	1.86	1.92	1.88	87.2
	54	1.88	1.88	1.96	1.91	86.9
column average		1.92	1.90	1.95	1.92±0.03	
column average for ß	ß=0.72	1.91	1.90	1.95	1.92±0.01	
	ß=0.85	1.93	1.90	1.96	1.93±0.03	
	ß=1.0	1.93	1.89	1.95	1.92±0.03	
	ß=1.2	1.87	1.90	1.96	1.92±0.03	

TABLE 4: Fractal Dimensions for Singlet Aggregation with the Hydrodynamic Radius as a Function of Size

RUN	$D_{C(r)}$	$D_{N(r)}$	D_{Rg}	row average	R_g (μm)
1	1.89	1.84	1.82	1.85	71.3
2	1.82	1.80	1.81	1.81	74.9
3	1.81	1.85	1.77	1.81	72.4
4	1.83	1.80	1.76	1.80	73.1
5	1.79	1.82	1.74	1.78	73.4
column average	1.83	1.82	1.78	1.81±0.02	

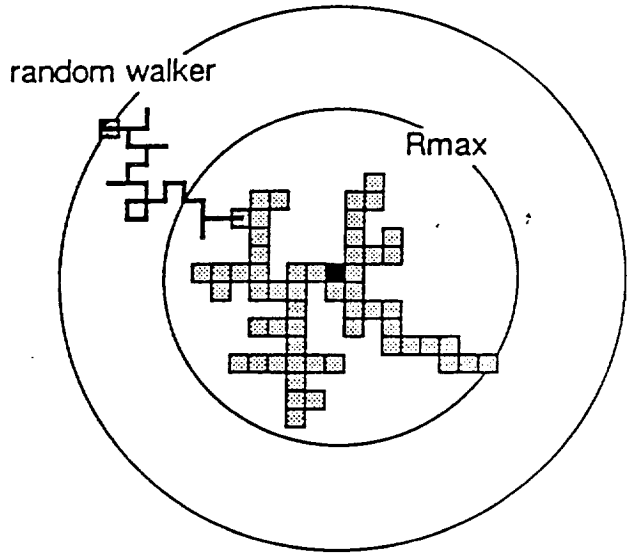

Diffusion Limited Aggregation

- random particle placement
- random walk until contact
- fractal growth: D ≈ 1.71 for 2-d

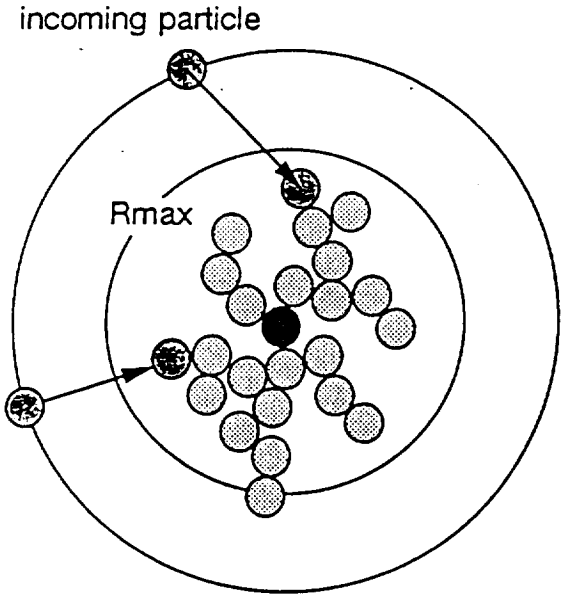

Ballistic Growth Model

- random particle placement
- random linear trajectory
- euclidian growth: D ≈ 2.0 for 2-d

Fig 1

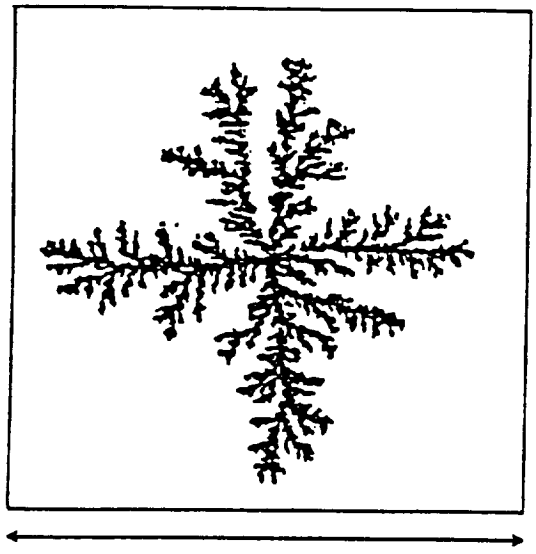

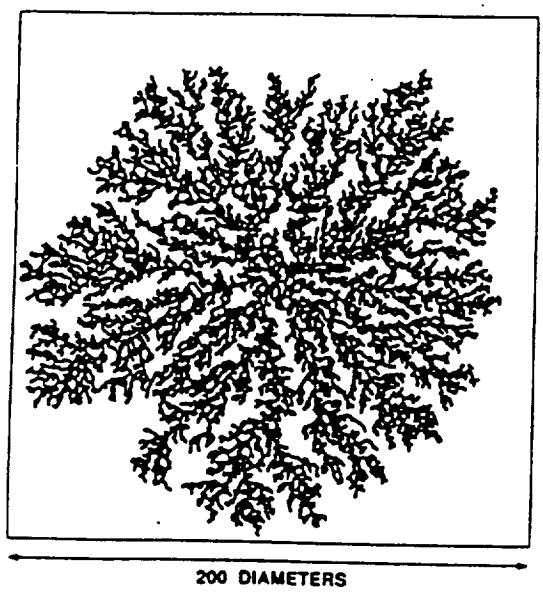

fig 2

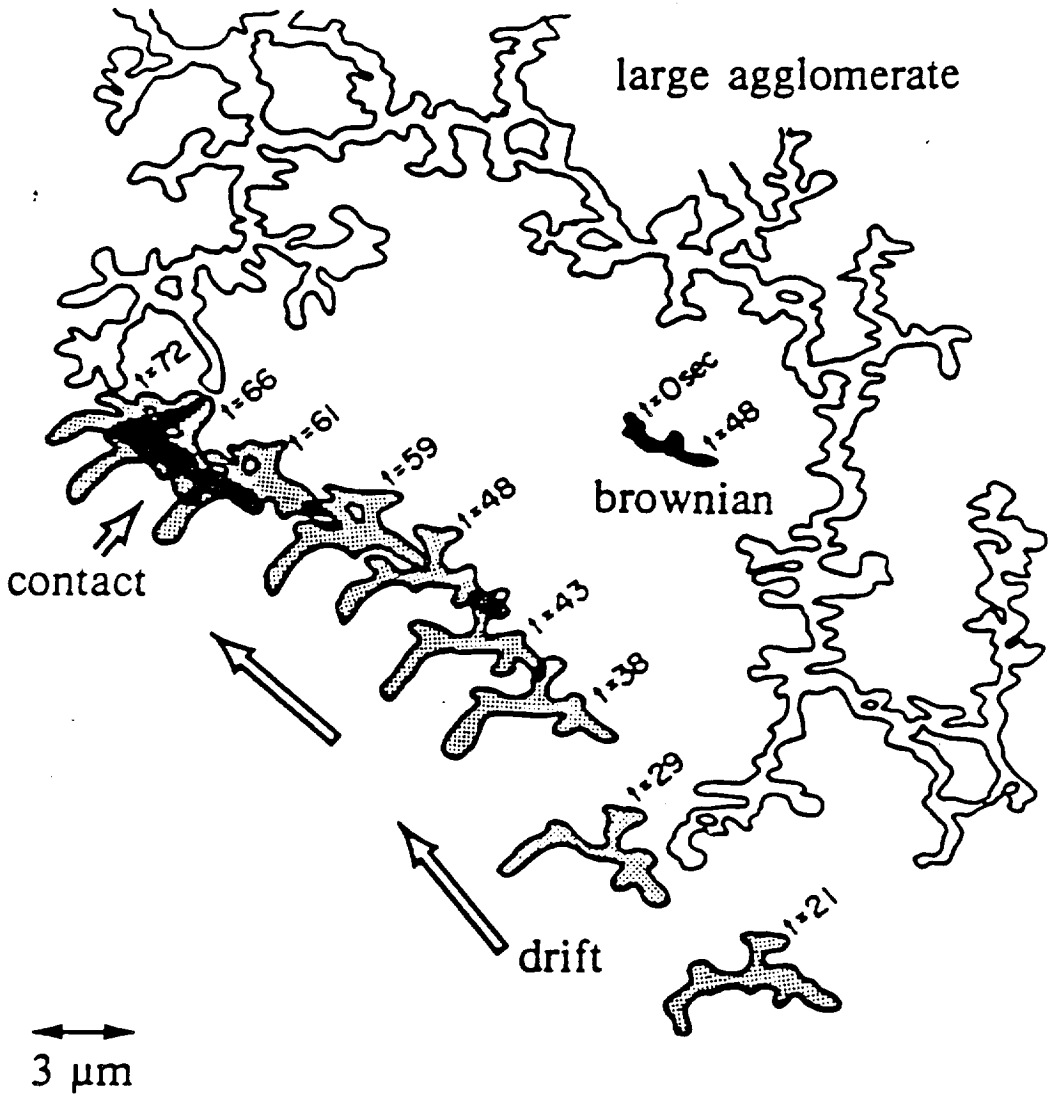
large agglomerate
t=72
t=66
t=61
t=59
t=48
t=0sec
t=48
brownian
contact
t=43
t=38
t=29
t=21
drift
3 µm

fig 3

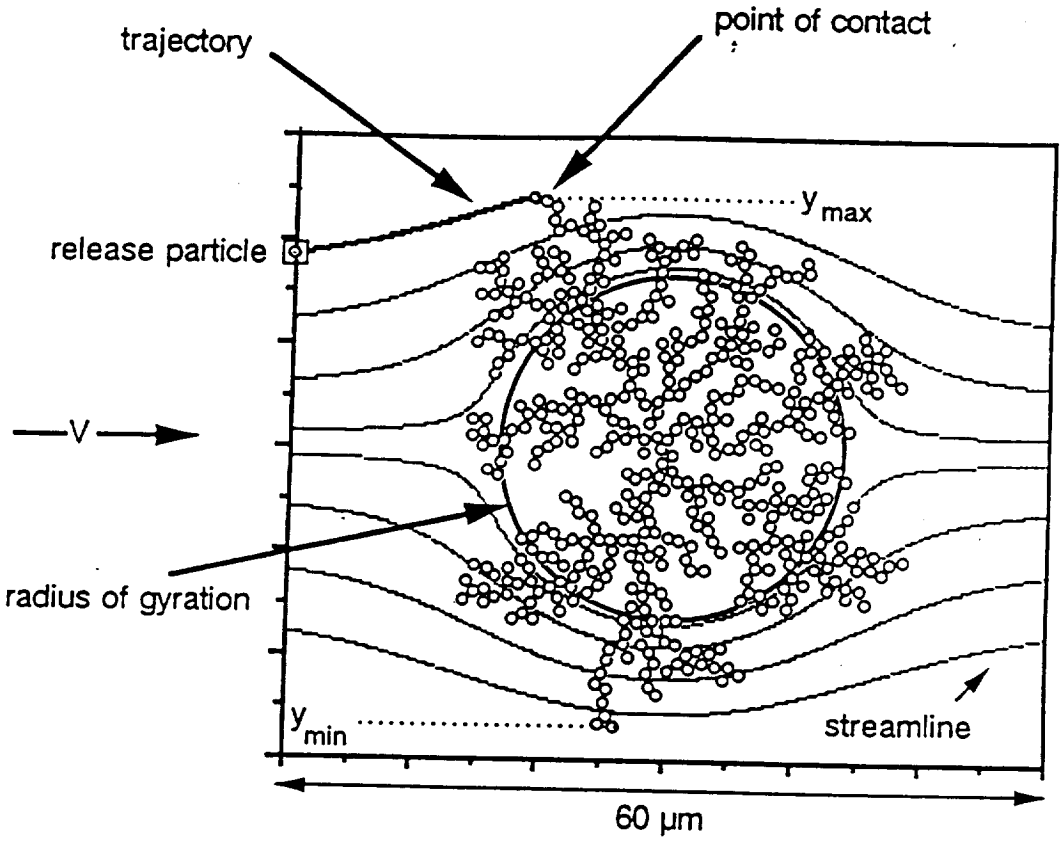

$R_{cylinder} = R_g = 13.8$ µm
$R_{particle} = 0.5$ µm
$V = 0.001244$ m/s
$\eta = 1$cp

Fig 4

Hydrodynamic Ratio as a Function of Aggregate Size

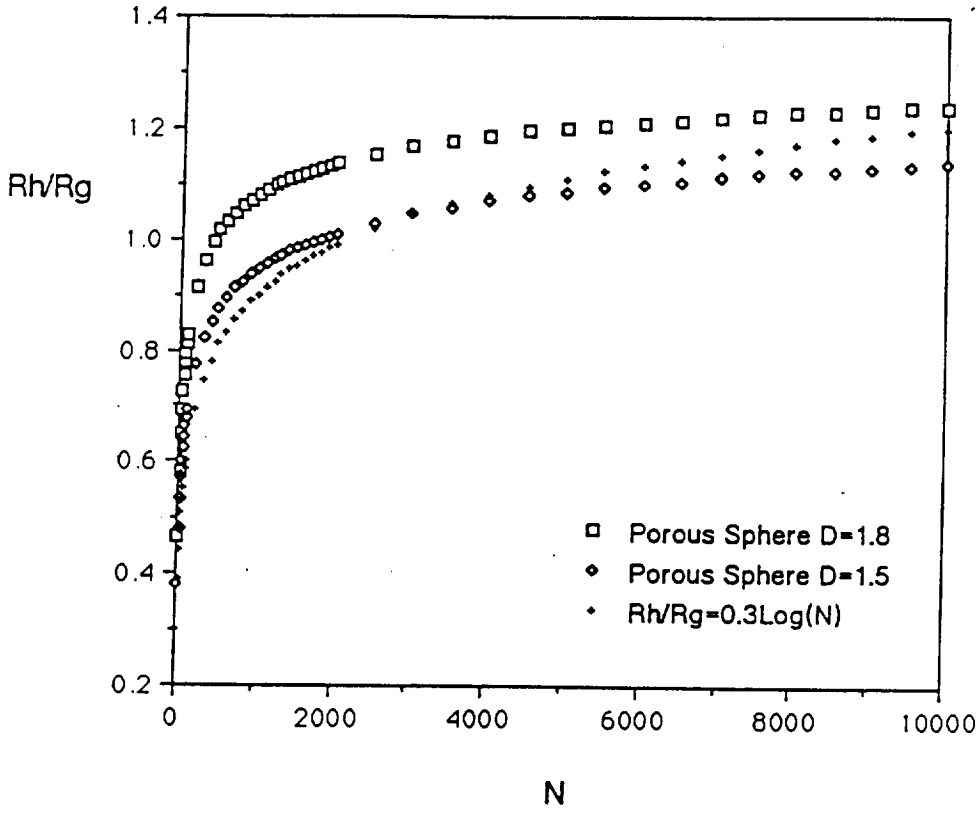

Fig 5

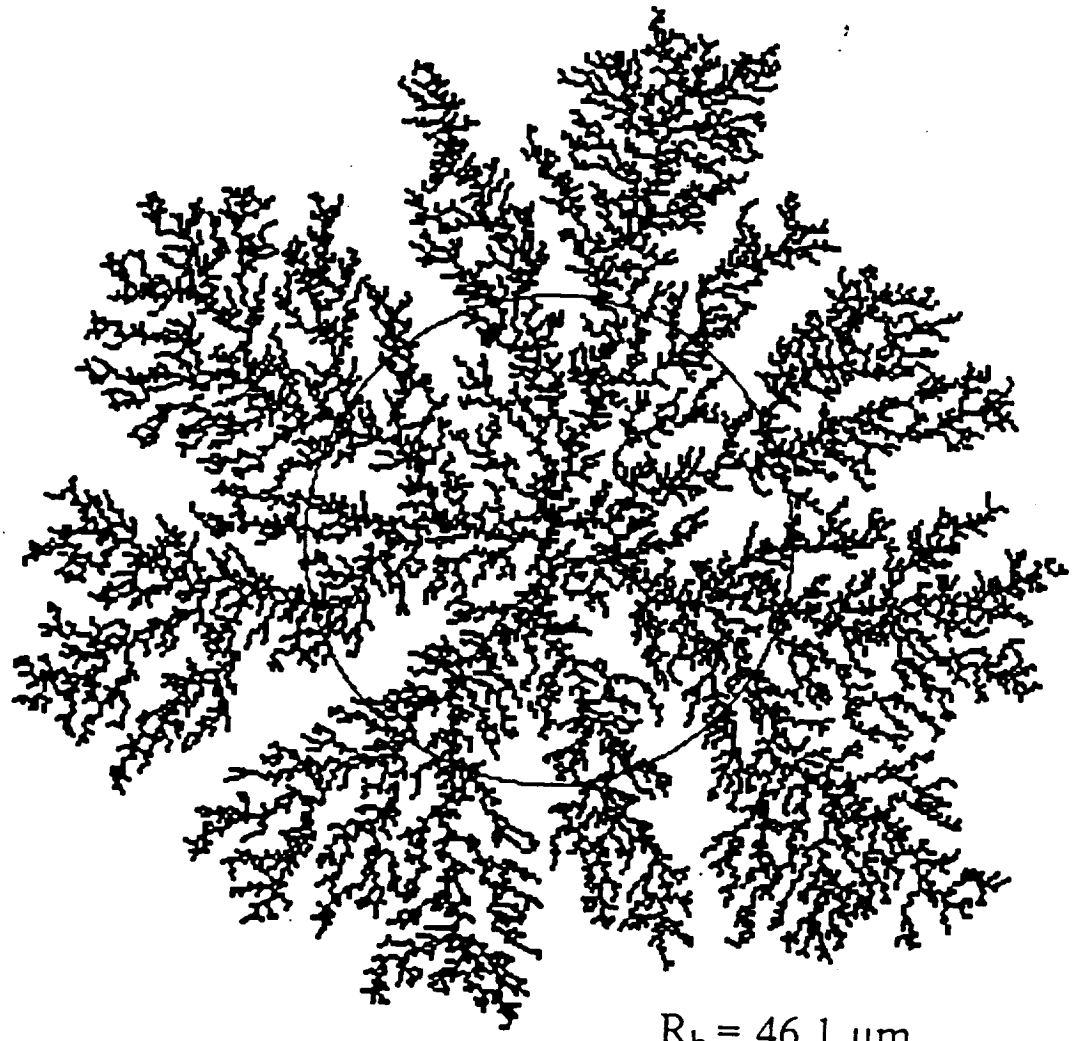

R_h = 46.1 μm

Fig 6

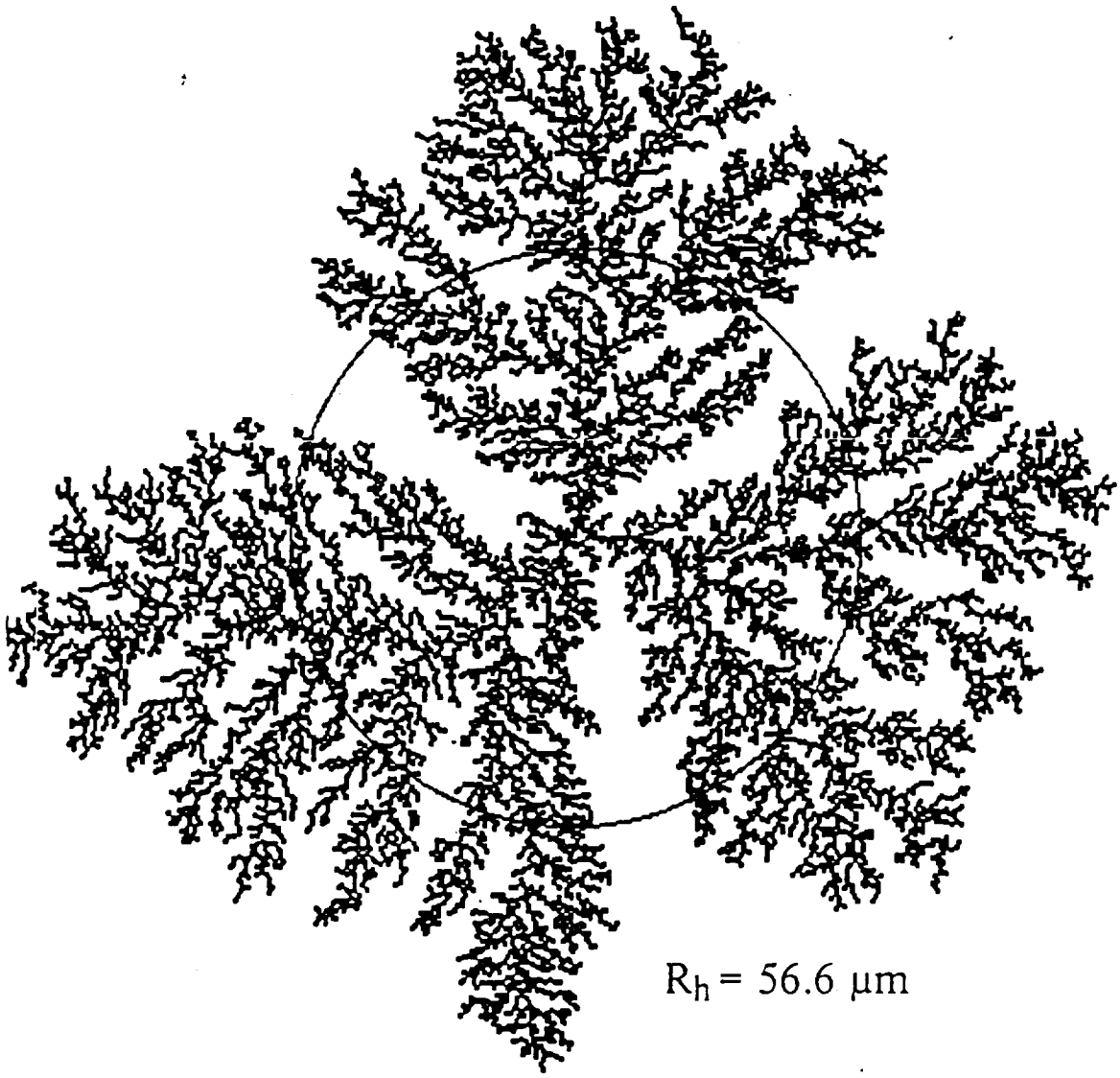

fig 7

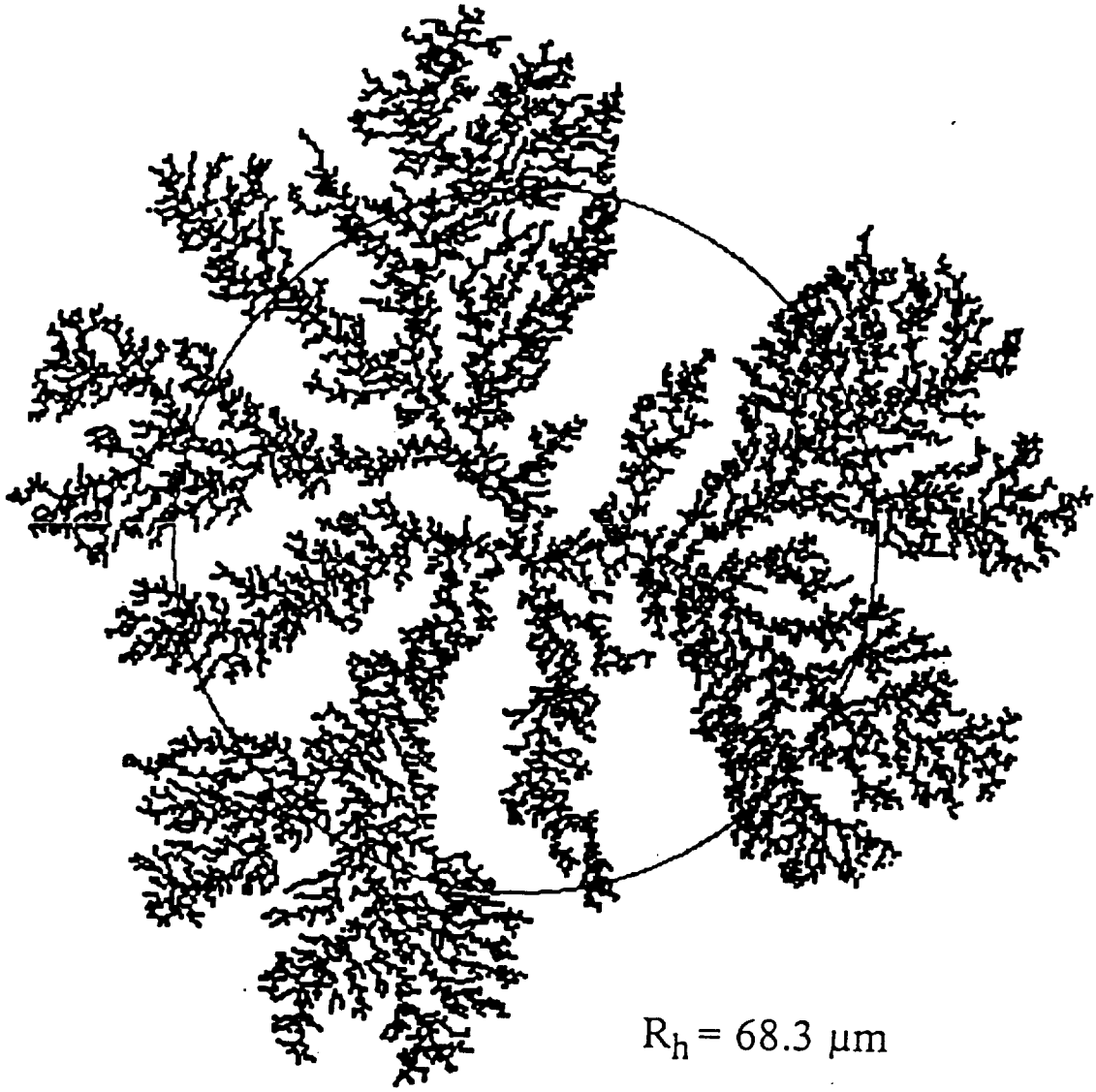

Fig 8

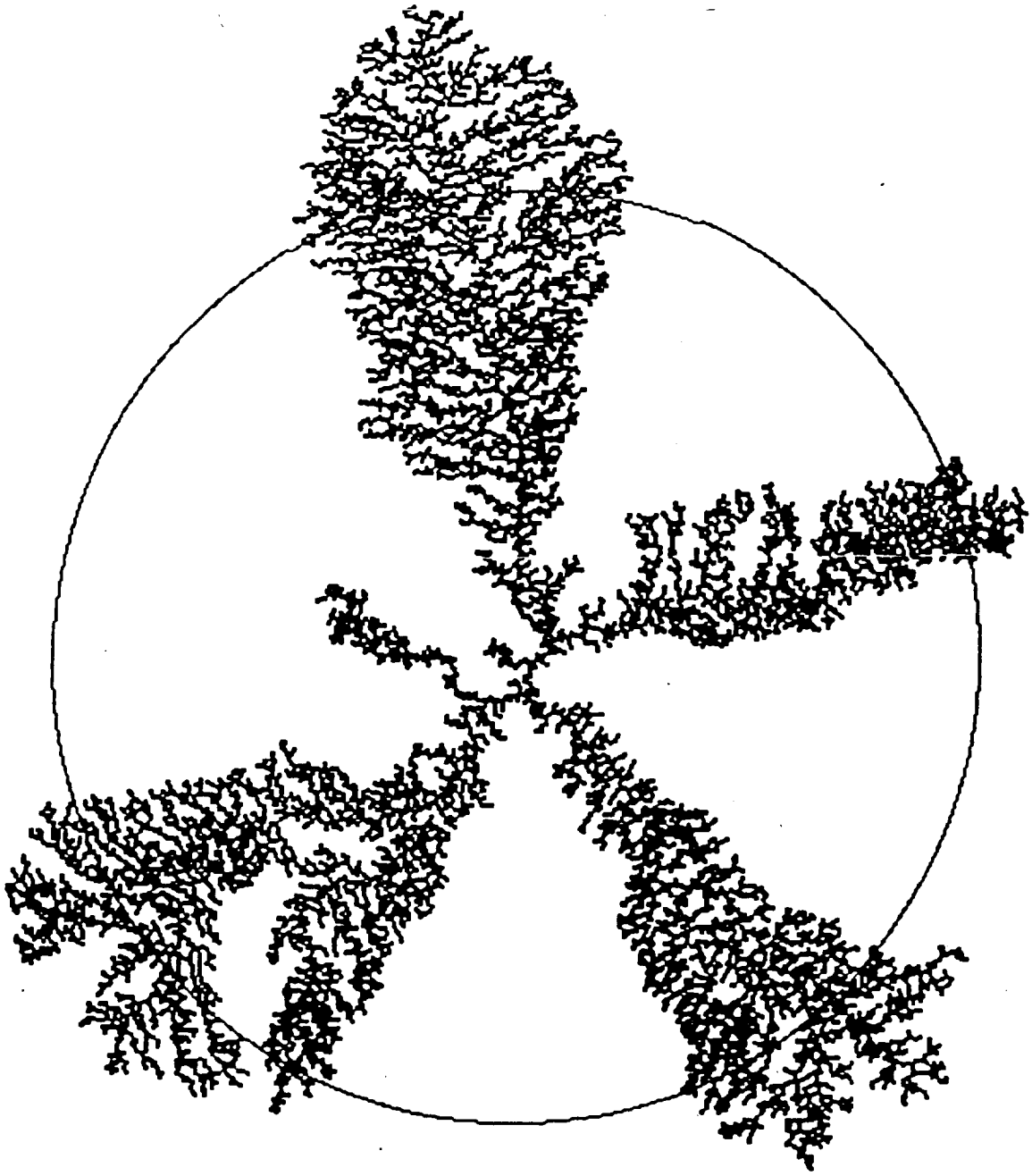

$R_h = 97.5\ \mu m$

fig 9

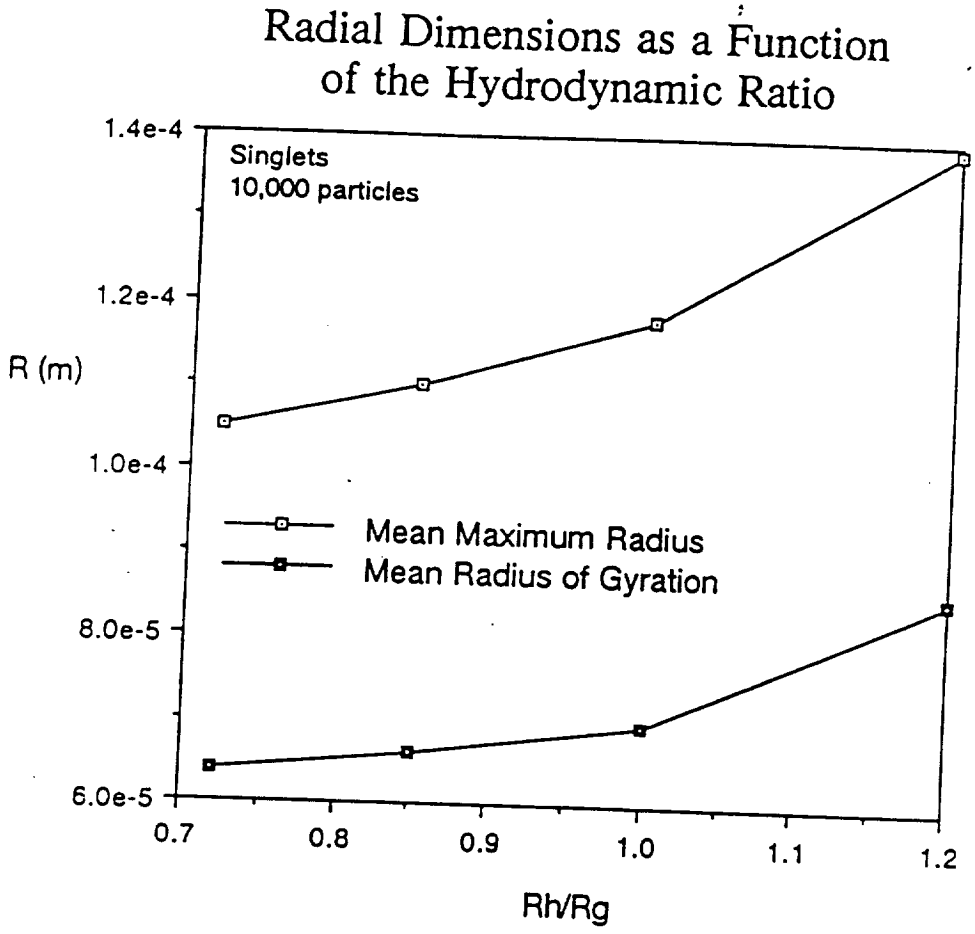
Radial Dimensions as a Function of the Hydrodynamic Ratio
Singlets
10,000 particles
R (m)
1.4e-4
1.2e-4
1.0e-4
8.0e-5
6.0e-5
Mean Maximum Radius
Mean Radius of Gyration
0.7
0.8
0.9
1.0
1.1
1.2
Rh/Rg

Fig 10

Fractal Dimension from the Correlation Function

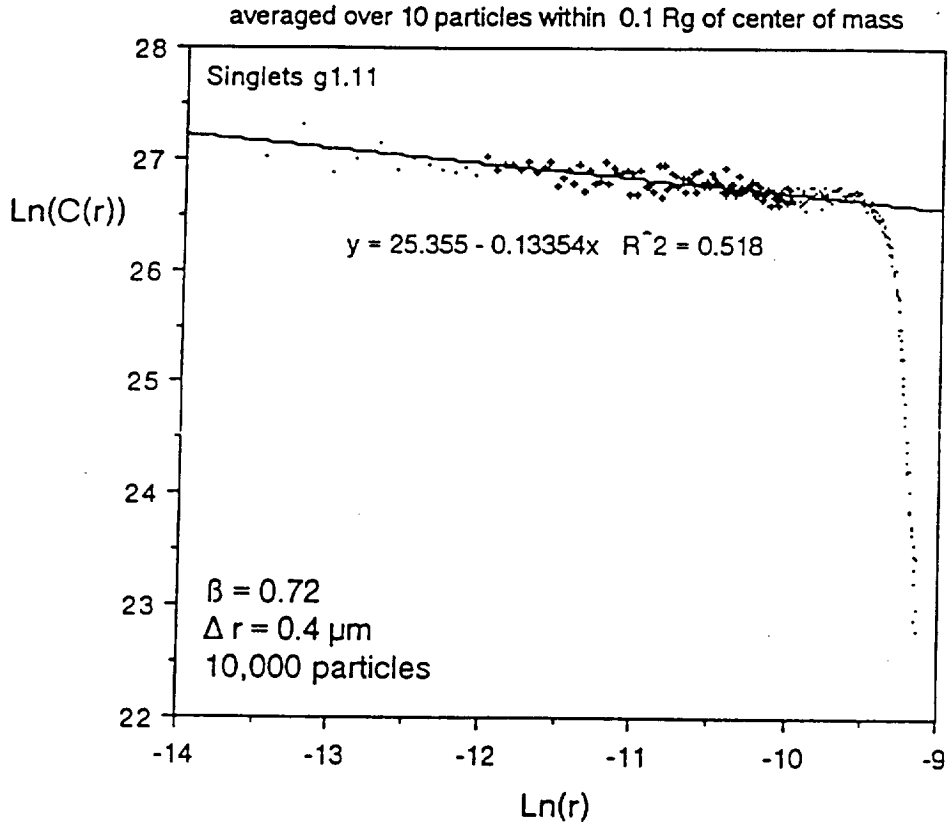

Fig 11a

FIGURE 18 continued

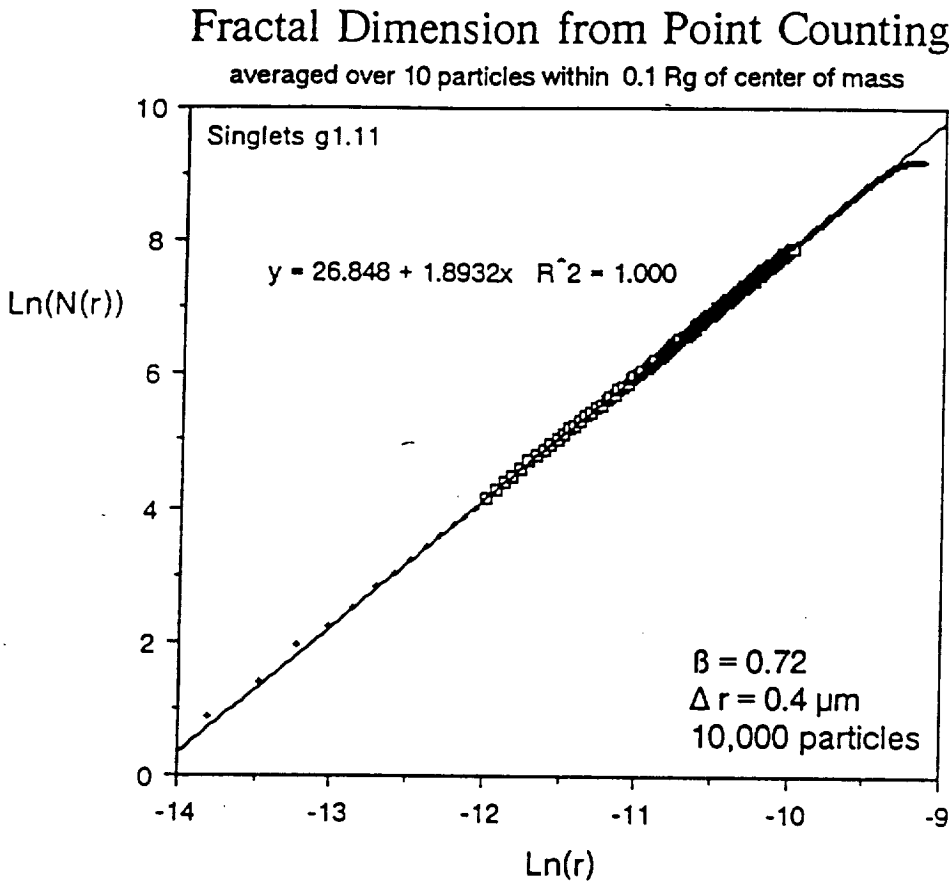

Fig 11b

FIGURE 18 continued

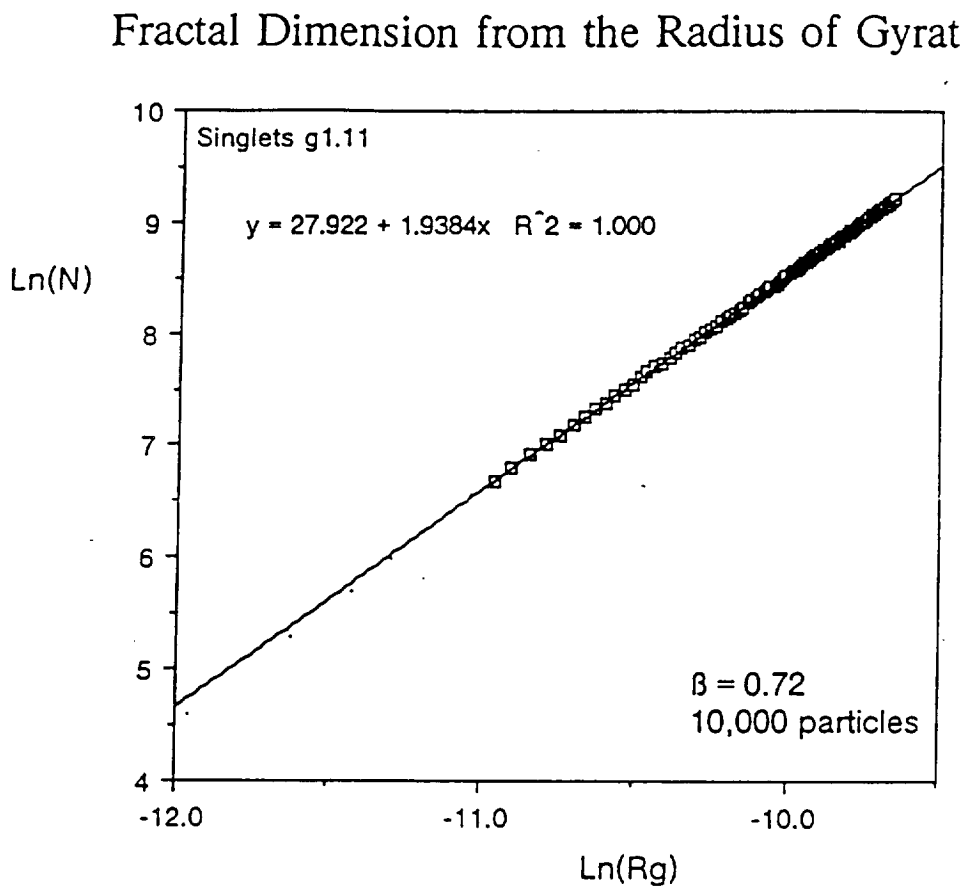

Fig 11c

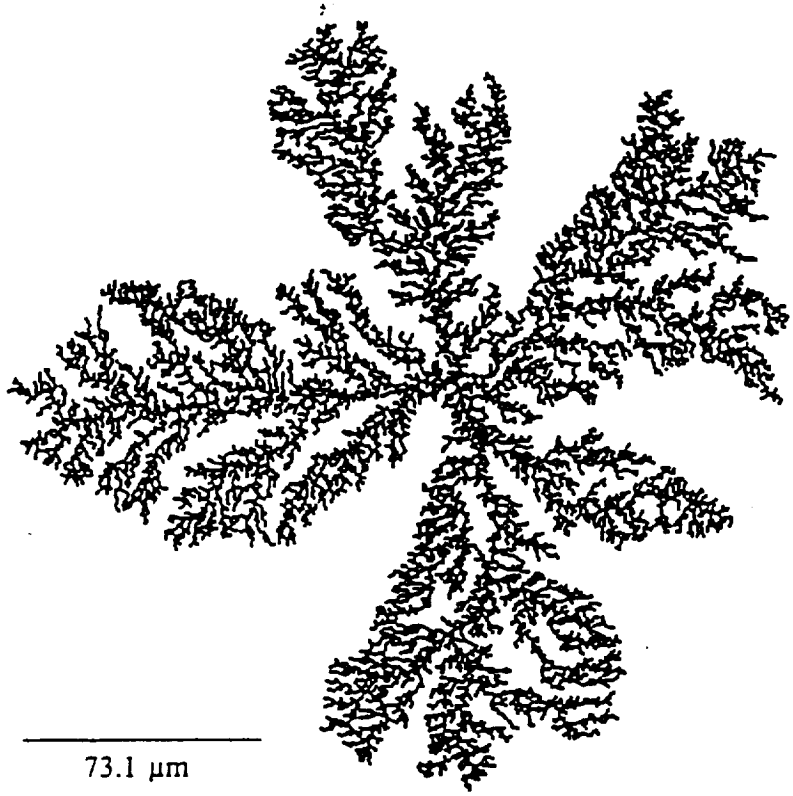

FIG 12

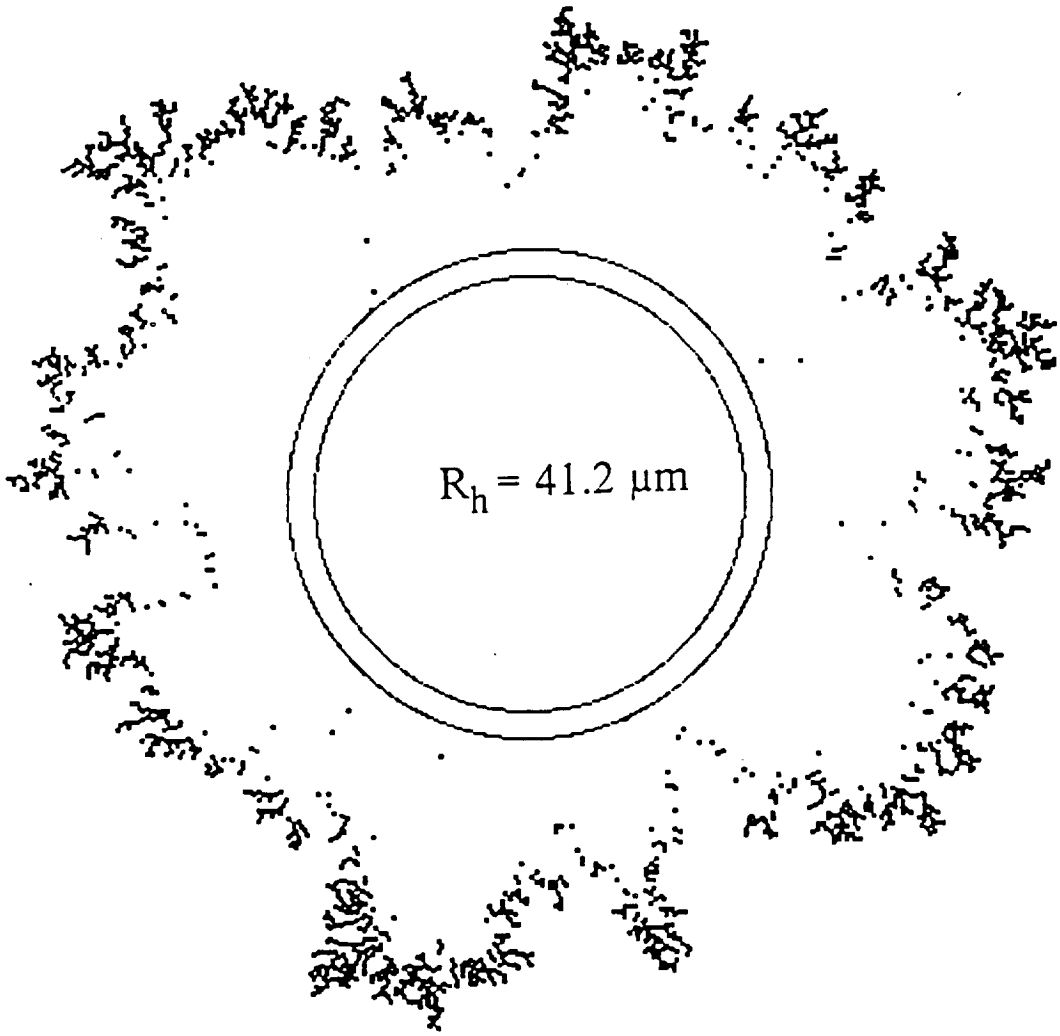

Fig 13

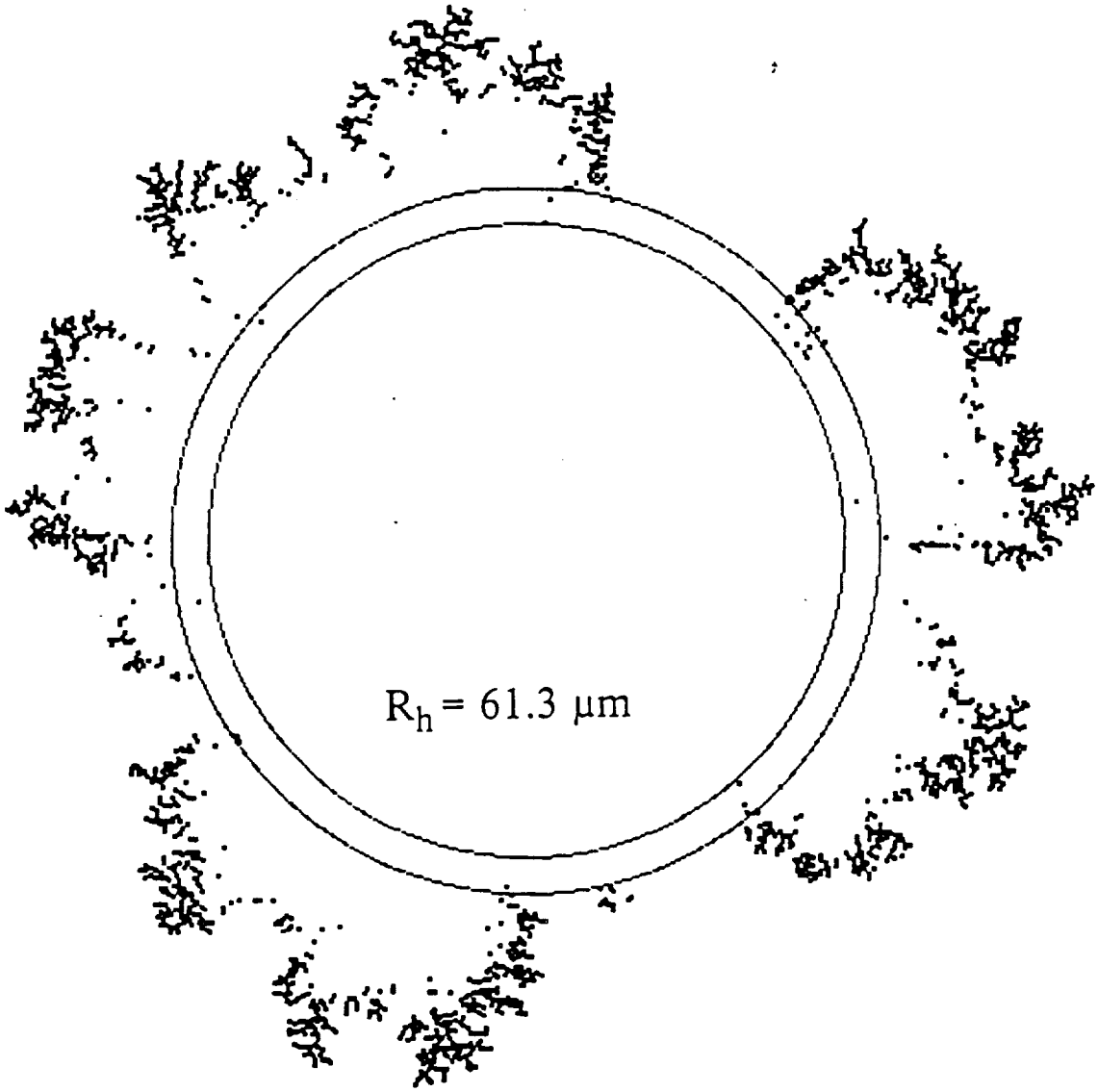

Fig 14

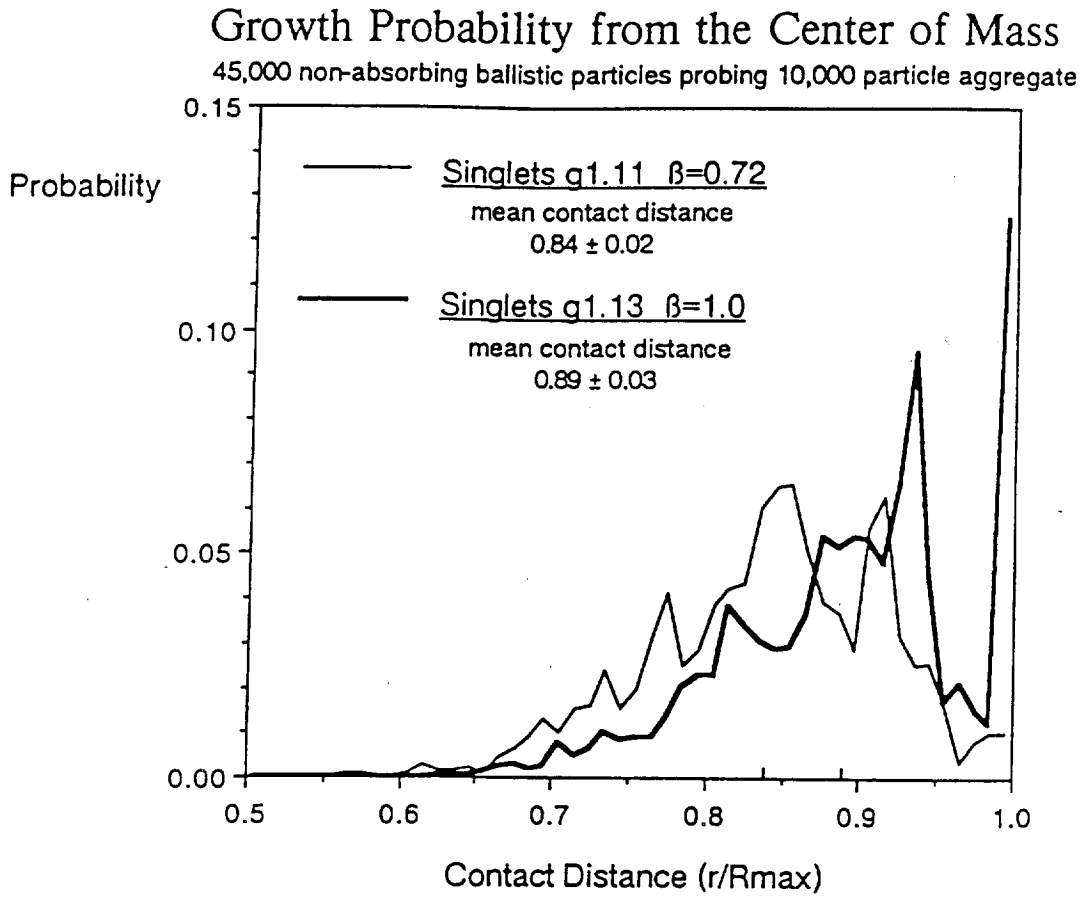
Growth Probability from the Center of Mass
45,000 non-absorbing ballistic particles probing 10,000 particle aggregate
Probability
0.15
0.10
0.05
0.00
Singlets g1.11 ß=0.72
mean contact distance
0.84 ± 0.02
Singlets g1.13 ß=1.0
mean contact distance
0.89 ± 0.03
0.5
0.6
0.7
0.8
0.9
1.0
Contact Distance (r/Rmax)

Fig 15

Numerical Simulation of Particle Rearrangement Within an Agglomerate During Settling Under Gravity

J. F. Dirkse* and J. D. Cawley**

Department of Materials Science and Engineering

Ohio State University

ABSTRACT

A numerical procedure based on the velocity form of the Verlet algorithm was developed and employed to model the behavior of van der Waals bonded agglomerates during settling under gravity. The results illustrate the effect of friction and hard agglomerates on restructuring after contact with an impermeable boundary.

This work was supported by National Aeronautics and Space Administration through grant NAG3-775.

* currently with Tresp Associates, Energy Associates Group, Oakland, CA.

** currently with Case Western Reserve University, Dept. of Materials Science, Cleveland, OH.

1. Introduction

One definition of an agglomerate is a ensemble of particles which move as a single flow unit. However, in many ceramic forming operations this definition breaks down during the last stages of processing. For example, during centrifugation a sufficiently small agglomerate may settle as a rigid body until it encounters the bottom of the container or, in the case of slip casting, small floccs may move as flow units until reaching the surface of the porous mold. In both of these cases, forces on the particles may become large enough to cause restructuring of the agglomerate after contact is made. Certainly, particle rearrangement occurs as the dimensions of the cake increase.

As discussed below, numerical scheme was developed, based on the Verlet Algorithm, to model the restructuring of a agglomerate under a gravitational load. This problem is technically relevant; it is also the simplest to model since the gravitational force on each particle is independent of the particle arrangement unlike the hydrodynamic drag in slip casting.

The restructuring process was examined using a two dimensional simulation with an aggregate consisting of 51 particles. This initial agglomerate was produced using a modified ballistic aggregation model[1]. Particles were added to growing agglomerate as triplets (equilateral triangles). No rearrangement was allowed during growth; particles of a given triplet were considered fixed as soon as contact was made and a new triplet introduced. This aggregate, with an identical initial particle positions, was used in all simulations and is illustrated in Fig. 1. This initial configuration represents the time at which the lowest particle has just established contact with the bottom of the container.

Both the particle interaction potentials and the strength of the gravitational field were allowed to vary in the simulations. In one class of simulations all of the fifity-one

particles were allowed to move independently, i.e. attractive interactions were due to van der Waals forces, as defined below. These simulations thus give an indication of the type of result to be expected for soft agglomerates of nearly spherical particles. In the second class, the particles within the seventeen original triplets interacted with a symmetric Hooke's law, i.e. behaved as hard agglomerates bonded by solid bridges, whereas attractive interactions between particles of different triplets were of van der Waals type. The latter are the easiest nonspherical shape to include in these type of simulations and have the general characteristic of all nonspherical particles, i.e. particular orientations of two such particles will lead to stronger bonding.

In addition, each particle was subject to a constant downward force due to gravity which varied from 0 to 1 to 100 times natural gravitation. One additional variable was the nature of the boundary condition at the bottom of the cell. In all cases gravitational force is removed as particles touched the bottom of the simulation cell. For one type of boundary condition, termed 'slip,' no further constraint was applied (i.e. particles were free to move parallel to the cell boundary) whereas the other type of boundary, termed 'stick' the position of the particle was fixed as soon as it touched the boundary. Any real surface will exhibit behavior in between these two limiting cases; the former corresponds to a frictionless surface whereas the later corresponds to infinite friction coefficient.

The interparticle potential consists of an elastic repulsive term and a macroscopic attractive term. For the purposes of computational efficiency, the simplified form of the Van der Waals potential was used,

$$\Phi_{vdw}=-Ar/(12s) \qquad (1)$$

where Φ_{vdw} is the interaction energy, A is the Hamaker constant (4.12×10^{-20} J for non-retarded interaction of alumina in water[2]), r is the particle radius, and s is the surface to surface separation. This form is accurate for surface-surface separations much less

than the particle radius (s<<r), and always over-estimates the energy of the full expression. Since the Hamaker expression predicts an infinite negative energy at contact, an equilibrium energy Φ_o is assumed. This energy is equated to the value of the potential energy (Eqn. 1) at s=0.01 μm so that Φ_o=-1.72x10^{-19} J, or about 42 times the thermal energy kT at room temperature. Using this expression the van der Waals force is equal to the gravitational force on a 1 μm alumina particle at s=0.29 μm for 1g and s=0.029 μm for 100g. At closer distances the van der Waals force is always larger than the gravitational force.

The repulsive energy term used in these simulations is of the form

$$\Phi_{rep} = (Cs^2)/2 + \Phi_o \qquad (2)$$

where C is a constant equal to 1.72x10-3 N/m. This value was chosen for the constant to give a repulsive force at s=-0.01 μm (i.e. particle overlap) of the same magnitude as the attractive force at s=+0.01 μm. The force between two particles, F_{ij}, was evaluated using the derivative of the sum of Eqns. 1 and 2 with respect to s, i.e.

$$F_{ij} = Ar/(12s_{ij}^2) - Cs_{ij} \qquad (3)$$

where s_{ij} is the separation between the surfaces of particles i and j. The attractive term is calculated only for s>0 and the repulsive term for s≤0. In calculating the attractive term, surface separations were shifted by +0.01μm to allow Φ to approach Φ_o at contact.

Particle motion, which allows the restructuring, is accomplished using the velocity form of the Verlet algorithm[3,4]. This algorithm is a central difference solution of Newtons law F=ma. The equation relating position, p, at time t+Δt to position p, velocity v, and acceleration, a, at time t is

$$p(t+\Delta t) = p(t) + v(t)\Delta t + \Delta t^2 a(t)/2 \qquad (4)$$

and the new velocity at the same instant, t+Δt, is

$$v(t+\Delta t) = v(t) + \Delta t\,[a(t)+a(t+\Delta t)]/2 \qquad (5)$$

where the acceleration term is calculated from a superimposition of gravitational forces on a pairwise sum of the interparticle forces according to Eqn. 3 substituted in Newton's law. The timestep Δt must be small enough for the acceleration term to be nearly constant during Δt. The error is on the order of Δt^2 for each pass through the equations[5].

The numerical stability of Verlet simulations is sensitive to particle interaction near the energy minimum. Without proper damping forces, the kinetic energy of particles can climb to artificially high values. The restructuring simulations are kept stable by maintaining a nearly constant kinetic energy for the N=51 particles. The total kinetic energy at time t is computed and compared to a constant thermal energy NkT, where k is Boltzmann's constant and T is room temperature. The square root of this ratio determines the magnitude of velocity scaling for time $t+\Delta t$. The scaling factor is multiplied against $v(t+\Delta t)$ to obtain an adjusted velocity in the form

$$v(t+\Delta t) = v(t+\Delta t)[2NkT/(m\Sigma v_i(t)^2)] \qquad (6)$$

where $\Sigma v_i(t)^2$ represents the sum of the squares of all of the individual particle velocities. Simulations assumed 1 μm diameter alumina particles with a mass, m, of 2.09×10^{-15} kg. The position and velocity data at 't' is then over written, the time counter incremented by Δt, and new values for position and velocity are calculated. This process is repeated until the desired time period has elapsed. All simulations were conducted for a total period of 0.1 seconds using a timestep of 10^{-7} seconds. Initial particle velocities and forces were set to zero at the start of the simulations. Forces acting on each particle were only computed for particles within 2 μm (or particle diameters) of the particle under consideration.

Simulation results include the initial and final positions as well as average coordination numbers.

2. Results and Discussion

The results of the simulation are presented in two forms. The first is a graphical images, Figs. 2-5. These figures were generated by superimposing the particle configurations for each time step on a gray background and then subsequently erasing it. Thus the particle paths trace out an unshaded region. The particle configuration corresponding to the last time step is shown by the positions of the filled circles.

The average coordination number as a function of the gravitational force, boundary conditions, and the particle configuration are listed in Table 1. A particle was considered to be coordinated with another when their center-center separation was less than or equal to 1.1 times their diameter. The coordination number was evaluated after the final time step (0.1 seconds) in all of the simulations.

The initial condition, Fig. 1, is characterized by point contacts between the triplets. The average coordination number must be in excess of two since each particle touches two others in the original triplets and further connections are established during the formation of the agglomerate. The average coordination number is 2.82 which is consistent with Fig. 1 in which it is evident that most particles are three fold coordinated, but a significant number (those around the periphery) are two fold coordinated.

Under 0 g, the restructuring is entirely due to the attractive potential. As is evident in Fig. 2, these structures have retained an overall structure similar to the initial agglomerate, but have become locally more densely packed. The nature of the boundary condition did not affect these results since the interparticle force causes all of the particles to move toward the agglomerate center of mass and therefore the lowest particle was drawn off of the boundary at the beginning of the simulation. Very

little difference is seen between the singlet and triplet interactions. Both appear nearly hexagonally close packed, but the triplet interaction result in slightly more efficient packing this is seen in the average coordination numbers (3.45 for triplets versus 3.26 for singlets) and can be visually detected in the figures (for example, in the left-hand most arm of the agglomerates where the ten particles making up this arm appear fully hexagonal for the triplets, but contain gaps for the singlets). It is presumed that if the simulations were allowed to run for additional time the singlets would assume the same configuration as the triplets. The latter achieve this local minimum in energy more rapidly due to the stronger nature of the Hookean interaction potential.

The results of the simulations run for 1 g yield structures, see Figs. 3 , which are very similar to those from the 0 g simulations except that they have rotated about the first contact point until they touch at a second location. In addition local rearrangement leads the flattening of the structure immediately adjacent to the contact points. The similarity is evident in comparing figures as well as the average coordination numbers. In the case of singlets the average coordination number increases slightly, from 3.26 to 3.29, due the presence of gravity. In contrast the average coordination number for the triplets decreases slightly from 3.45 to 3.41. It is believed that this results from a disruption in the local packing efficiency in the regions adjacent to the point contacts as the structure attempts to confirm to the flat surface. As in the 0 g case, the nature of the boundary condition does not produce any effect on the nature of the structure which is consistent with the fact that gravity is insufficient to break the agglomerate structure.

At 100 g's the effect of both the boundary condition and the nature of the particle interaction (singlets versus triplets) is very evident. Fig 4 shows the results of a simulation assuming a stick boundary condition. For triplets the results are very similar to the 1 g simulation. Apparently pinning the two contact points is sufficient to stabilize the entire structure except for most right-hand arm of the agglomerate which pivots as

a rigid structure until it lays on top of the portion of the agglomerate in direct contact with the cell boundary. In contrast, the singlets collapse to a much greater degree leaving far less void space at the bottom of the simulation cell and no extended arms anywhere on the structure. These results demonstrate the potentially dramatic effect of small hard agglomerates (or more generally nonspherical particles) on restricting local rearrangement to achieve more efficient packing under an applied load. This is also evident in the average coordination numbers, 3.45 for stick boundary and 3.88 for the slip boundary. The former is the same as for the triplet structure at 0 g whereas the latter is substantially greater than the values observed for singlets under either 0 or 1 g.

The difference is nearly as dramatic for simulations run with the slip boundary condition, see Fig. 5. In this case the singlets have achieved a nearly hexagonally close packed structure with a low center of mass whereas the packing of the triplets is far less efficient and fewer particles are in contact with the cell boundary. Again these observations are evident in the average coordination numbers, 4.47 for singlets and 3.80 for triplets. Although the latter is significantly higher than that observed for triplets with the stick boundary condition, a larger difference is observed between the former and singlets with the stick boundary condition.

3. Summary

The algorithm which was developed based on a standard molecular dynamics procedure appears to be robust and suitable for modeling the behavior of agglomerates under settling. The results are consistent with the fact that under 0 and 1 g particle rearrangement in these small agglomerates is dominated by the interparticle forces rather than gravity. This leads to restructuring only on a local level. The effect of friction and particle shape are directly observable in these simulations. Under high g-fields, the sticking condition restricted lateral movement on the bottom of the simulation cell and lowered the final particle coordination. This effect was more pronounced with

triplets.

REFERENCES

[1]J. F. Dirkse and J. D. Cawley, "A Modified Ballistic Aggregation Model," submitted to the J. Am. Ceram. Soc.

[2]S. Ross and I. D. Morrison, Colloidal Systems and Interfaces: p226, John Wiley and Sons, Inc., New York, 1988.

[3]L. Verlet, "Computer 'Experiments' on Classical Fluids. I. Thermodynamical Properties of Lennard-Jones Molecules," Phys. Rev., 159 [1] 98-103 (1967).

[4]M. P. Allen and D. J. Tildesley, Computer Simulation of Liquids:p81, Oxford University Press, New York, 1987.

[5]C. F. Gerald and P. O. Wheatley, Applied Numerical Analysis: p21, 3rd Ed., Addison-Wesley Publishing Co., Reading MA., 1984.

Figure Captions

1. Initial configuration of particles used all simulations. This arrangement was generated using a modified ballistic aggregation routine in which triplets of particles (arranged in equilateral triangles) were added to the growing structure. In all of the simulations termed "triplets" a symmetric Hooke's law potential was assumed between particles within a given triplet and a van der Waals potential was used between particles in different triplets. For simulations termed singlets, a van der Waals type potential was used between all particles including those which arrived as part of the same triplet.

2. Particle configurations after 0.1 seconds under zero gravity. The particles have moved in response to local coordination as a result the attractive interparticle potential. Very little difference is seen between the singlet and triplet results. Identical particle packing is observed for both the slip and stick type boundary conditions.

3. Particle configurations after 0.1 seconds under a 1 g gravitational field. The particles have moved in response to the local environment and, in addition, the entire structures have rotated to establish two points of contact with the cell boundary. The type of boundary condition does not significantly affect the packing.

4. Particle configurations after 0.1 seconds under a 100 g gravitational field assuming a stick type boundary condition. For the triplets the structure is only modestly different from that observed for for a 1 g load. In contrast, for the singlets a much denser packing is observed.

5. Particle configurations after 0.1 seconds under a 100 g gravitational field assuming a slip type boundary condition. Denser packing are observed for both triplets and singlets. In the case of the triplets, the shape of the hard agglomerates interferes with the local packing efficiency resulting in a more open arrangement.

TABLE 1 Average Coordination Numbers after 100 ms

	Singlet	Triplet
	2.82 initial	
0 g	[3.26] (3.26)	[3.45] (3.45)
1 g	[3.29] (3.29)	[3.41] (3.41)
100 g	[3.88] (4.47)	[3.45] (3.80)

() = slip boundary condition
[] = stick boundary condition

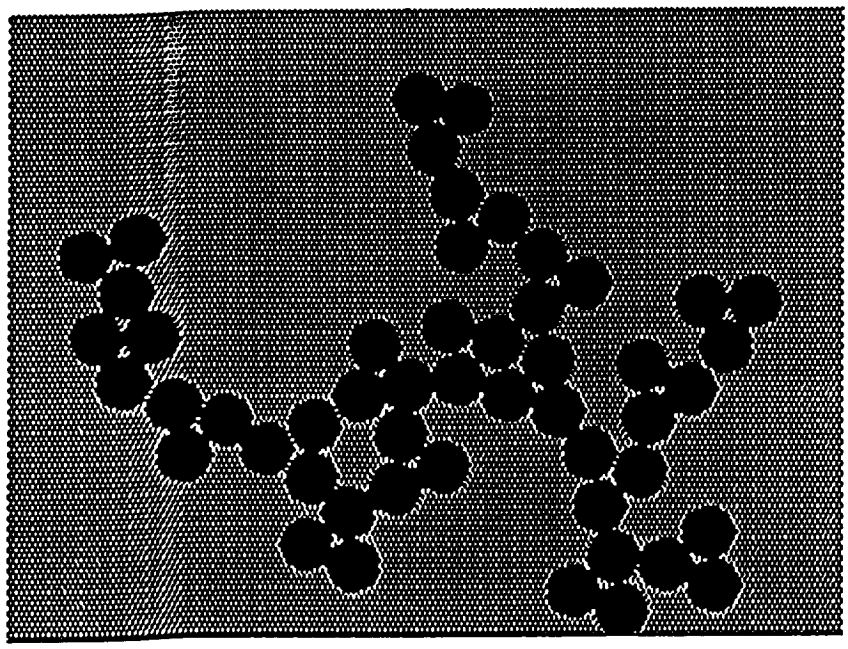

FIG

Singlet Interaction

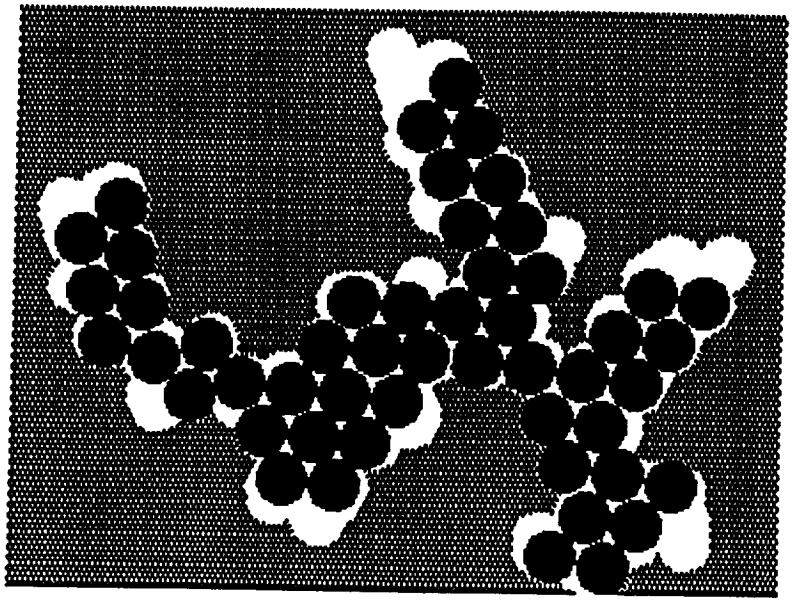

Triplet Interaction

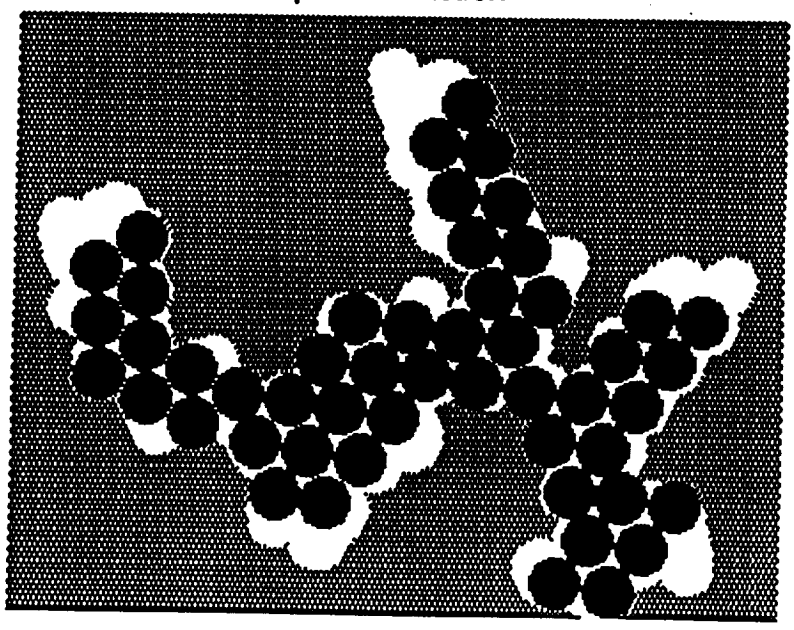

Singlet Interaction

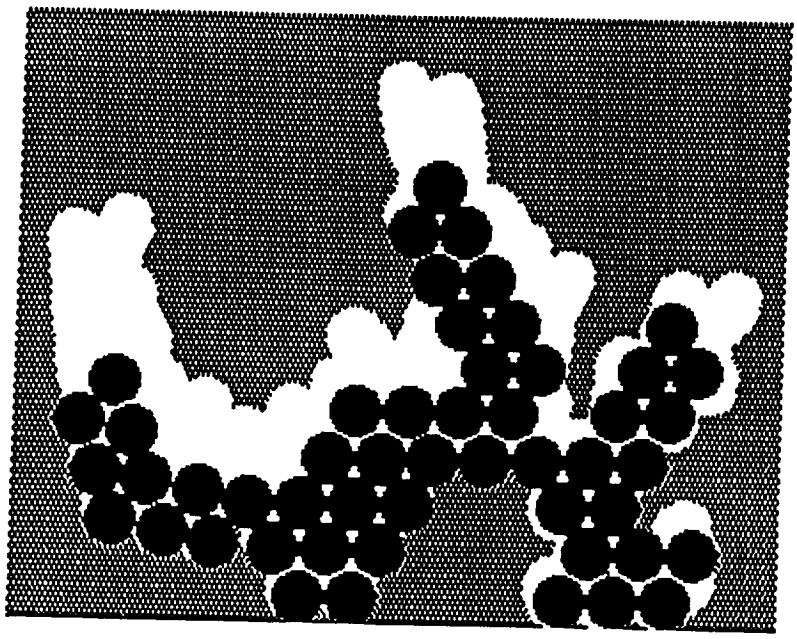

Triplet Interaction

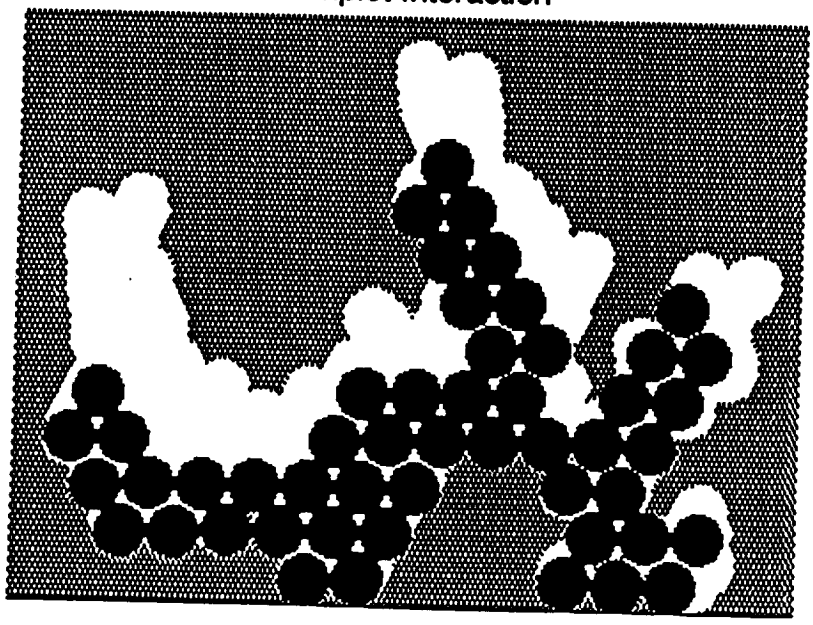

Fig 3

Singlet Interaction

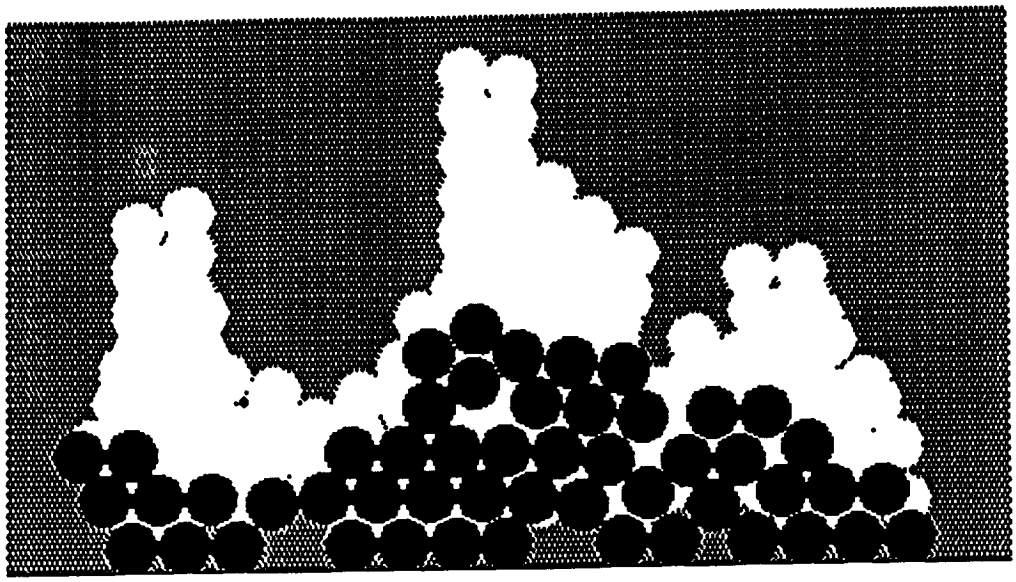

Triplet Interaction

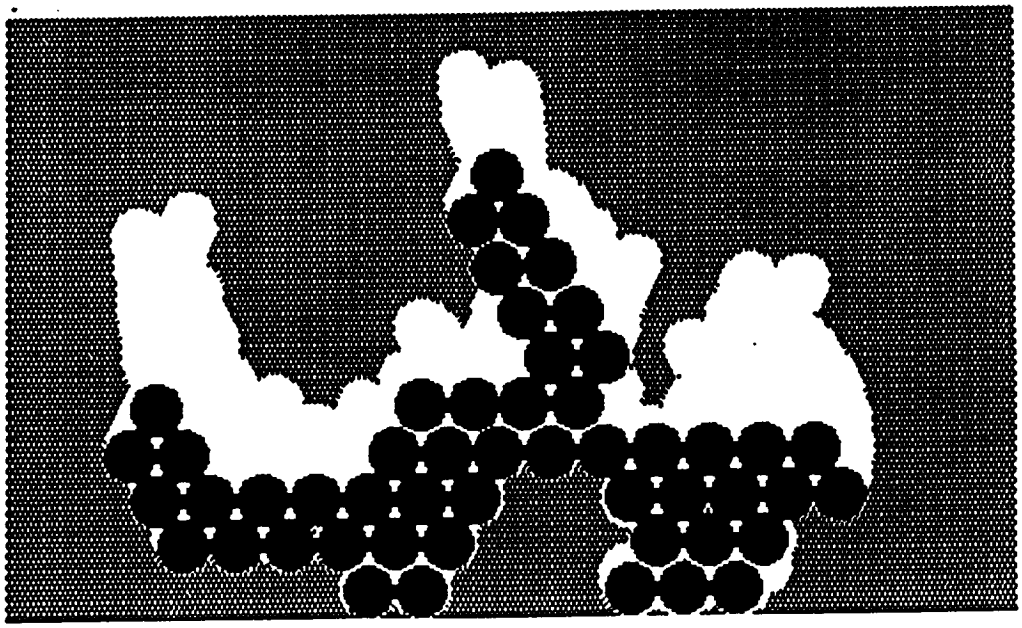

Singlet Interaction

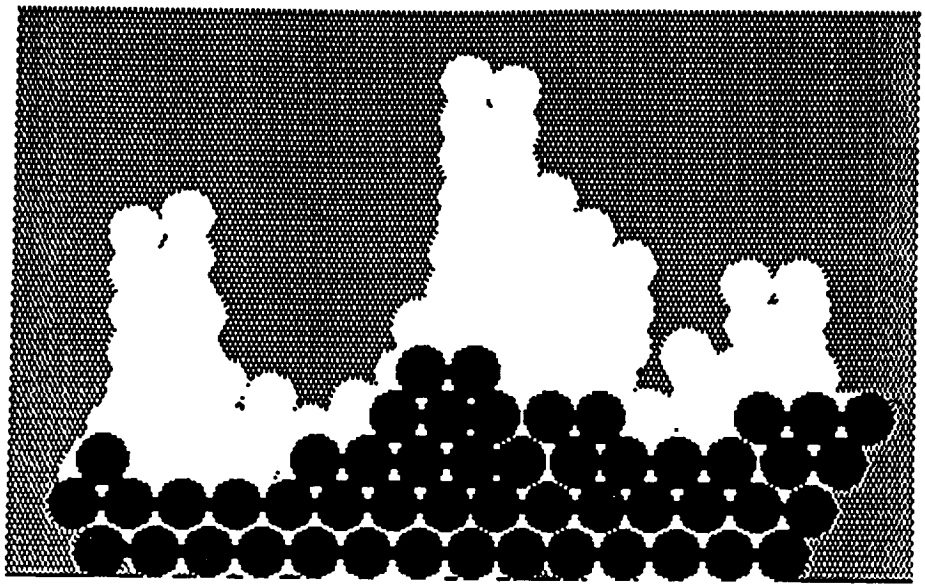

Triplet Interaction

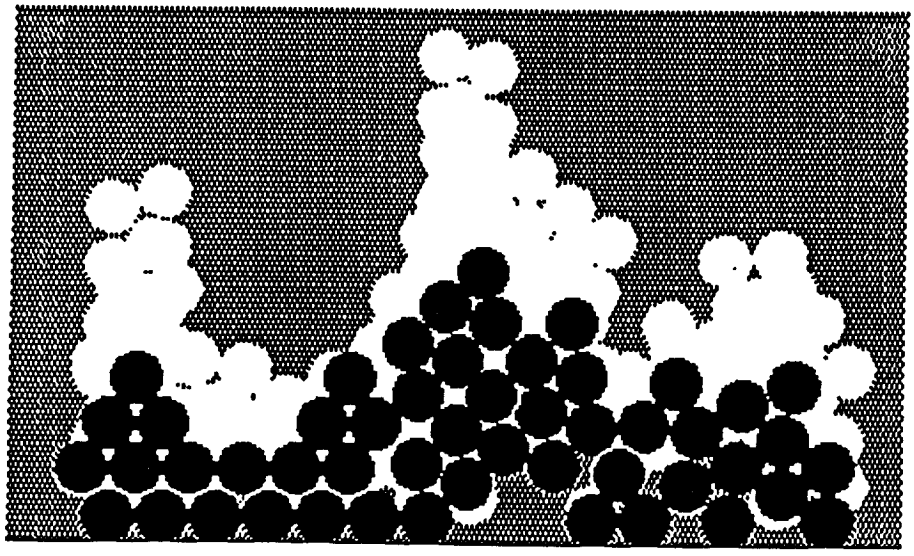

Fig 5